# DEVELOPMENT OF LIFE PREDICTION MODELS FOR ROLLING CONTACT WEAR IN CERAMIC AND STEEL BALL BEARINGS

**A thesis submitted in fulfillment of the requirements for the degree of Master of Engineering**

**Fazul M Huq**
**B.E**

**School of Aerospace, Mechanical and Manufacturing Engineering**
**Royal Melbourne Institute of Technology**
**Melbourne, Victoria, Australia**

**April, 2007**

# ABSTRACT

The potential for significant performance increases, using ceramic materials in un-lubricated rolling element bearing applications, has been the subject of research over the past two decades. Practical advantages over steel include increased ability to withstand high loads, severe environments and high speeds. However, widespread acceptance has been limited by the inability to predict wear life for ceramic bearing applications.

In this thesis, the rolling contact wear of 52100 bearing steel and Over-aged Magnesia-Partially-Stabilised Zirconia (OA-Mg-PSZ) ceramic are examined using a newly developed rolling contact wear test rig. The new wear test rig simulates the system geometry of an un-lubricated hybrid (ceramic and steel) ball bearing. The new wear test rig is versatile in that it allows low cost samples to be utilized resulting in a larger number of samples that can be tested.

Wear samples of 52100 bearing steel and OA-Mg-PSZ produced by the new wear test rig were examined for mass loss and wear depth. The wear behavior of both the steel and ceramic material showed a dependence on operating variables time and load. Load was varied between 300N to 790N. Typical mass loss after 1 hour of testing 52100 bearing steel at 790N was 0.03 grams as compared to OA-Mg-PSZ which was 0.001 grams. The rolling contact wear of the OA-Mg-PSZ was an order of magnitude lower than that of the 52100 bearing steel.

The wear mechanism for 52100 bearing steel was typical of plastic deformation and shearing near and below the surface of rolling contact. Once cracks extend to reach the surface, thin flat like sheets are produced. In OA-Mg-PSZ the wear mechanism initially is that of plastic deformation on the scale of the surface asperities with asperity polishing occurring followed by lateral cracks and fatigue spallation.

Results obtained using the new rolling contact wear test rig led to the establishment of a new equation for wear modeling of 52100 bearing steel and OA-Mg-PSZ ceramic materials.

# ACKNOWLEDGEMENTS

I wish to thank my first supervisor, Mr Varikan (Tom) Thomas for his patience, kindness and encouragement during the course of this project. He has provided me with an opportunity to succeed. I am indebted for all that he provided for me.

Many thanks to my second supervisor, Dr Mehdi Mahdavian for the review of this thesis and Dr S Lathabai of C.S.I.R.O for assistance in preparing and examining the Zirconia ceramic studied.

I am grateful to Mr Ron Fraser, of the Department of Mechanical and Manufacturing Engineering for his help in setting up and using the Talysurf 4 - profilometer and light microscope.

I would like to acknowledge Mr Safar Shawal, of the Chemical and Metallurgy group for his help in using the scanning electron microscope work and EDS.

I would like to thank Eric Lock, Lab Manager, Department of Mechanical and Manufacturing Engineering for purchasing of parts for building the rolling contact test rig.

Much appreciation to my friend Mr Ron Cocks, of RL Welding Fabrications, for the many hours and long nights spent manufacturing the rolling contact test rig.

I would like to thank C.S.I.R.O for providing Ceramic Specimens, and specialised equipment for advanced engineering materials.

The project funding and department scholarship from RMIT during the programme is gratefully acknowledged.

Finally, I must express my greatest love for my father whose only desire was to help me learn.

# DECLARATION OF ORIGINALITY

I, Fazul M Huq, hereby declare that this thesis has not been submitted, partially or fully for the award of any other degree or diploma in any university. To the best of my knowledge and belief, this thesis contains no material previously published or written by another person, except where due reference is made in the text.

**Fazul M. Huq**

April,2007

# CONTENTS

# CONTENTS

**Page No.**

# CONTENTS

**Page No.**

# CONTENTS

**Page No.**

# CONTENTS

**Page No.**

# CONTENTS

## List of Figures

# CONTENTS

## List of Figures

## List of Figures

## List of Figures

## List of Figures

## List of Graphs

# CONTENTS

## List of Tables

# Chapter 1

# Introduction – Hybrid Bearings

There is much interest in the use of ceramic materials for hybrid bearings applications where bearing steel races are used in combination with ceramic balls [10,13]. Hybrid bearings are considered for high speed and lubricant starved applications. Under these operating conditions, traditional steel bearings cannot operate [2]. The performance of ceramic materials like traditional bearing steels have been shown to depend heavily on the conditions of use, such as load and geometry of the contact as well as environmental effects [10]. It has been difficult to predict the performance of candidate ceramics since it appears that for each ceramic material there is a different dependence on wear rate for each usage condition. In addition, material properties such as composition, microstructure, porosity, toughness, hardness and surface finish may greatly affect the wear rate [10].

For rolling element bearing usage, sought after properties identified in the literature for candidate ceramic materials are listed below [7,11].

- Fracture toughness – High
- Hardness – High
- Elastic modulus – Low
- Density – Low
- Bend Strength – High
- Corrosion resistance – High
- Upper use temperature - High
- Failure mode by spallation - Small
- Porosity - Low

Failure modes must be typical of that seen in traditional steel bearings which are fatigue by spallation rather than catastrophic failure. Any ceramic that is to be considered viable for rolling element bearing must exhibit this failure mode. Only fully dense Silicon

Nitride and transformation toughened Zirconia fail by spallation [7]. Alumina and Silicon Carbide are not advocated as rolling elements for bearings due to this reason.

Silicon Nitride by far is currently the most used ceramic material for rolling element applications [7]. It has a high fracture toughness, high hardness, low elastic modulus and density. It has high corrosion resistance and fails by fatigue spallation.

Transformation toughened, Partially Stablised Zirconia (Mg-PSZ) has similar advantages to Silicon Nitride. Mg-PSZ has a higher fracture toughness than Silicon Nitride [10] and comparable strength and an elastic modulus very close to steel. In the case of ceramic rolling elements with steel races, an elastic modulus lower or close to that of the steel is required due to its relationship to Hertzian stress at a given bearing load. The lower the elastic modulus, the lower the contact stress. Thus one would expect that Mg-PSZ would be utilized as ceramic rolling elements. Rolling tests by Katz [8] show bearing life of PSZ to have two or three orders of magnitude less than the Silicon Nitrides therefore, fully dense Silicon Nitride remains the preferred ceramic for rolling element bearing applications.

Based on the results of Katz [8], high fracture toughness, high hardness, low elastic modulus and density alone cannot account for the wear behavior of ceramics in rolling contact. Studies reporting reduced life of PSZ as compared to Silicon Nitride have shown that lower life values of PSZ as compared to Silicon Nitride relate to microstructure [26]. The larger number of pre-existing defects, greater size of surface defects in PSZ is life reducing factors that shadow the qualities mentioned for PSZ.

Kelly [57] also proposed that microstructure played a significant role in the rolling contact wear life of this material. The stress-induced phase transformation was determined to be a significant factor in the wear behavior of Mg-PSZ in rolling contacts. Kelly [57] studied the rolling contact wear behavior of Mg-PSZ subeutectoid aged to a range of toughness values. This included AF (as fired - low toughness), MS (maximum strength - mid toughness), TS (thermal shock resistant – high toughness) and OA (over-aged). Of the four studied, the over-aged (OA-Mg-PSZ) showed significant resistance to wear. Kelly [57] concluded that the increased resistance of the OA material to the removal of material from the wear track is due to a combination of effects. The

transformable tetragonal precipitates assist in formation of a compressive layer due to volume change associated with phase transformation. In addition, the increased amount of softer monoclinic phase present, increases the amount of deformation able to be accommodated before large-scale damage occurs. The increase in monoclinic content, as well as the amount of transformable tetragonal phase contributes to increasing the number of cycles required to initiate wear.

In this work, the potential for un-lubricated hybrid Mg-PSZ bearing application is investigated by conducting rolling contact wear tests on OA-Mg-PSZ and 52100 bearing steel. A summary of the existing knowledge of wear of un-lubricated rolling contact of ceramic and steels is detailed in Section 2 - Literature Review. Section 3 discusses the design of new rolling contact wear test rig used to produce wear data. Section 4 – Results, documents the results from the rolling contact wear tests.

To enable application of hybrid bearings using Mg-PSZ requires a wear equation based on experimental data. Sections 5 & 6 presents a wear equation for 52100 bearing steel and Mg-PSZ based on the data and results obtained by the new rolling contact wear test rig.

# Chapter 2

# Literature Review

## 2.1 Wear and the Variables Affecting Wear

Vast documentation [27,30,32] exists in the literature describing wear behavior and its relationship to the variables that affect wear. Wear investigations typically monitor and vary some of the variables while measuring the wear volume and wear scar produced [5,16,32]. The majority of these wear investigations are conducted for un-lubricated sliding wear. The typical test configuration used consists of a pin sliding against a rotating disc. The wear of the pin and disc are then measured and analyzed. Section 3 provides a detailed description of the test configuration.

In roller bearings, a combination of rolling and sliding motion occurs. The slide to roll ratio will vary for each application and is typically dependent on the geometry, material of the material pair and surface friction [28,26] . As such it would be expected that the wear mechanisms and behavior would differ between rolling contact and sliding contact.
Experimental data in the literature [28,32,26] however, shows similarities in wear behavior and as such wear models for sliding wear have also been initially applied to wear produced by rolling contact.

As steel bearings typically contain a lubricant, most rolling contact tests are conducted with lubricant, thus the study focuses only on fluid film degradation and fatigue failure mode of the components rather than wear in rolling contact.

Hybrid bearings which contain steel races and ceramic balls are being investigated for their potential to be used in environments where the lubricant is removed [10,13]. This is for high speed applications or conditions where there would be adverse chemical reactions of the lubricant with the environment. When the lubricant is removed for rolling contact then the key failure mode is wear [13].

As steels are ductile and the ceramics are brittle [26] it is expected that wear mechanism will be different for steels and ceramics. This is indeed the case with steels materials which fail by plastic deformation associated with ductility, while ceramic fail by brittle fracture [13,57].

## 2.2 Variables to be Studied in this Investigation

This work is an attempt to fill a gap in the knowledge base for un-lubricated hybrid bearings applications by conducting un-lubricated wear investigations in rolling contact for both 52100 bearing steel and OA Mg-PSZ (Over –aged transformation toughened Partially Stablized Zirconia).

As it is impossible to cover all variables that affect wear as described in Table 2.1 in a single test facility, only operational variables load / pressure and cycle duration are varied. Material, geometric and environmental conditions defined in Table 2.1 are kept constant. The section to follow provides a summary of wear behavior observed for the operation variables load / pressure and cycle duration in ceramic and steels in rolling contact. Although surface finish and all material variables are kept constant in this work, they are still detailed. The selected microstructure for Mg-PSZ and surface finish used in this investigation, is based on the outcome of existing studies by Kelly [57] and Shetty et al. [14] which are documented in the section to follow.

## 2.3 Wear Behavior

### 2.3.1 Effect of Time on Wear

Skim, K.Kato, K.Hokkirigawa, H.Abe [13], studied the wear of a number of ceramic materials $Al_2O_3$, TiO2, SiC, $Si_3N_4$ and SUJ2 bearing steel in un-lubricated rolling contact as illustrated in Graph 2.1. They found that steady state wear occurs after 104 to 105 cycles. In steady state wear the wear volume was proportional to the number of revolutions. The wear loss of Silicon Nitride was smaller than any other ceramic materials and bearing steel in un-lubricated rolling contact.

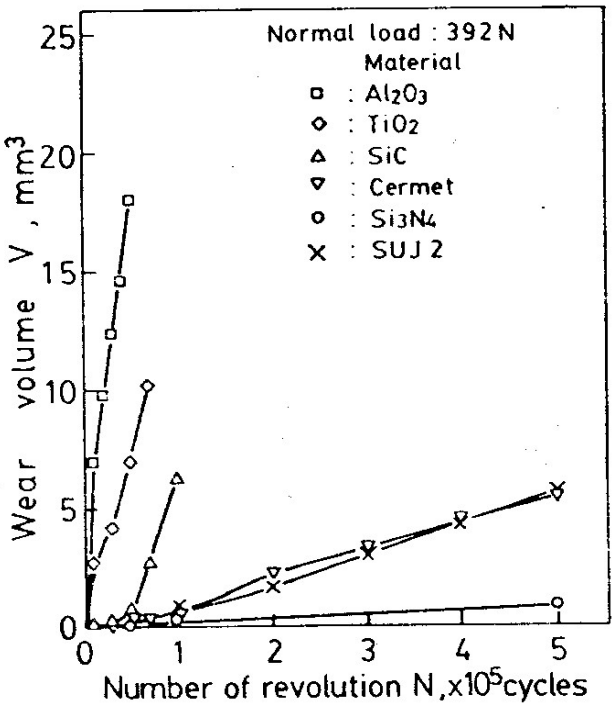


Graph 2.1 Wear Volume vs Number of Revolutions Relationship (392N) for Ceramic Materials on Bearing Steel. Ref: K.Kato, K.Hokkirigawa, H.Abe [13].

### 2.3.2 Effect of Load / Pressure on Wear

As load is increased the wear rate will increase in an un-lubricated bearing, Bayer [32]. Eventually a point will be reached where the wear rate will increase drastically. This increase will usually be due to the generated high temperatures which soften the material. Wang & Hsu [5] in their study of the wear and wear transition of alumina ceramic found that time-dependant wear transitions phenomena of alumina exists. When the normal load was increased without changing any other parameters an abrupt increase in wear scar diameter occurred in shorter time, as per Graph 2.2. The time-dependant wear transitions usually occur at certain load and speeds which are close to but not exceeding the critical fracture criteria of the materials.

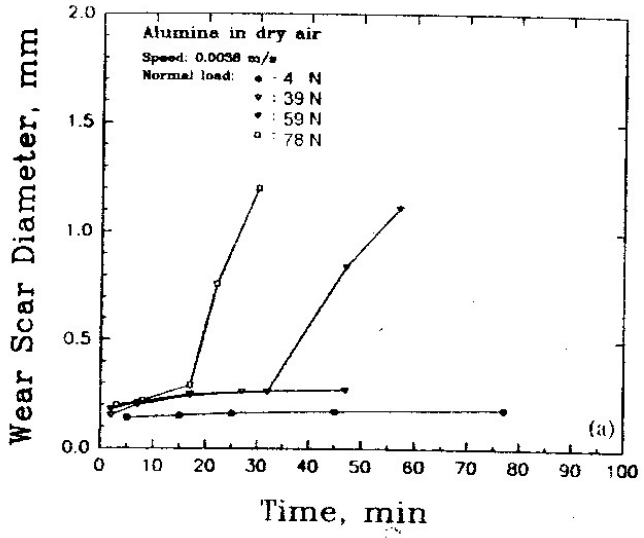


Graph 2.2 Wear as a Function of Time for Alumina in Dry Contact at Various Loads. Ref: Wang & Hsu [5]

Similar results are reported for Mg-PSZ in dry rolling contact, Kelly[57].

### 2.3.3 Effect of Surface Finish on Wear

Lakshminarayanan, L-Y. Chao, N.Iyer and D.K Shetty [14] studied the wear of bearing steels AISI M-50 and AISI 52100 in rolling contact with Silicon Nitride. They found that steels can suffer significant wear in rolling contact with Silicon Nitride with as ground ($R_a$ = 0.18um) silicon nitride rods. The steel balls suffered negligible wear when in contact with ground and lapped silicon nitride rods ($R_a$ = 0.08um) as per Graph 2.4.

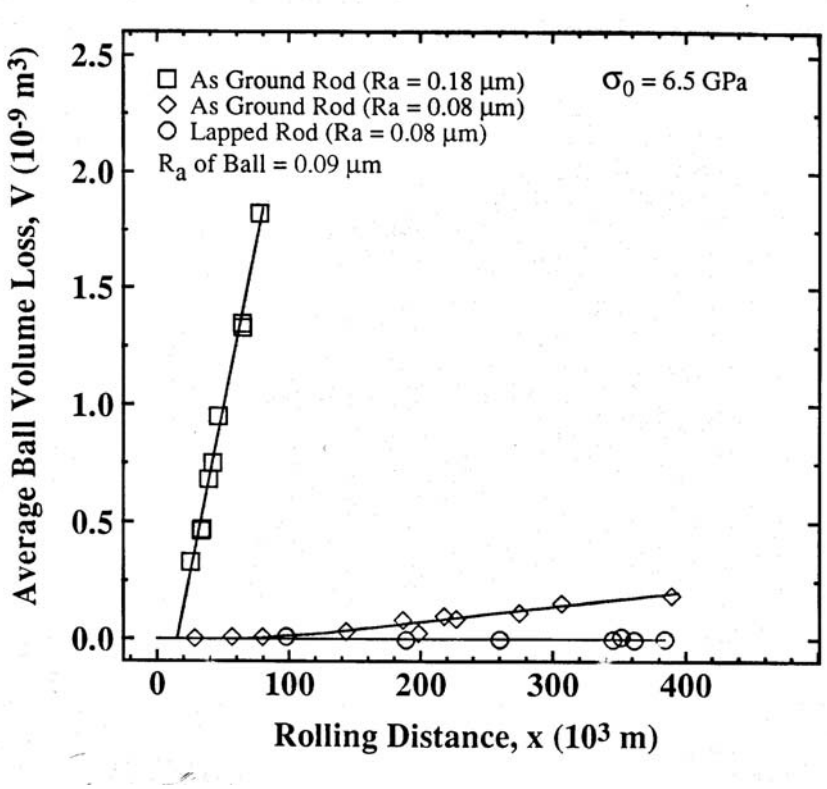


Graph 2.4: Comparison of the Wear Volume Loss of AISI 52100 Steel Balls in Rolling Contact with three types of $Si_3N_4$ Surfaces, Rough Ground ($R_a$ = 0.18um), Fine Ground Surface ($R_a$=0.08um) and Ground-and-Lapped Surface ($R_a$=0.08um). Ref: Lakshminarayanan, L-Y. Chao, N.Iyer and D.K Shetty [14]

In this work, $R_a$=0.08, OA – Mg-PSZ samples are produced based on the findings above.

### 2.3.4 Effect of Materials - Composition, Microstructure, Hardness, Fracture Toughness, Stress Induced Transformation Toughening

#### 2.3.4.1 Hardness, Toughness, Composition

The composition, properties and metallurgical structure of materials will determine their wear rates under different conditions of operation. Properties of particular significance are hardness, impact strength, toughness, porosity, modulus of elasticity, corrosion resistance and fatigue resistance.

For rolling elements density should be as low as possible to maintain low centrifugal loads, thus enabling attainment of high rotational speeds but should not be achieved by increase in porosity. It is well know that ceramic bearing life increases as porosity decreases [26,27]

Bremble & Brothers [16], conducted a study on the wear rate of rollers in un-lubricated metal roller bearings. In the case of metals dependence of wear rate is approximately inversely proportional to hardness, that is the lower the hardness the higher the wear rate. In the case of ceramic materials it is quite different from metals. S.Kim, K.Kato, K.Hokkirigawa, H.Abe [13] in their study of un-lubricated rolling friction of ceramics showed that although alumina and silicon carbide are harder than silicon nitride the wear rates of alumina and silicon carbide are much higher than that of silicon nitride.

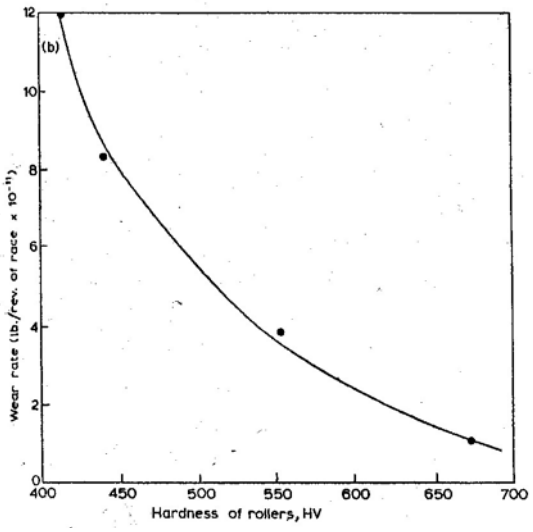


Graph 2.6 Wear Rate vs. Hardness in Bearing Steels in Un-lubricated Rolling Contact. Ref: Bremble and Brothers [16]

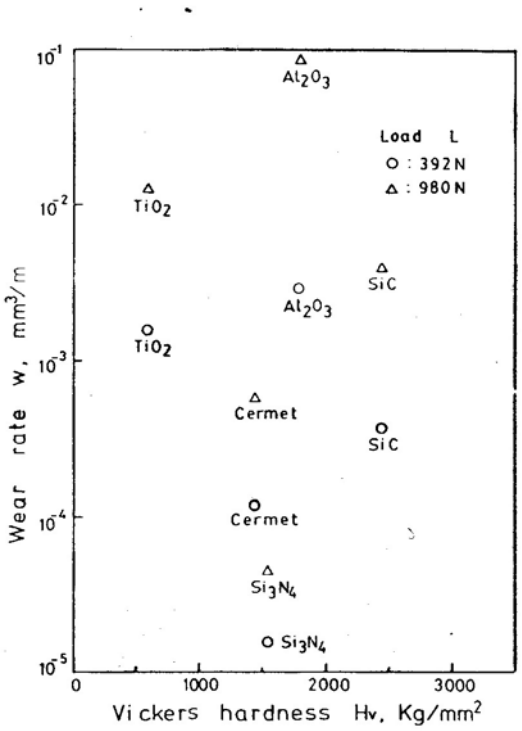


Graph 2.7 Hardness vs. Wear Rate for Ceramics. Ref: Kato [13]

Fracture toughness is often listed as a desired property of a bearing material however in the same study S.Kim, K.Kato, K.Hokkirigawa, H.Abe, [13] showed fracture toughness by itself is not a good function to represent the wear property of ceramic material either. Ceramic materials with higher fracture toughness such as Cerment (10.2 Mpa.$m^{1/2}$) and PSZ (8-10 Mpa.$m^{1/2}$) had a faster wear rate than Silicon nitride (5.2 Mpa.$m^{1/2}$)

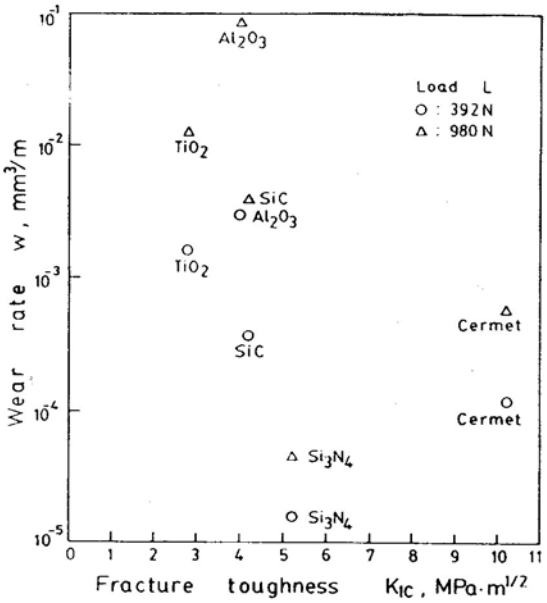


Graph 2.8 Fracture Toughness vs Wear Rate. Ref: Kato [13]

Governing equations of wear of ceramics described in the following sections show inverse proportionality to hardness and fracture toughness. Hardness and fracture toughness taken by themselves do not account for the wear behavior of ceramic materials.

Predictive equations that are based solely on hardness and fracture toughness only in part reflect the wear resistance, based on the literature described in this section.

More precise predictions of ceramic wear behavior require additional information regarding the microstructures. Of particular interest is stress induced transformation toughening observed in Zirconia ceramics.

### 2.3.4.2 Microstructure - Transformation Toughening

Transformation toughening is a mechanism used to improve wear resistance of Zirconia ceramics. This phenomenon occurs in Partially Stablised Zirconia (PSZ) and is described by Martin [42] below. Zirconia particles can transform from tetragonal to monoclinic ahead of a propagating crack. Ahead of a propagating crack there is a dilational stress field; this interacts with the constraining stress field around a metastable particle and initiates transformation. Transformation will occur to some distance within the stress field, and thus behind the crack tip there will be a wake or process zone of transformed particles, see Fig. 2.1 below. The volume expansion of these particles acts as a crack closure strain and thus reduces the stress intensity at the crack tip. This means that a further stress has to be imposed to continue crack propagation, so the failure stress (and hence toughness) increases.

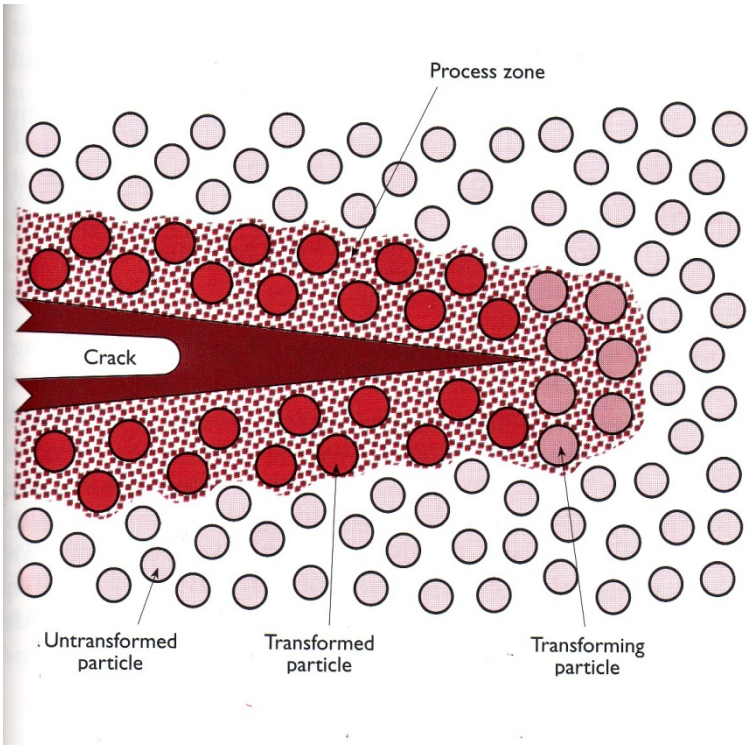


Figure 2.1 Mechanism of Transformation Toughening in Zirconia Ceramic. Ref: Martin [42]

Kelly [57] observed and quantified the amount of tetragonal to monoclinic transformation in four grades of Mg-PSZ.

Kelly [57] concluded that the increased resistance of the OA material to the removal of material from the wear track is due to a combination of effects. The transformable tetragonal precipitates assist in formation of a compressive layer on the surface, as previously discussed. In addition, the increased amount of softer monoclinic phase present in the OA material, increases the amount of deformation able to be accommodated before large-scale damage occurs.

In this work, OA-Mg PSZ identified by Kelly [57] as having the best wear resistance is used with surface finishes of 0.08μm.

## 2.4 Wear Prediction Techniques

Wear prediction is making an estimate of how much wear will occur after a given amount of time.

There are three different approaches to predict wear in service:

**Analytical** – Wear equations are proposed and attempts are made to account for significant variables either directly or through the use of wear coefficients. Wear coefficients are obtained from bench tests.
**Component** – Wear is measured under controlled conditions in component bench tests or prototype tests. These results are then extrapolated to service usage.
**Service Wear Measurements** – Wear is measured either directly or indirectly on components in service or those temporarily removed from service. Wear rate is usually determined only as a function of operating time. Wear of similar components in the same application are predicted using the wear time behavior.

In this work, existing analytical wear equations relating to un-lubricated rolling contact wear are reviewed. Wear equations for steels and ceramics are reviewed. Component bench tests are presented in section 3.

### 2.4.1 Analytical Wear Equations - Steel

Tribologists divide basic wear mechanisms into a few major categories:

Adhesion
Abrasion
Surface Fatigue
Delamination Wear
Corrosion (Oxidative wear)

Adhesion, Abrasion and Delamination wear models are detailed in this section. Surface fatigue is a combination of adhesion and abrasion due to repeated rolling. Oxidative wear is briefly discussed, but is not observed in the load range of this work. Figure 2.2 and 2.3 following provide a pictorial view.

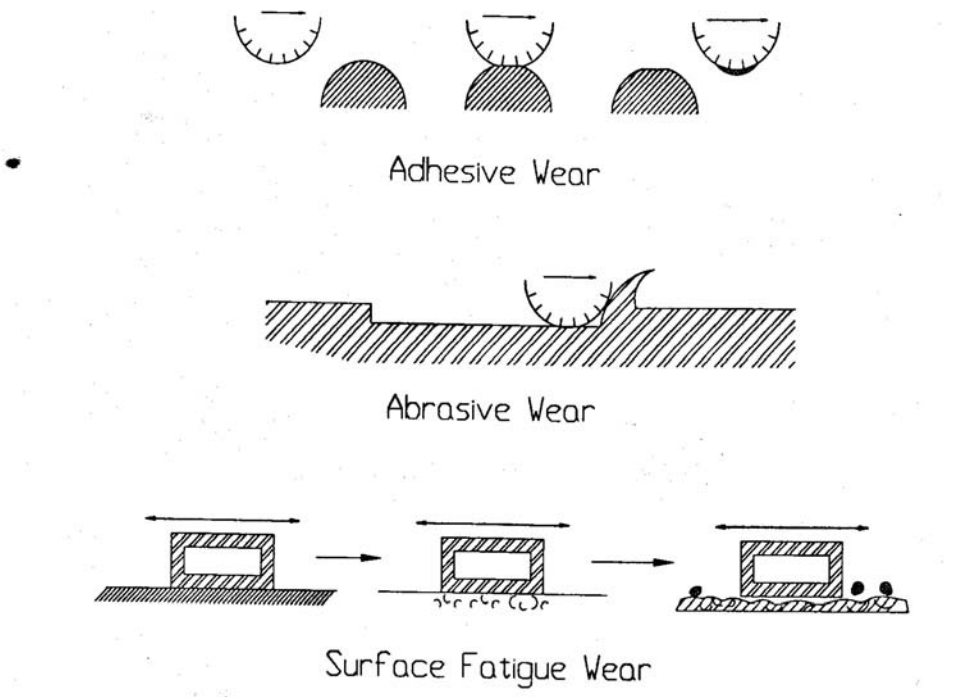


Figure 2.2 Graphical Representation of Adhesive, Abrasive and Surface Fatigue Wear. Ref: Wear Control Handbook [30]

#### 2.4.1.1 Adhesive Wear

Adhesive wear is wear by transference of material from one surface to another during relative motion due to a process of solid phase welding. When two surfaces come into contact they adhere to one another at least in localized sites. As the two surfaces move relative to one another, wear occurs by one surface pulling the material out of the other surface at these sites.

Archard [29] derived a mathematical model for adhesive wear that has been found to be in good agreement with experimental observations. Equation (1) has been used extensively in describing adhesive wear behavior.

$$V = \frac{K}{3p} Px \qquad \ldots(1)$$

Where x is the sliding distance, P is the normal load pressing the two surfaces together, p is the penetration hardness of the softer material and K is the probability that the rupture of any given junction will result in adhesive wear.

In this equation:

- The volume of material worn is proportional to the sliding distance.
- The volume of material worn is proportional to the load
- The material worn is inversely proportional to the hardness of the softer material

#### 2.4.1.2 Abrasive Wear

Abrasive wear mechanisms are generally considered to be any mechanism by which the hard asperities or particles cause damage in a single action. The damage, or wear, that they produce is of two general types, deformation or particle formation (material removal).

Three general situations for abrasive wear are identified [30]. One situation is when hard asperities of one surface are pressed into a softer surface. The abrasive wear situation is generally referred to as two-body abrasive wear. The second contact situation is one in which hard loose particles are trapped between two surfaces and the forces between the two surfaces are transmitted through these particles. This abrasive wear situation is referred to as three-body abrasion. The third contact situation is when hard particles directly impinge on a surface. In this case the particles are contained in a fluid such as a slurry.

From a practical standpoint, the equation for abrasive wear is often written as:

$$V = K\frac{L}{p}x \qquad \ldots(2)$$

Where K is a combined factor taking into account sharpness, probability of wear and nature of the wear process. p is the indentation hardness of the softer material, L is the total load and x is the sliding distance.

This equation is generally used for two-body and three-body abrasive wear situations.

#### 2.4.1.3 Delamination Theory of Wear

The delamination theory of wear was proposed by Suh [20,21,22,23,24,25] and is documented throughout the literature. Jahamir [55], provides a summary of the process and this is detailed below.

When two sliding surfaces come into contact, asperities of the softer surface are easily deformed by the repeated loading, caused by the normal load. As the process continues, the surface becomes smooth and the sub-surface deforms plastically due to the surface tractions.

As the sub-surface deformation continues, voids are nucleated below the surface (Figure 2.4). Void nucleation below the contact surface is controlled by two factors. Deformation by the shear component of stress promotes void nucleation, while the triaxial state of compression stress opposes void nucleation. Since the compressive stress is a maximum at the surface, voids do not nucleate at the surface. However, below a certain depth, where the deformation induced stress exceeds the compressive stress, void nucleation becomes possible. At depths far away from the surface void nucleation cannot occur since the stresses diminish very quickly. In materials which contain hard particles (e.g. second phase or inclusions) void nucleation is preferentially initiated at the particle-matrix interfaces.

Upon further deformation and repeated loadings, cracks extend and propagate, joining the neighboring ones. Cracks tend to propagate parallel to the surface since the state of loading is repeated along the surface (Figure 2.5).

When these subsurface cracks reach a critical length and become unstable they propagate to the surface, generating thin wear sheets. The thickness of the wear sheet depends on the magnitude of the normal and tangential loads at the surface, since they control the magnitude and depth of the maximum tensile stress. When the sheets become detached from the surface (Figure 2.6), shallow craters are produced on the worn surface.

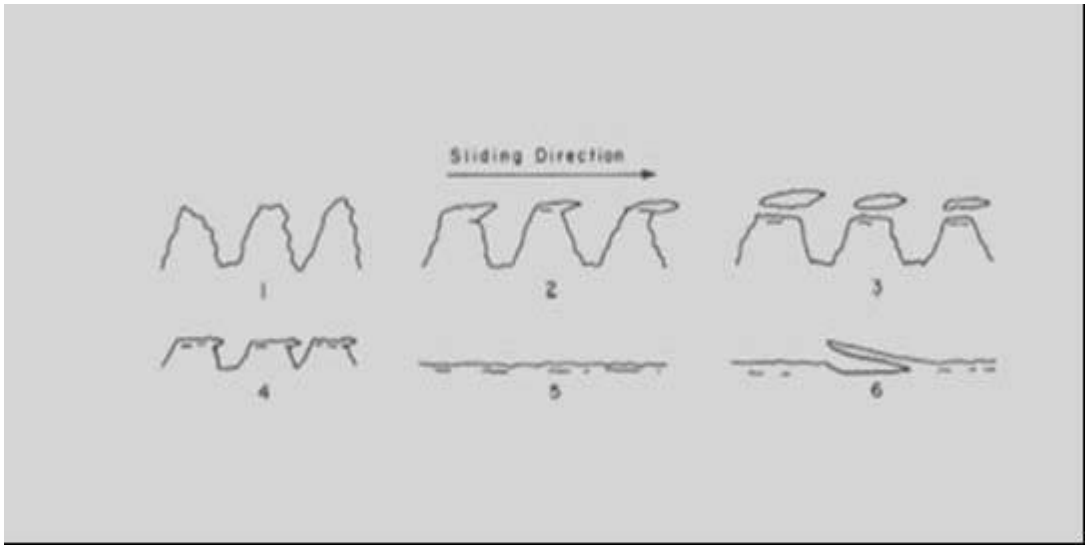


Figure 2.3 Schematic representation of the Delamination Process during Sliding Wear; Asperity Deformation and Fracture 1-5, Subsurface Crack Nucleation, Propagation, and Wear Sheet Formation 5-6. Ref: Jahamir [55]

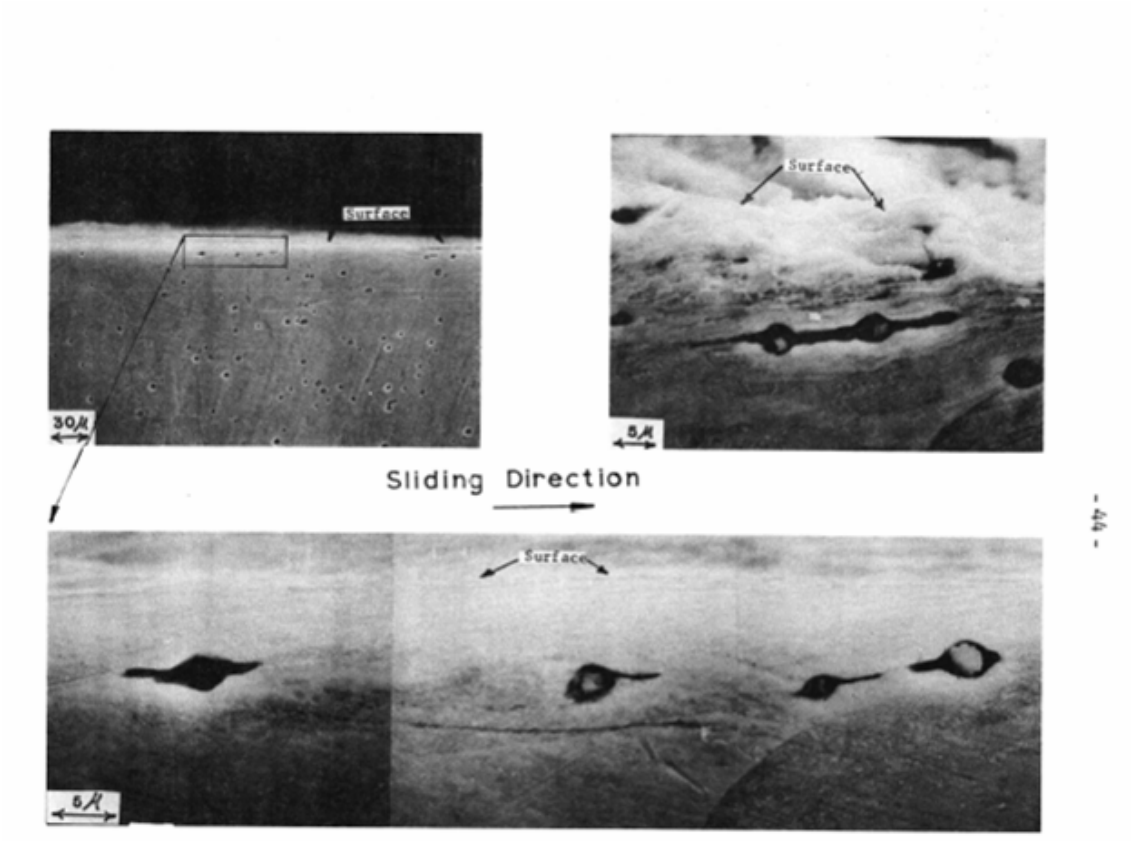


Figure 2.4 Void Formation around Inclusions and Crack Propagation from these Voids near the Surface in Annealed Fe -1.3% Mo. Ref: Jahamir [55]

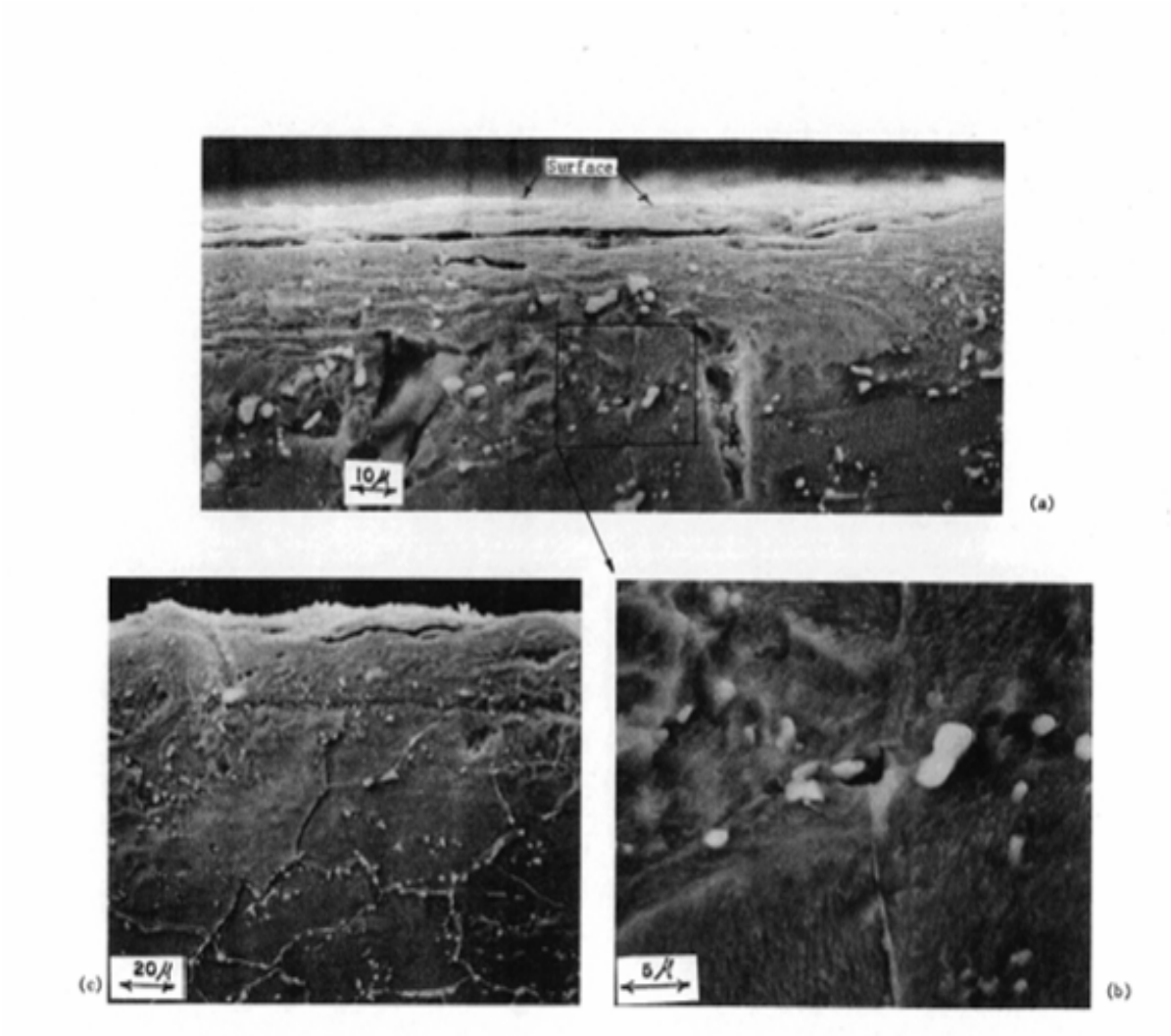


Figure 2.5 Subsurface Cracks and Deformation in annealed AISI 1020 steel. Ref: Jahamir [55]


Figure 2.6 Wear Sheet Formation. Reference- Said, Jahamir [55]

The wear equation based on delamination theory has been developed by Suh [20].

$$\frac{V}{S} = \Delta L^2 d(\Delta C_L + \Delta C_R) / \lambda 1c \qquad \text{... (3)}$$

Where:

V = wear volume, $\lambda$ =the spacing of asperity contacts, 1c=crack spacing, $\Delta L$ =total crack length, $\Delta C_L$=the average crack propagation rate at the left end of the crack, S = sliding distance, d =depth of crack.

Wear rate is directly proportion to the depth of crack and average crack growth rate. Wear is inversely proportional to the asperity spacing (which is an element related to surface topography) and crack spacing.

#### 2.4.1.4 Oxidative Wear

Surface layers of a chemically reacted species can be formed (e.g. iron oxide) in materials. Wear then occurs by one of the other three mechanisms either in this reacted layer or at the interface between the layer and the parent material. The wear rate then is influenced and possibly controlled by the growth and formation of that layer. This wear mechanism is confined to low loads under un-lubricated rolling contact.

### 2.4.2 Analytical Wear Equations - Ceramics

The application of linear elastic fracture mechanics (LEFM) to wear is confined to brittle materials [27,28], in which crack growth is accompanied by only low plastic deformation. This means that the principles of LEFM may be applied to wear problems in ceramics. Authors, Evans, Marshall, Kato, Wang & Hsu [53,37,13,15] have developed wear models for ceramics based on LEFM and are detailed in this section. Equations for modeling the reduction in critical stress due to stress induced phase transformation observed in Mg-PSZ is also detailed. An overview of LEFM is described below based on the literature.

#### 2.4.2.1 Fundamentals of LEFM

Understanding the strength of ceramics requires an understanding of the behavior of microcracks under stress. Liner elastic fracture mechanics is a theory that treats cracks in a continuous body.

Cracks in a body under uniform stress far from the crack will propagate catastrophically for values of this stress slightly exceeding a critical value given by

$$\sigma_f = \frac{K_c}{Y_c^{1/2}} \qquad ...(4)$$

where $K_C$ is the critical stress intensity factor , c is the appropriate crack size and $Y_C$ is a geometrical factor.

The central assumption of linear elastic fracture mechanics is that for a given material there is some critical value of $K_i$ usually termed $K_{ic}$ at which the crack is in equilibrium and above which rapid crack propagation will take place. The fracture condition in this formulation is taken as the equilibrium point so that fracture condition becomes:

$$K_i = K_{ic} \quad \ldots(5)$$

The quantity on the left is the applied stress intensity factor, and that on the right is a property of a particular material under consideration. $K_{ic}$ is usually measured.

The applied stress intensity factor at the crack tip is affected by internal stress caused by the interaction of the crack with the microstructure as the crack advances.

#### 2.4.2.2 Evans, Wilshaw & Marshall Model

Evans and Wilshaw [53] developed an equation for providing a basis for estimating material removal rates based on studies of lateral crack extensions in ceramics.

$$V_{wear} \alpha \frac{1}{K_{IC}^{3/4} H^{1/2}} \sum_{i=1}^{i=N} P^{5/4} D \quad \ldots(6)$$

In this model wear is proportional to load (P), Sliding Distance (D) and inversely proportional to fracture toughness ($K_{IC}$) and Hardness (H). As load and sliding distance are increased wear is increased. As fracture toughness and hardness are increased wear rate decreases.

The material removal analysis considers the extension of the lateral cracks normal to the motion. Evans & Marshall [54], derived the following equation for the volume removed.

$$V = C \frac{P^{9/8}}{K_{IC}^{1/2} H^{5/8}} \left( \frac{E}{H} \right)^{4/5} D \quad \ldots(7)$$

where C is a material-independent constant and E is the elastic modulus.

### 2.4.2.3 Kato Model

Kato [13] developed a new parameter for evaluating wear rate of ceramic materials in un-lubricated rolling contact. As described in earlier sections, this was based on his findings that fracture toughness and hardness alone do not correlate well with wear rate in ceramics. A new dimensionless parameter $S_c$ describes the severity of contact in actual rolling friction.

$$Sc = Pm\sqrt{R\max} / K_{IC} \qquad \ldots(8)$$

$S_c$ gives the microscopic and geometrical information of the wear surface. $K_{ic}$ is the fracture toughness, $R_{max}$ is the maximum surface roughness, $P_m$ is the mean Hertzian Pressure.

The wear rate of ceramic materials is given by

$$w = \alpha \bullet Sc^n \qquad \ldots(9)$$

where $\alpha = 1.56x10^{-5}$ and n=5.46

### 2.4.2.4 Wang and Hsu Model

Wang and Hsu [15], studied the wear mechanisms of ceramic materials in un-lubricated sliding contact. Wang and Hsu found that the difference in surface roughness correlates well with difference in wear rate in each material. Brittle fracture and surface cracks are observed on the wear track where debris is generated.

Wang & Hsu [15] introduced a new variable $\sigma_d$. When the contact stress exceed the critical stress $\sigma_d$ cracks propagate and wear particles are produced. The cracks and wear particles change the stress distribution in the contact. The contact stress at the tip of these particles can be larger than the critical stress and more cracks would result. The chain reaction produces more damage and causes more cracks.

$$V = C\frac{\sigma_{\max}}{\sigma_D}\frac{DP}{H} \qquad \ldots(10)$$

where V is the wear volume, C is a coefficient derived from experimental data. $\sigma_{max}$ and $\upsilon_d$ describes at any time the ratio of the applied stress to the critical damage stress for brittle materials. D is sliding distance, P is load and H is hardness.

$\sigma_d$ needs to be measured experimentally for any particular ceramic material. When the maximum tensile stress $\sigma_{max}$ equals or exceeds $\sigma_d$ cracks appear on the surface.

The threshold theoretically should be unity. When the ratio exceeds the threshold, wear transition occurs and the C value signifies the controlling wear mechanism of microcracks during the wear process.

The equation indicates that ceramic wear under the control of tensile stress depends not only on load, sliding distance and hardness but also on the surface stress ratio, $\sigma_{max}$ and $\sigma_d$ which is primarily dependent on friction state, Hertzian pressure and pre-existing surface damage.

### 2.4.2.5 Stress Induced Phase Transformation - Toughening Equations.

Equations for the change in stress intensity factor due to stress induced phase transformation are detailed below.

Marshall, Evans and Drory as detailed in Watchman [28] treated the toughening induced by transformation through direct calculation of the change in the applied stress intensity factor caused by transformation.

For dilatational stress (no shear stress)

$$\Delta K_c^{\ T} = 0.3 V_f \varepsilon^T E w^{\frac{1}{2}} \qquad \ldots (11)$$

$V_f$ = volume fraction of tetragonal grains transforming to monoclinic, w = width of wake (transformed zone), $\varepsilon^T$ = permanent strain associated with transformation. E is the Young's modulus.

The value of w is given by:

$$w = \frac{3^{\frac{1}{2}}(1+\nu)^2}{12\pi}\left(\frac{K_\infty}{\sigma^c}\right)^2 \qquad \ldots(12)$$

Designing and producing microstructures to increase toughness $\Delta K$ have thus become the main goals of research on structural ceramics. To maximize toughness, the number of particles that will readily transform under an applied stress must be maximized and thus increase wake width w.

## 2.5 Hybrid Bearing – System Modelling

The purpose of this investigation is to produce wear data that can be used to develop life prediction models for the wear of ceramic and steel materials when combined in a hybrid bearing with no lubrication. Ultimately the data and models would be used to predict service life in the field. Figure 2.7 presents a pictorial view of the system under investigation.

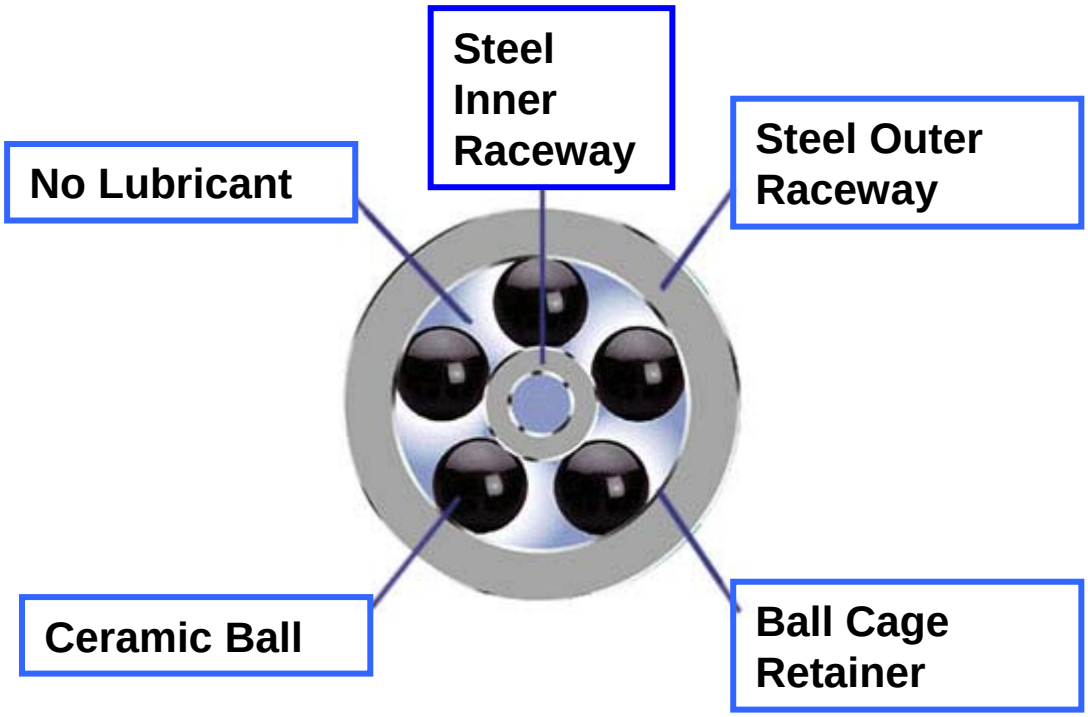


Figure 2.7: Pictorial view of Hybrid Ceramic Bearing System

Full scale bearing tests for investigating rolling contact fatigue and wear life of candidate ceramic materials and steels constitutes the ultimate proof of bearing materials. However, the reality is these tests are very expensive. This is due to high material costs, duration time of tests, and large number of specimens that have to be tested as data must be treated statistically [49, 52].

The alternative is to design a test rig that simulates the bearing system, allowing materials to be evaluated quickly and larger amounts of data to be obtained. In this section, details of the development of a new rolling contact wear test rig for the hybrid bearing system are provided. The development begins first with reviewing system level modeling methodology, followed by a review of existing wear test rigs. The design of a proposed new test rig is then detailed.

A new rolling contact test rig is built based on the requirements of system modeling a hybrid bearing and is presented in this section. The test procedure for producing wear data using this test rig is documented. Pre and post test sample preparation and measurement systems used to evaluate wear results are also presented in this section.

The tests to be conducted to investigate the wear of steel and ceramics in rolling contact are summarized in this section and the test results are documented in Section 4.0 Results.

## 2.6 Wear System Methodology

To ensure a new test rig is capable of simulating the system described in Section 2.5, a systems level approach is applied to the wear process. Czichos [50] presents a systems level description of wear process and is detailed below.

Czichos [50] explains that elements and materials directly involved in the process must be hypothetically separated from other components of the technical system under consideration. The directly involved parts and materials are called the elements of the system concerned. As shown in Figure 2.8 these are the elements (1) and (2) i.e. the interacting bodies which would be the ceramic ball in contact with the steel raceways. The interfacial medium (3) would be for instance a lubricant. In this investigation there is no interfacial medium (no lubricant). Finally the surrounding medium (4) is the external environment.

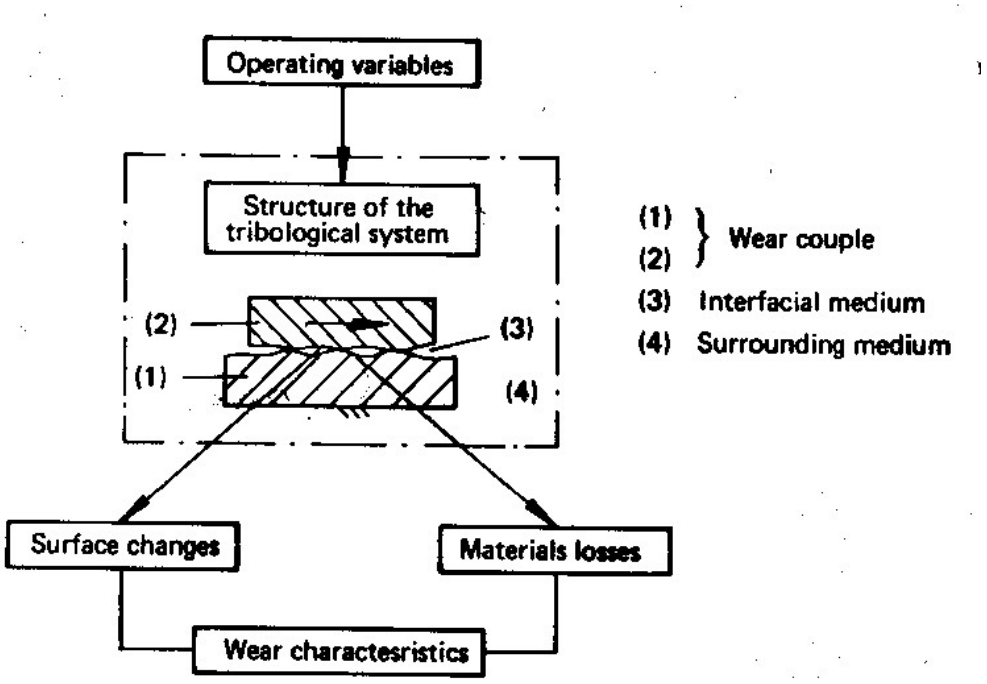


Figure 2.8 Description of a Wear System Ref: Czichos [50]

The elements directly involved in a wear process and their relevant properties and interactions form the structure of the system.

The wear resulting through the action of the operating variables on the structure of the system produces the wear characteristic. This data characterizes the surface changes, i.e. the appearance of wear and material losses induced by the wear.

The new test rig based on a system approach needs to include the relevant operating variables, correct structure of the system, which includes the elements involved in wear, the relevant properties of the elements and correct interactions between the elements (geometry of bearing). The test rig would also need to allow for evaluation of the wear characteristic as a function of the operating variables and system structure.

The systems analysis of the wear process is summarized in Figure 2.9.

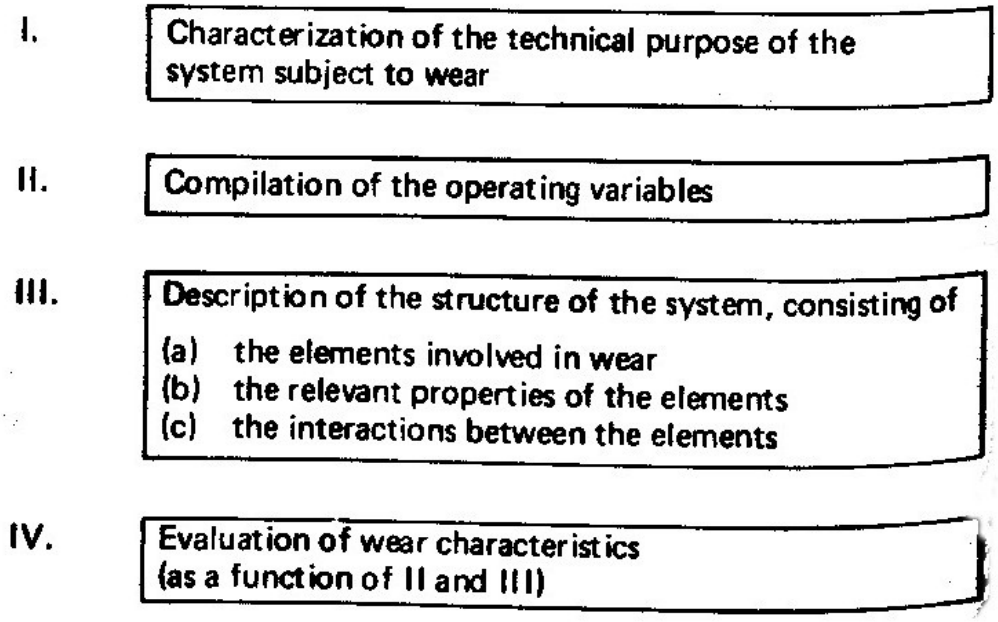


Figure 2.9 System Analysis of wear process. Ref: Czichos [50]

Zum Gar [27] presents a pictorial summary of the literature in Figure 2.10. Figure 2.10 displays the parameters and mechanisms which affect service life under rolling-sliding contact. In the case of a un–lubricated hybrid bearing, the inputs are the rolling contact

geometry and operating conditions. The outputs are surface damage characterized by plastic shearing, surface indentation, cracking, spalling and chemical reaction. The test rig needs to include the correct geometry and operating conditions to produce the relevant surface damage as seen in full scale bearing.

The following section reviews existing wear test rigs. They are evaluated for their suitability for this investigation based on the system level methodology described above. Finally, a design is proposed that meets the system level requirements.

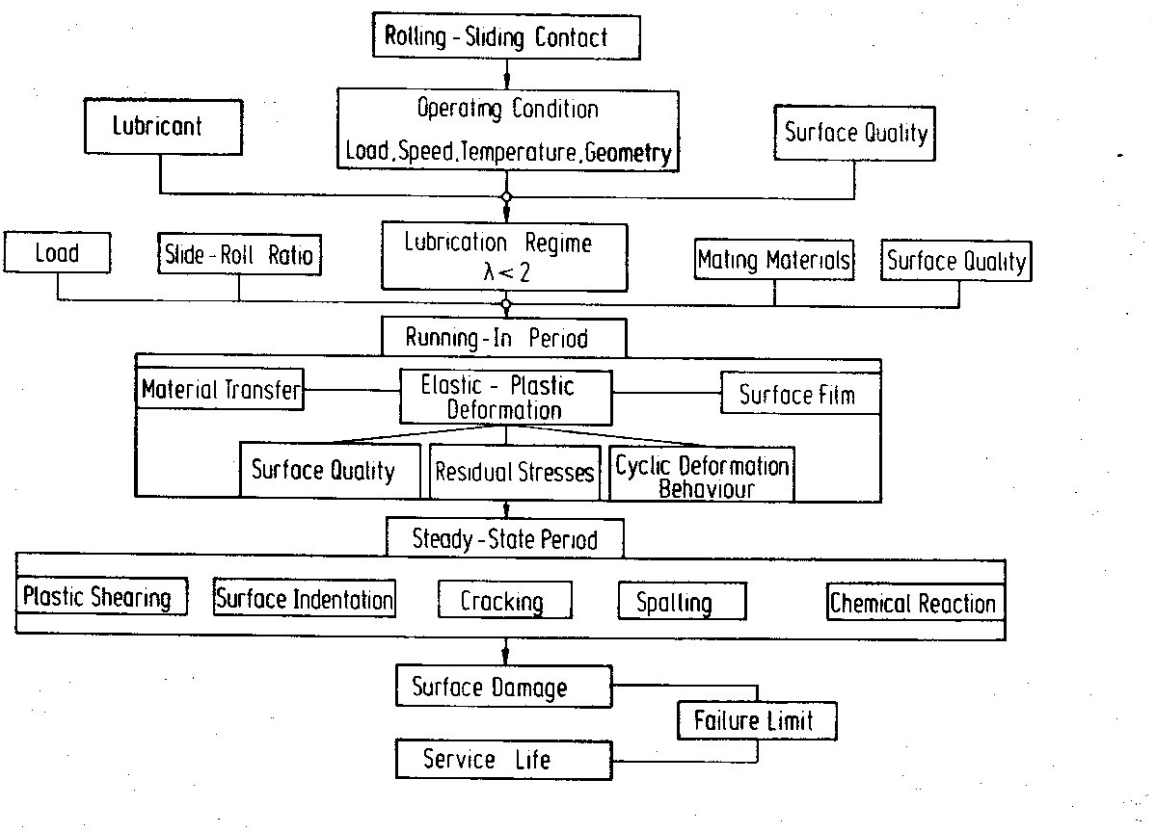


Figure 2.10 – Factors and Mechanisms influencing the Service Life of Rolling-Sliding pairs in Marginally Lubricated or Un-Lubricated contact. Ref: Zum Gar [27]

## 2.7 Wear Test Rigs – Evaluation of Current Systems

### 2.7.1 Pin on Disc

Pin on Disc is one of the most commonly used test rigs in the literature for evaluating sliding wear of material pairs. Figure 2.11 show the schematic of the test set-up. In a hybrid set-up a steel pin slides against a ceramic disc. The wear of the pin and the wear track produced on the disc are measured. Normal load and frictional force are recorded along with sliding distance.

This set-up is not suitable for the current investigation as it contains pure sliding rather than a degree of sliding and rolling observed in bearings. Additionally the contact geometry of a flat plane on pin is not representative of a bearing geometry.

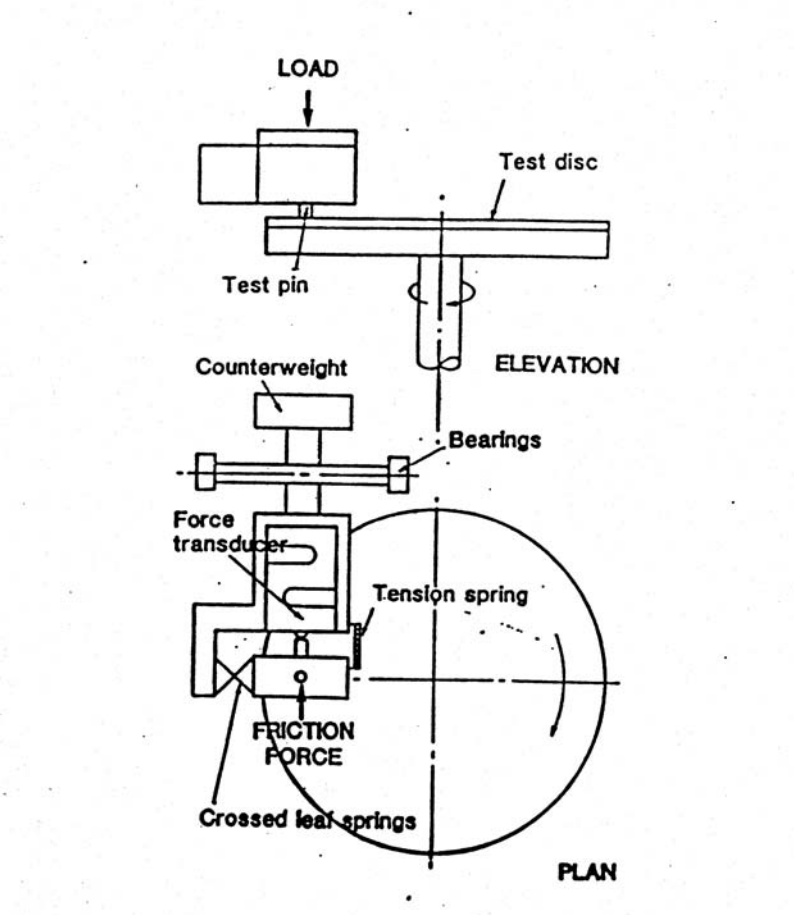


Figure 2.11: Pin on Disc Schematic. Ref: Kelly [57]

### 2.7.2 Modified Pin on Disc – Roller on Disc

Kelly [57] in rolling contact investigations modified the pin – on disc test machine to include a roller rather than a pin as shown in Figure 2.12. The wear of both the roller and disc were then evaluated. As this configuration has a roller in contact with a flat plane, the Hertzian Stress distribution would differ to that produced by the ball in contact with the inner and outer race of a bearing [Hertz,1881]. This limitation means that the system elements would not interact in the same way as that seen in a bearing and would not be suitable for this investigation.

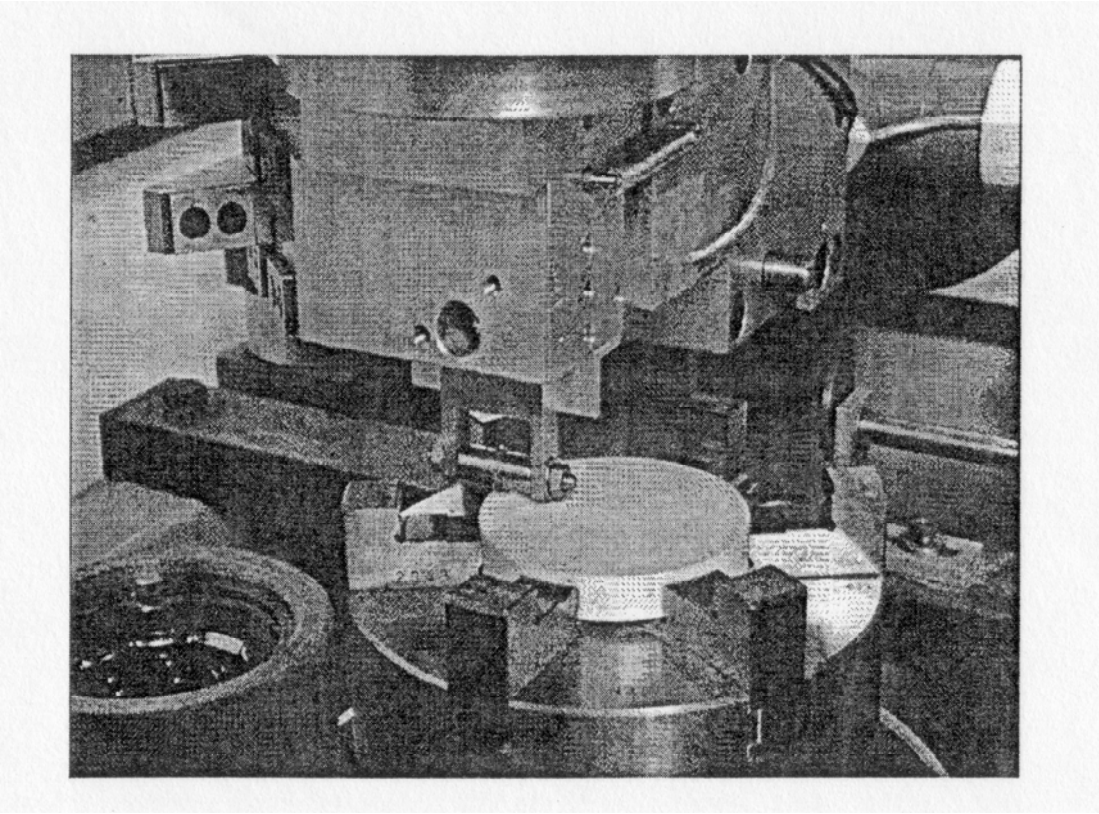

Figure 2.12 Modified Pin on Disc Machine to include Roller. Ref: Kelly [57]

### 2.7.3 The Ball - Rod – RCF Tester

Glover [49] describes this test in detail. A rotating cylindrical test specimen is alternately stressed by rolling contact with three radially loaded balls. The three balls, separated by a retainer, are radially loaded against the test specimen by two tapered bearing cups thrust – loaded by three compression springs. The test specimen is held in a vertical position by a precision collet. The specimen is rotated by a direct drive motor mounted in line with the specimen

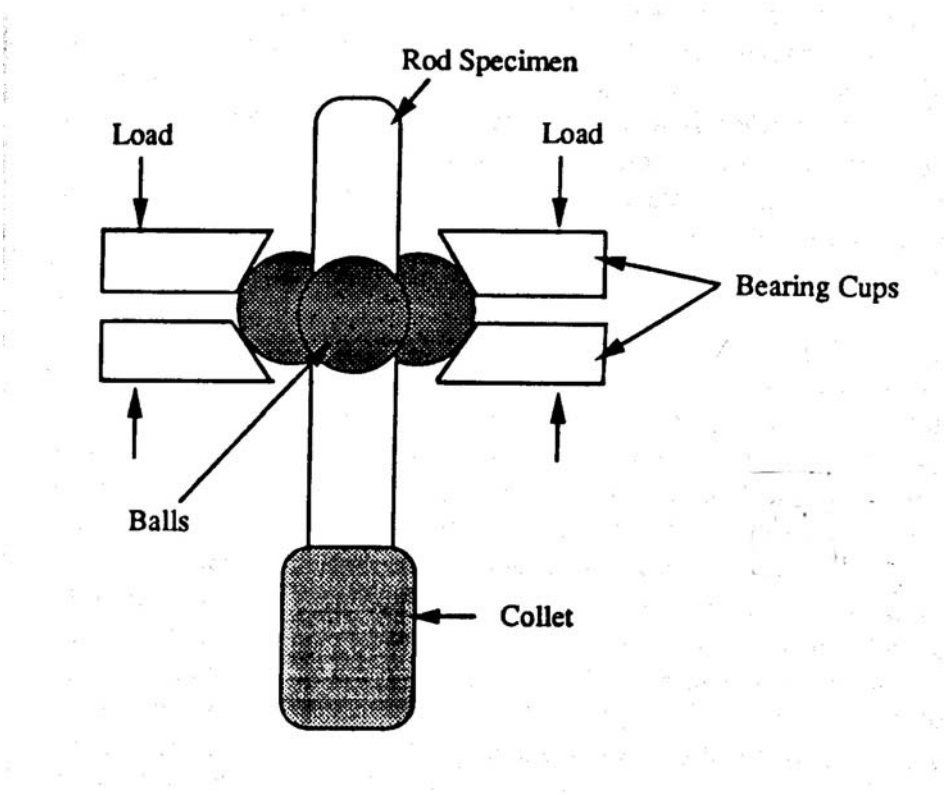


Figure 2.13: Ball Rod- RCF Tester Ref: Glover [49]

This configuration does meet the system requirements for rolling contact and is used widely in the literature to produce rolling contact wear data. The test specimen however is supported by 3 balls. In the bearing system under consideration in this investigation, the ceramic ball would make two contacts only, one with the inner and one with the outer race as shown in Figure 2.14.

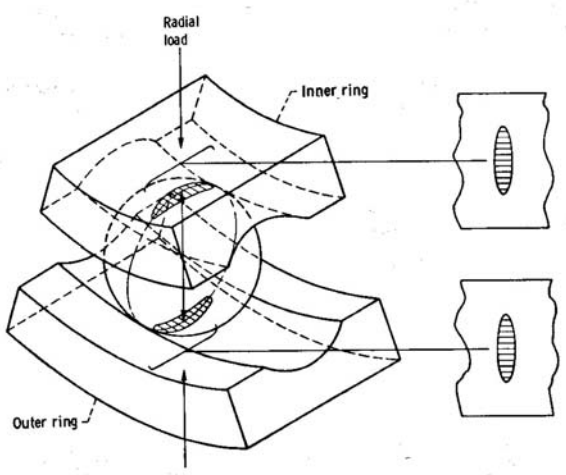


Figure 2.14: Contact Geometry of Ball Bearing System. Two Elliptical Contacts with Inner and Outer Race are shown. Ref: Hamrock [43]

### 2.7.4 Rolling - Element-on-Flat Test

The rolling element-on-flat tester was originally used by Dalal et al. [48]. Figure 2.15 shows a cross section view of the test rig. The test unit has a unidirectional thrust bearing configuration, which consists of three balls or rollers equally spaced at 120 degrees by a retainer and loaded between a stationary flat washer (at the bottom) and a rotating grooved washer (at the top). The rotating washer produces ball motion and serves to transmit load to the balls and the flat washer. In this investigation a radially loaded bearing is investigated rather than thrust load thus it is not suitable. Additionally the stationary flat washer would not represent the correct geometry as described in earlier sections.

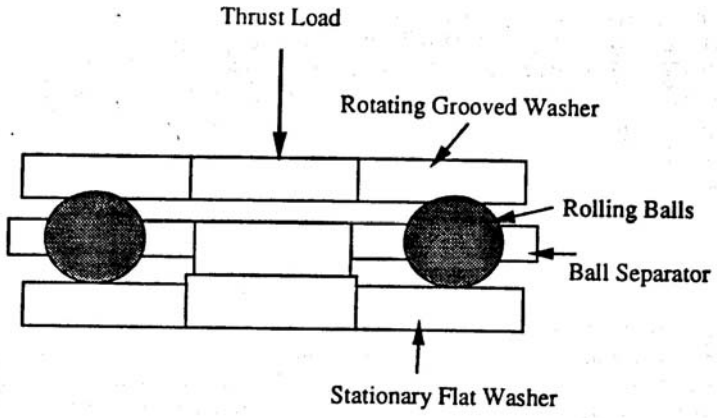


Figure 2.15: Rolling Element on Flat Test Rig. Ref: Shetty [48]

### 2.7.5 Rotating Five - or Four - Ball Fatigue Test

The five-ball fatigue tester was first used by Carter and Zaretsky at NASA Lewis Research Centre [48]. Figure 2.16 shows the contact geometry and the rotating mechanism of the test rig. The test assembly consists of a driven test ball on top of four lower balls positioned by a separator, in the form of a pyramid. The four lower balls rotate in a race driven by the upper ball, thus simulating the rolling and sliding produced in angular contact ball bearings. It would be possible to use this configuration but ceramic test samples would be difficult to produce for this investigation.

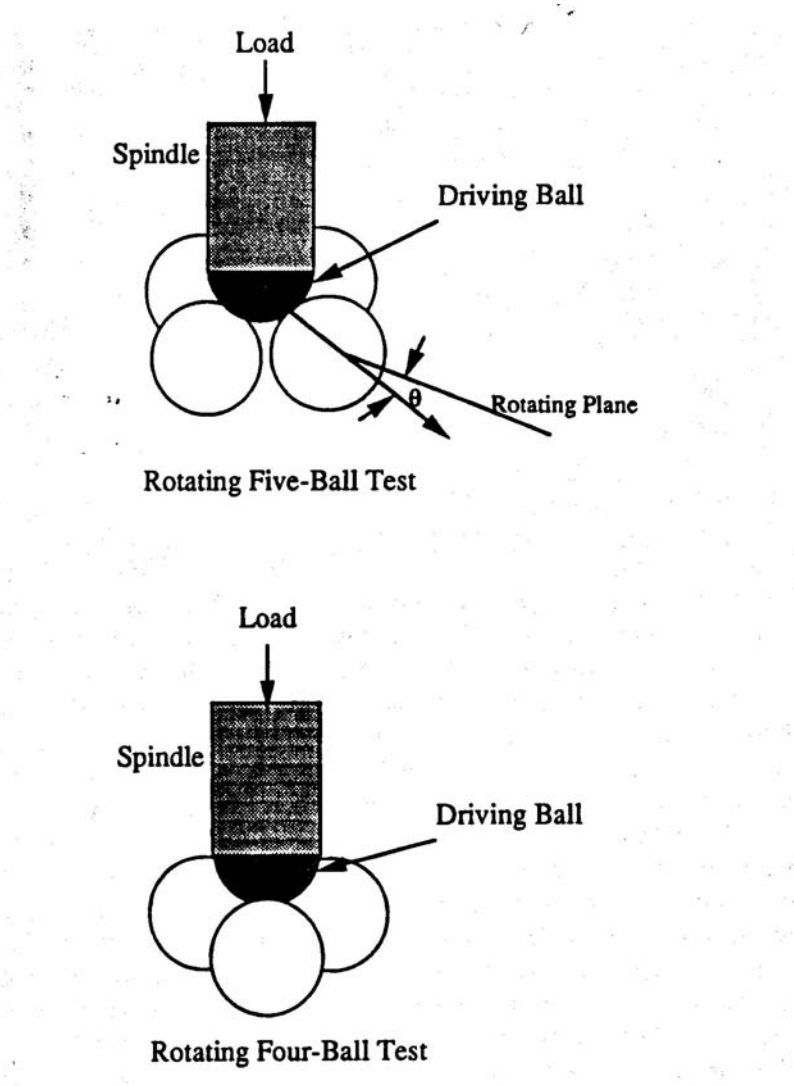


Figure 2.16: Rotating Five Ball and Four Ball Wear Test Rigs. Ref: Shetty [48]

### 2.7.6 Disk on Disk Type Tester

The disk on disk type tester has been used by Kato and Bremble [13, 16]. The apparatus uses two disk-shaped specimens rotating against each other on their outer surfaces. A schematic is shown in Figure 2.17. Tests can be conducted in dry conditions. Profiles of the wear scars on the contact surfaces can be used to estimate the wear volume.

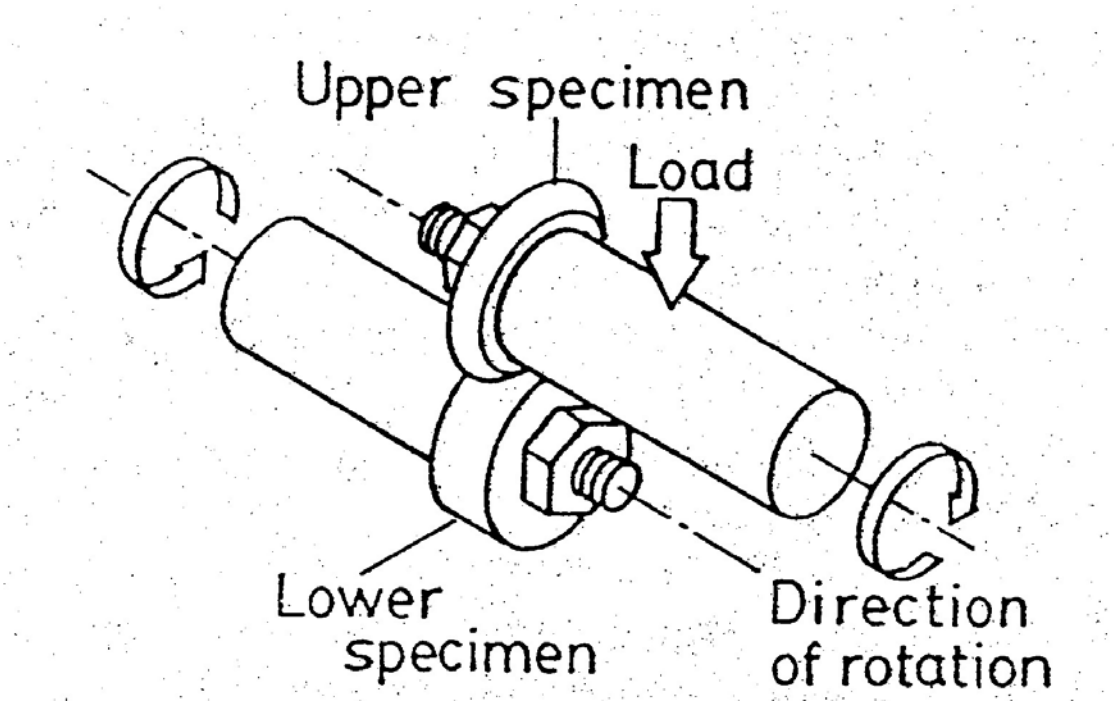


Figure 2.17: Wear Test Rig as used by Kato Ref : [13].

Bremble [16] also used a similar test configuration which is shown in Figure 2.18. The inner race of the bearing is mounted on shaft S and held in position by a lock nut. The outer race is fixed to the annular housing H, with a groove in its outer surface. A one inch ball B is mounted on a shaft in the housing K to which a load transducer T is attached. The load is applied by locating the ball B in the groove of the outer race housing and screwing up the collar C against the outer supports L.

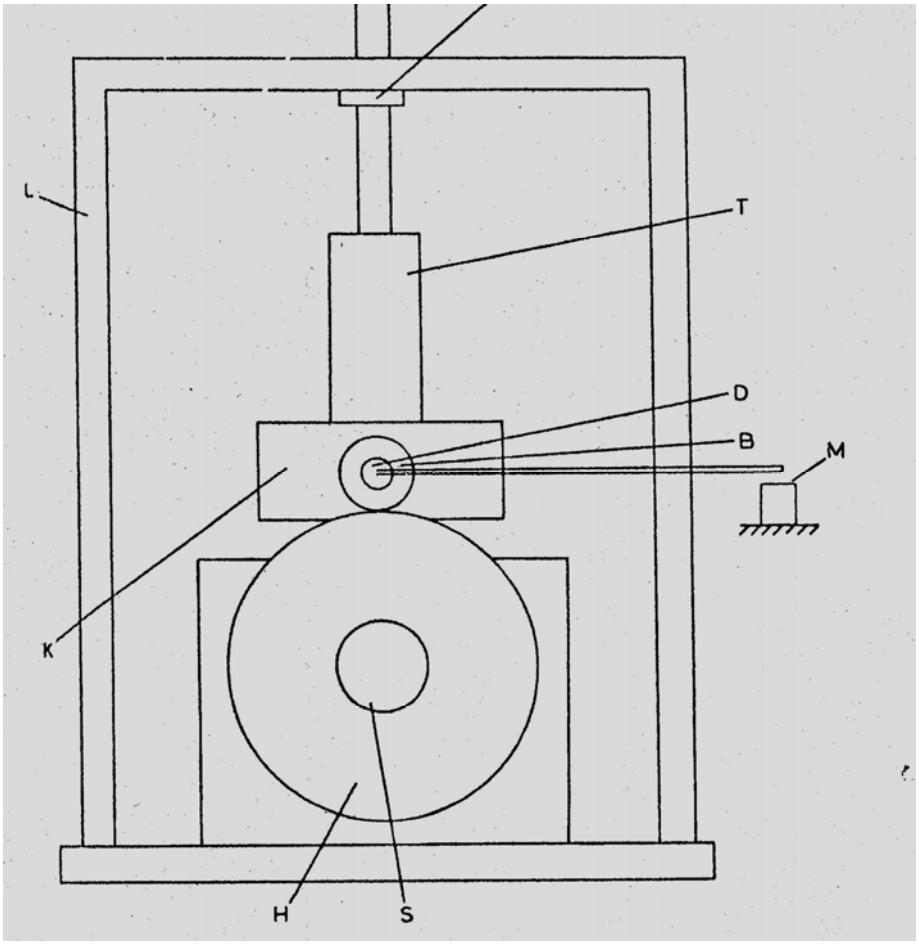


Figure 2.18 Drawing of Bearing Test Rig used by Bremble and Brothers Ref: [16].

In summary the test rigs reviewed are not suitable for this investigation as they either do not contain the correct bearing geometry or the samples would be too difficult to produce. The next section documents a test configuration which eliminates these issues and details the proposed test configuration.

In this section the current state of knowledge on the variables affecting wear, the influence of these variables on wear behavior and empirical models for wear prediction modeling of steel and ceramic materials have been reviewed.

Methods for modelling the hybrid bearing system under investigation were also reviewed based on system level methodology. The purpose is to develop a new rolling contact test rig that can be used to produce wear data for steel and ceramic materials in rolling contact. Data produced by the test rig will be documented in Section 4.0 Results.

In Section 5 Discussion, the wear data will be fitted to suitable empirical models that have been reviewed in the Section 2 Literature Review.

# Chapter 3

# Design of a new Rolling Contact Wear Test Rig and review of Experimental Procedure

## 3.1 Proposed Test Configuration

Muro and Tsushima [51] investigated rolling contact of various hardness steels using a test configuration shown in Figure 3.1. The cylinder and ball wear tracks were evaluated for wear.

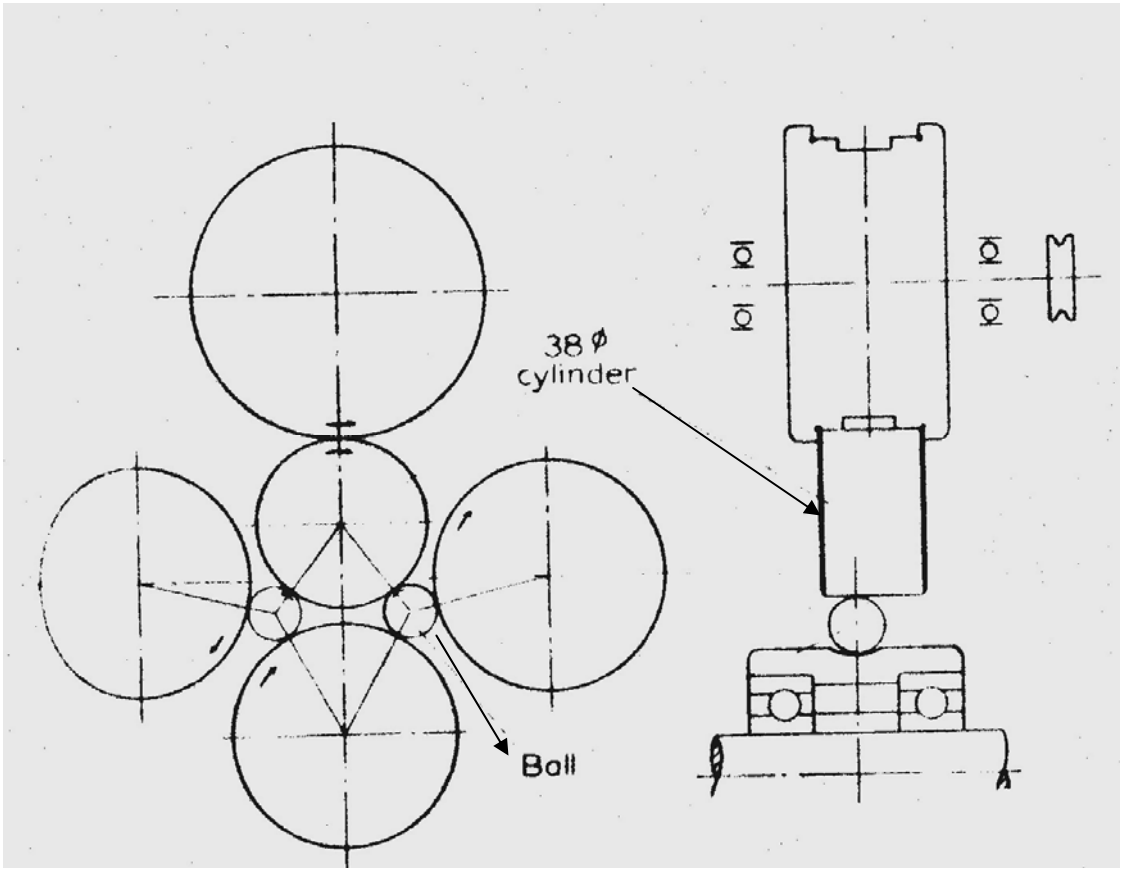


Figure 3.1: Rolling Test Configuration used by Muro and Tsushima Ref: [51]

In this investigation it is proposed that this geometry may be modified as shown in Figure 3.2 to simulate the hybrid bearing of section 2.? successfully.

The upper guide roller (1) and lower guide rollers (2) support a rod specimen (3) and two steel balls (4). The rod specimen is edge driven by the upper guide roller which would be connected to a driving shaft. The rod specimen has two point contacts with the two steel balls which simulate the inner and outer race contact of a real ball bearing as described previously in Figure 3.8.

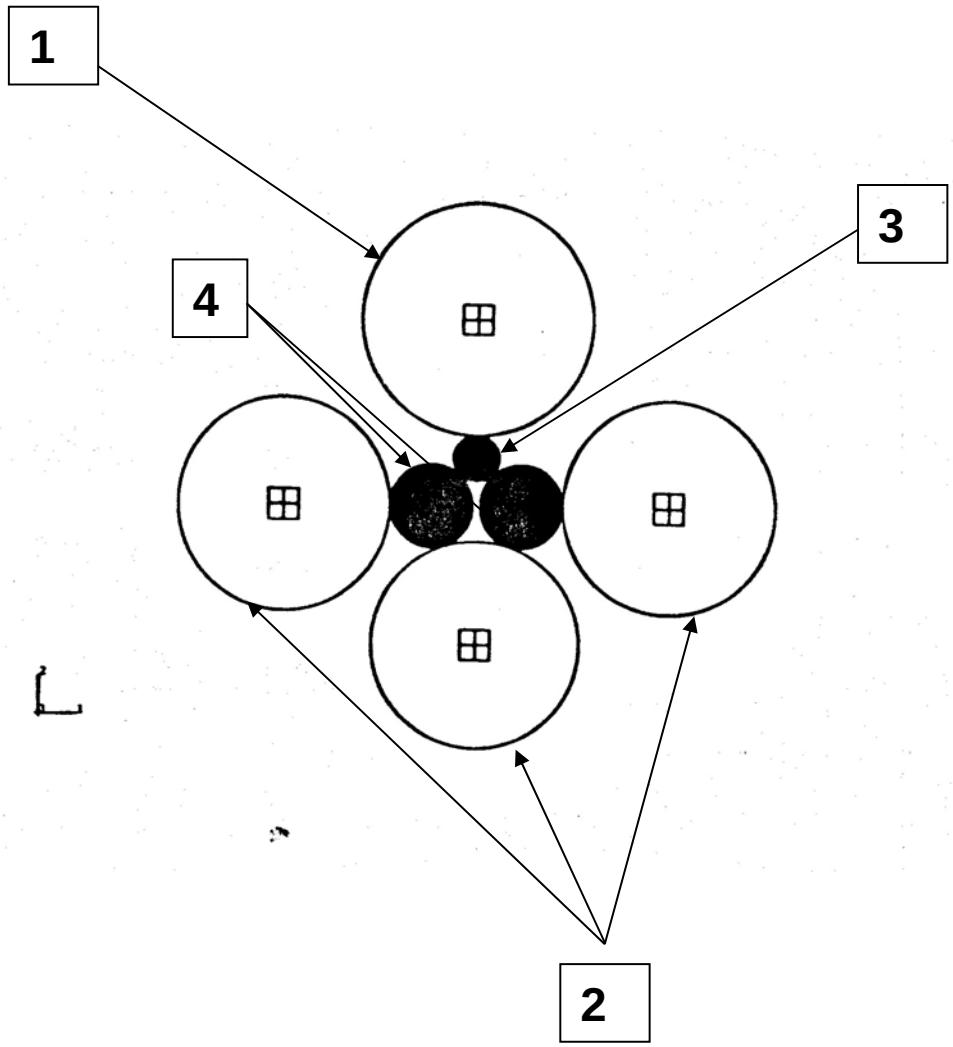


Figure 3.2: Proposed Geometry of the New Test Rig. (1) Upper Drive Roller (Load applied Vertically), (2) Lower Guide Rollers, (3) Ceramic or Steel Rod Specimen, (4) Steel Balls (Simulate Inner and Outer Race).

## 3.2 Design of New Rolling Contact Test

The concept of Figure 3.2 was applied in practice and a test rig built with the configurations shown in Figure 3.3 and 3.4. It was found in practice however that edge driving the test specimen using the upper roller proved difficult. The specimen would either dislodge or suffer from lateral movement.

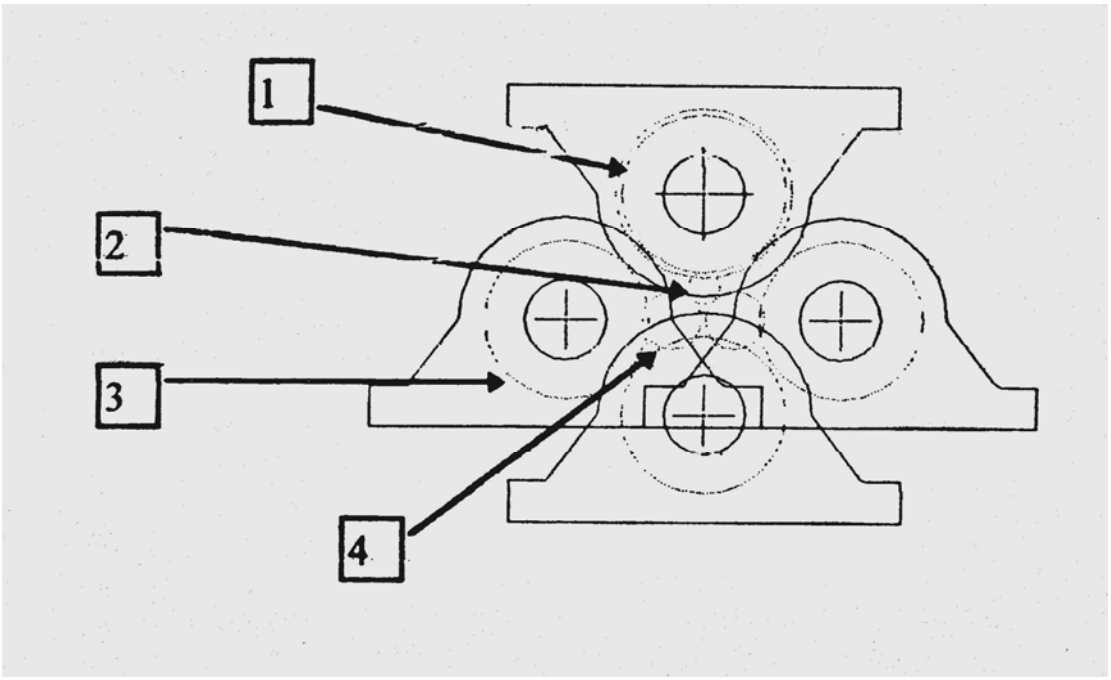


Figure 3.3: Actual Geometry of the New Test Rig. (1) Upper Drive Roller (Load applied Vertically), (2) Ceramic or Steel Rod Specimen, (3) Lower Guide Rollers, (4) Steel Balls (Simulate inner and outer race).

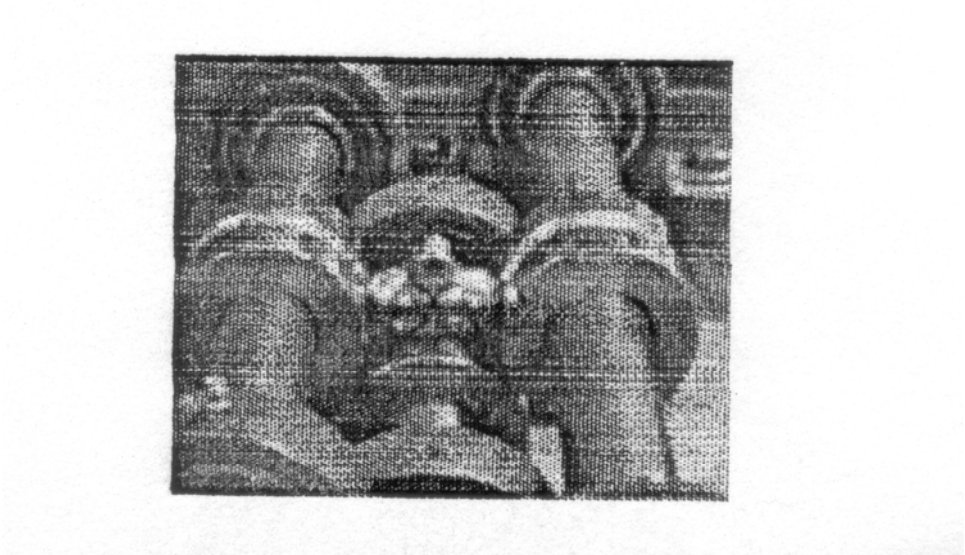

Figure 3.4 Lower Section of the New Test Rig. (Driving Roller not shown)

### 3.2.1 Modification to Test Rig.

The test rig was modified to remove the upper guide roller. A new design for mounting the test specimen was developed. The specimen was loaded into the driving shaft. Four grub screws were used to locate the test specimen in the driving shaft. The shaft is supported by two bearing blocks which are mounted to the top cover of the machine. The top cover is hinged so that it can be lowered into position. Once in position the test specimen contacts the steel balls which are in contact with the lower guide rollers. A schematic view of this is shown in Figures 3.5 and 3.6

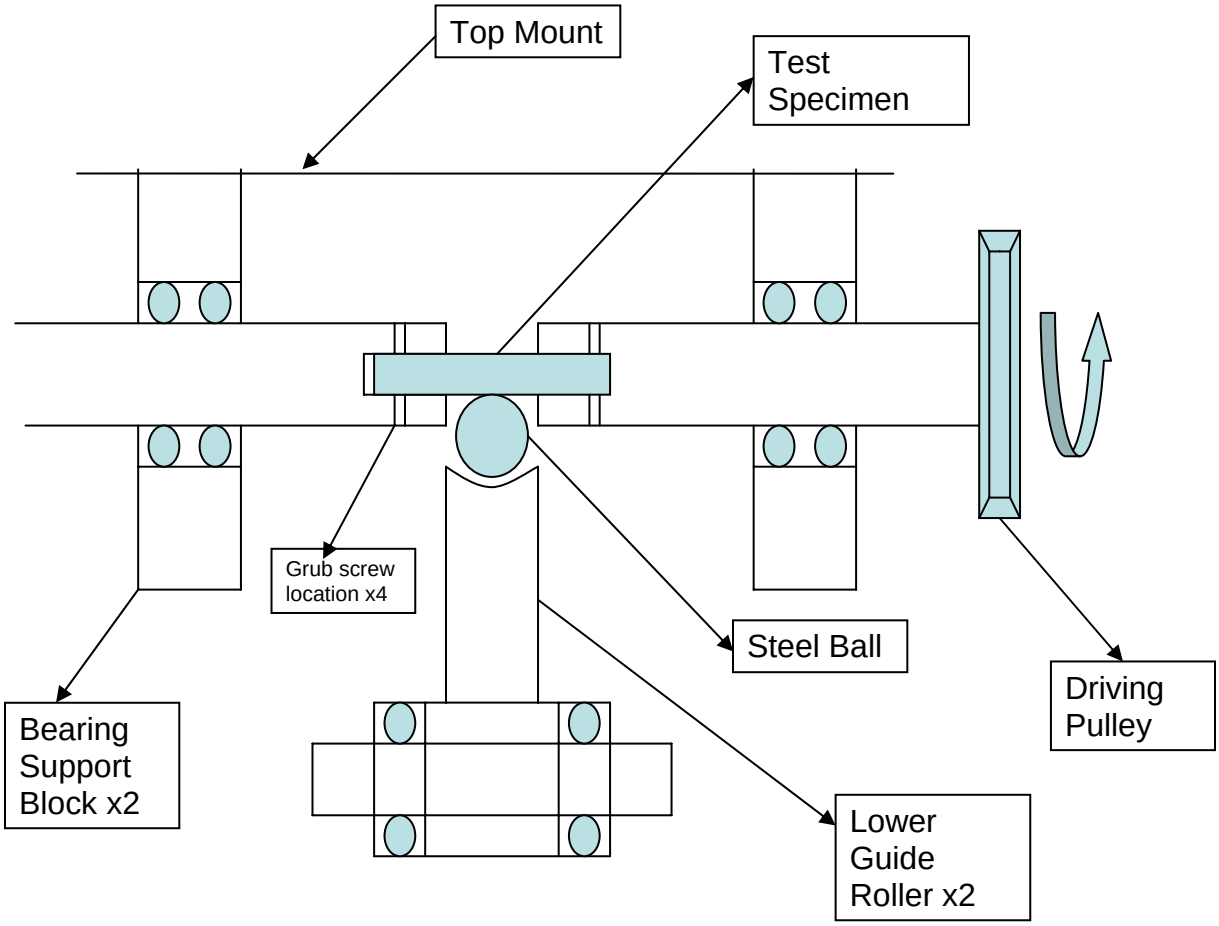


Figure 3.5: Pictorial View of updated Mounting Design of Test Specimen

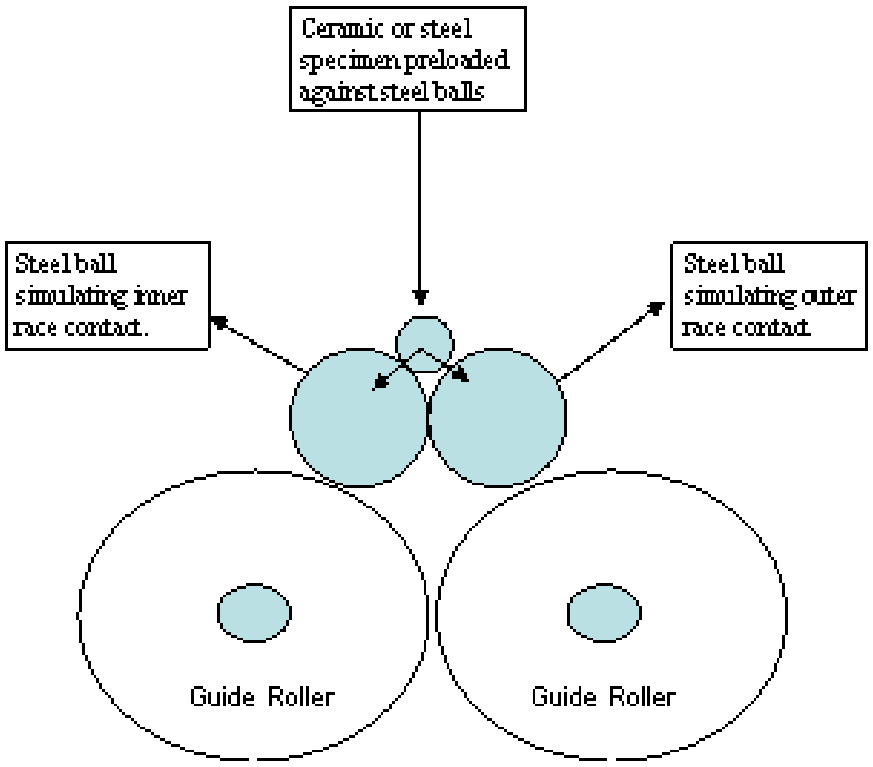


Figure 3.6: Pictorial view of updated Wear Test Rig Geometry

### 3.2.2 The Rolling Contact Wear Test Rig - Summary

To simulate the contact geometry of a bearing a two ball on rod testing machine was designed and built and is shown in Figures 3.7 – 3.9. The two balls simulate the inner and outer race of a ball bearing. The two balls are commercial grade 52100 steel ball bearings which are loaded against either a cylindrical 52100 bearing steel or ceramic specimen. Guide rollers maintain the contact geometry. Load is controlled via a load cell which is pre-calibrated. A data logger is used to record the rpm of the loaded cylinder. The current and revolutions per minute of the motor are recorded also to enable calculation of the friction coefficient if required. Each test was run using the same diameter specimens. Tests were carried out over a period of 12 months in the same laboratory using the same test rig.

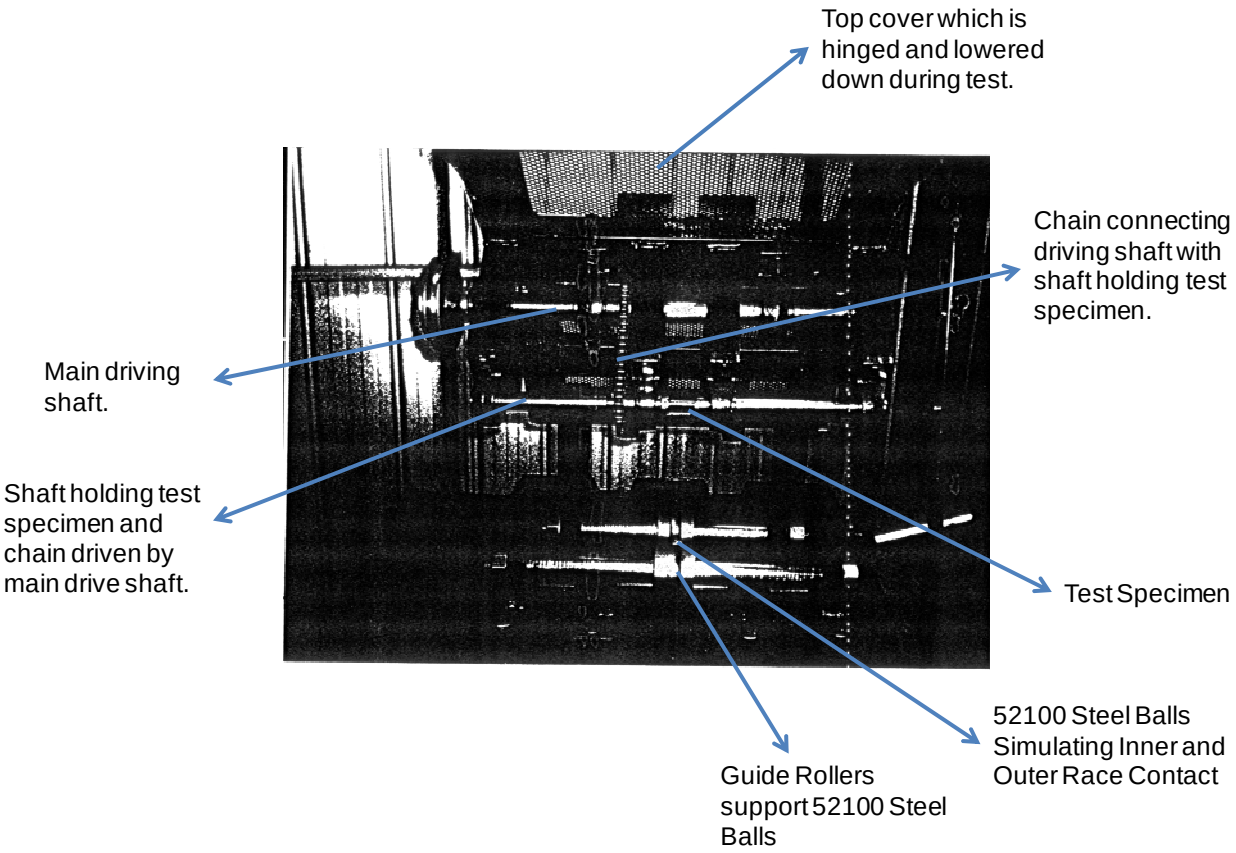


Figure 3.7: New Rolling Contact Test Rig.

This is the test rig used for all wear data produced in this investigation.

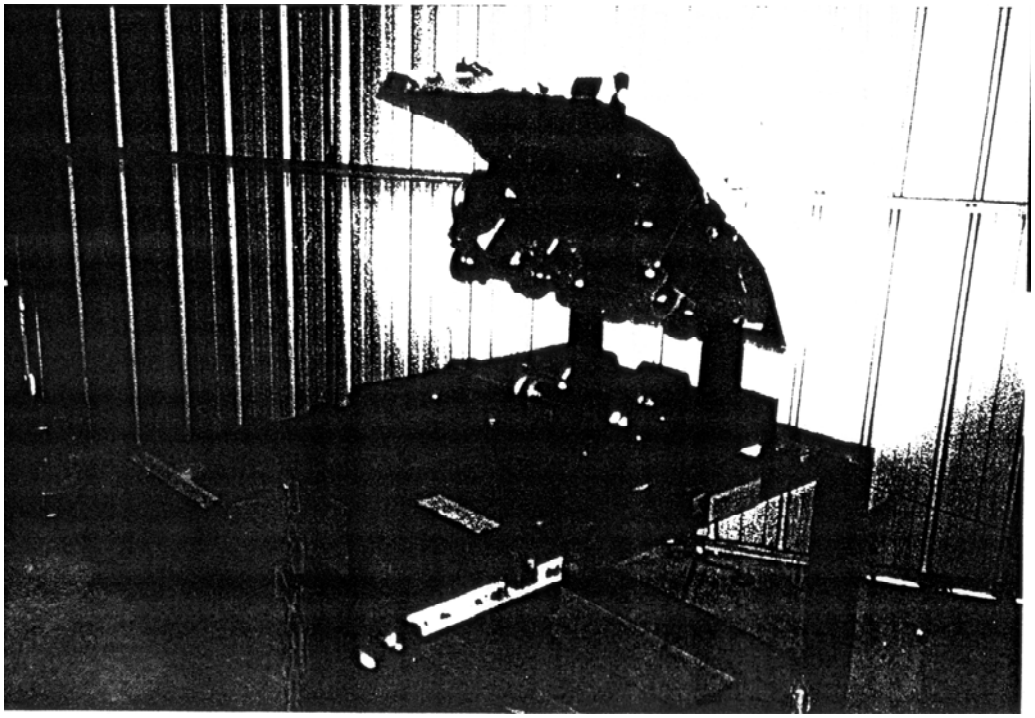

Figure 3.8 Side view of New Test Rig, Cover open ready to load Specimen.

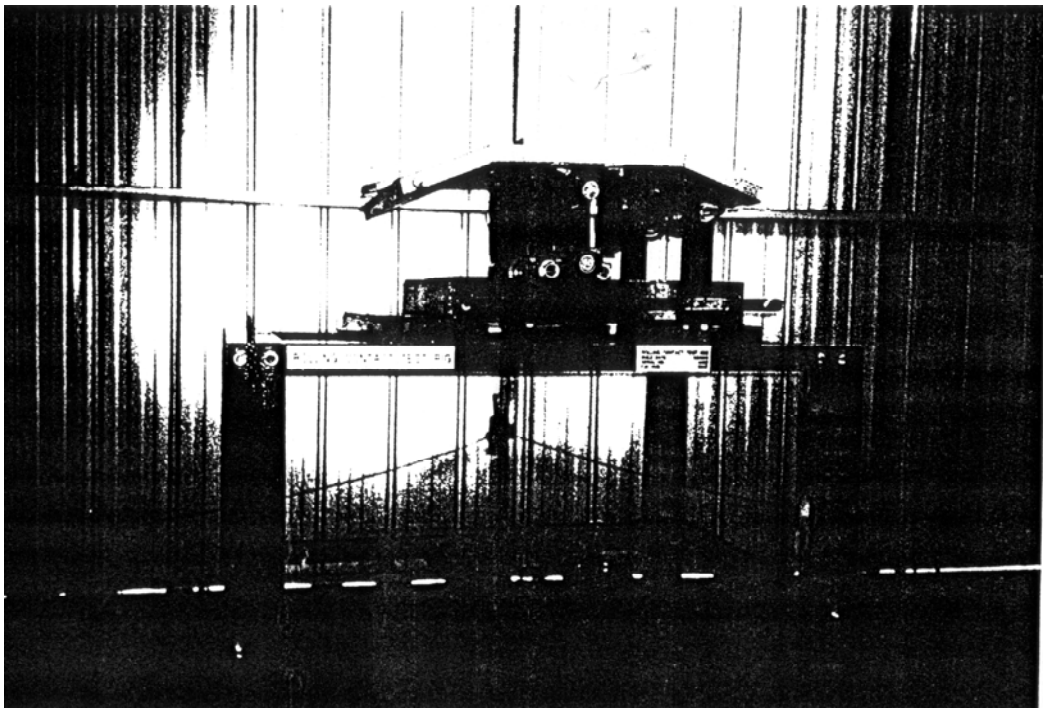

Figure 3.9 Side view of New Test Rig with cover down when tests are running. Load Cell and Locking Down Mechanism not shown.

Figures 3.10 to 3.12 show a second generation test rig that was planned for future testing. The purpose was to enable more tests to be done at one time. This machine was not completed and was not used to produce wear data. The pictures are only presented here to show work that was being conducted and discussion of future work in Section 7.0. A suitable fixture for loading the test specimen would be the next step in working on this test rig but could not be completed by the current author.

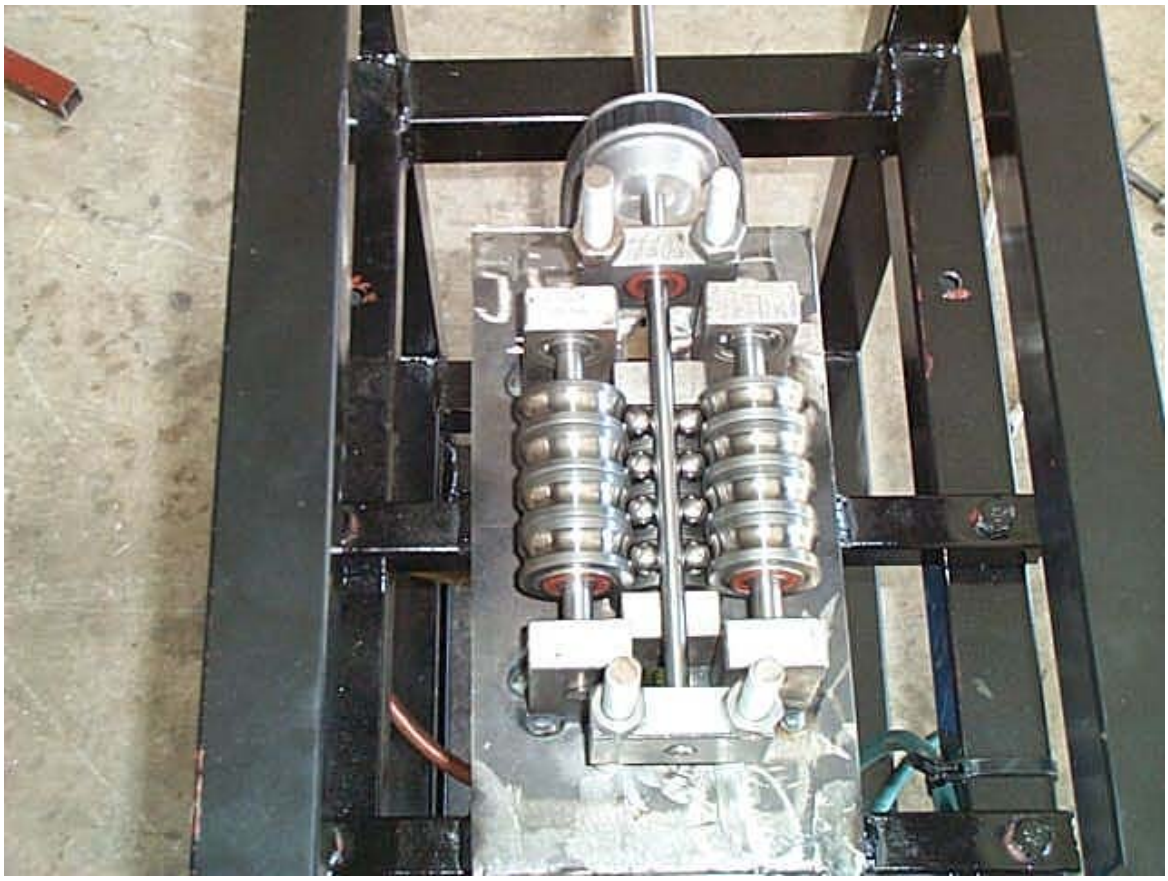

Figure 3.10: Base Section of 2nd Generation Test Rig. Sample loading fixture not designed.

Figure 3.11: 2nd Generation Test Rig Assembly

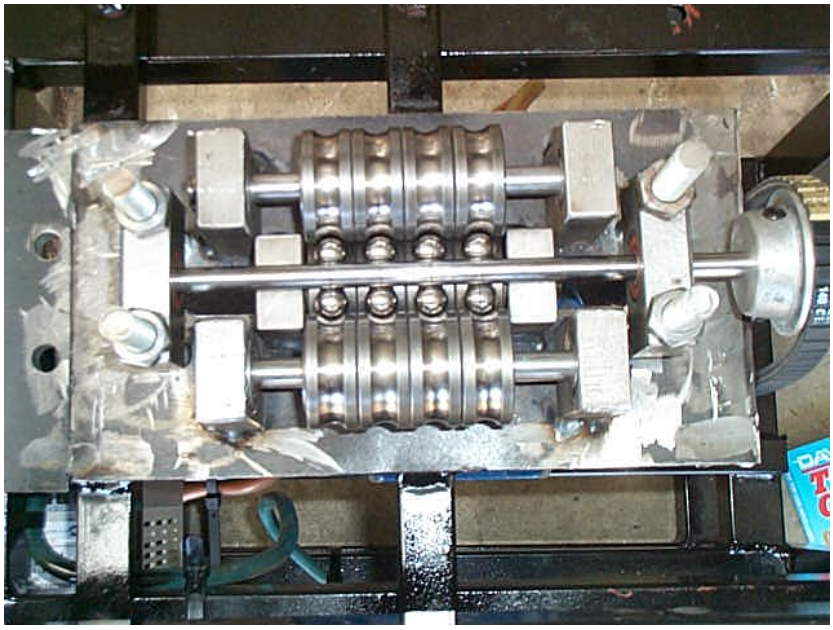

Figure 3.12: View of 2nd Generation Test Rig Proposal Base Plate.

## 3.3 Rolling Contact Wear Tests

### 3.3.1 Test Procedure

Samples were loaded into the test rig as shown in Figures 3.5 and 3.7. The test rig would be pre-loaded using the load cell. The motor speed was set using the motor controller. All tests were run with continuous observation till completion. All data was continuously sent to the data logger with a pre-determined sample rate. The duration of the test was recorded using a stop watch.

### 3.3.2 Analytical Procedure

All samples (balls and specimen) were weighed before and after testing to calculate mass loss. All tests were repeated three times due to the inherent variability in fatigue and wear results. All samples were cleaned in an alcohol solution prior to the test starting. They were then weighed and positioned in the test rig. All tests were conducted under laboratory conditions at ambient temperature about 20 degrees and relative humidity about 65%.

On completion of the tests a Talysurf Profilometer was used to measure the wear groove dimension.

### 3.3.3 Steel Sample Preparation

Commercial grade 52100 bearing steel rod samples of 12mm diameter were used in the initial study of steel to steel contact. Samples were cut to fit the test rig.

### 3.3.4 Partially Stabilized Zirconia Sample Preparation

Samples were made at CSIRO laboratories from base powder. Isostatic pressing method was used to prepare the samples. The process consisted of a flexible elastomeric mould (Figures 3.13 and 3.14) in which the cavity was filled with ceramic powders and sealed tightly.


Figure 3.13: Flexible Elastomeric Mould (Size of mould 150mm length diameter 30mm)


Figure 3.14: Flexible Elastic Mould Assembly (Size of mould 150mm length diameter 30mm)

The moulds were then placed inside a pressure vase as shown in Figures 3.15 and 3.16. The mould was pressed isostatically through the action of a pressurized fluid. The fluid, when pressurized, compressed the mould in all directions generating the compact to green state.


Figure 3.15: Autoclave Pressure Vase


Figure 3.16: Autoclave Open Position

Figure 3.17: Samples out of Autoclave – Ready for Oven.


Figure 3.18:  The samples are then Fired in an Oven.

The samples are then ready for grinding. Grinding requires end caps to be fabricated and glued onto the ends of the test samples as shown in Figures 3.19 to 3.21.

Figure 3.19 End Caps for Grinding Ceramic Rods.

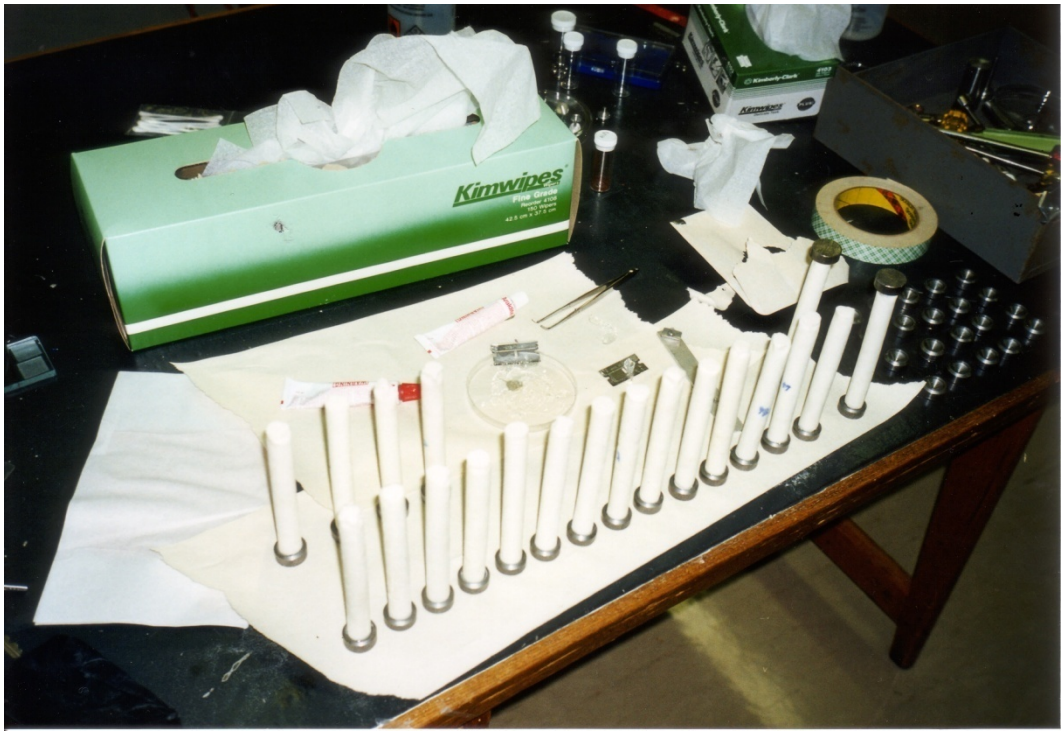


Figure 3.20 End caps being glued to the Ceramic Rods.

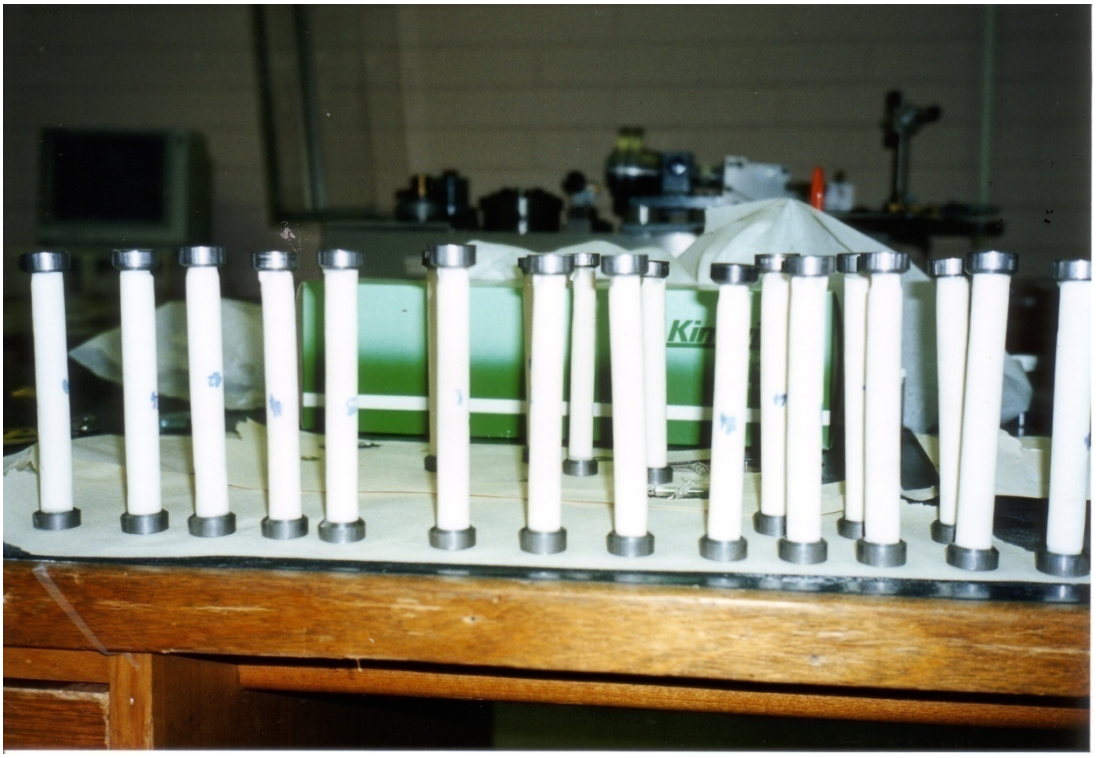

Figure 3.21 Ceramic rods ready for Grinding Process.

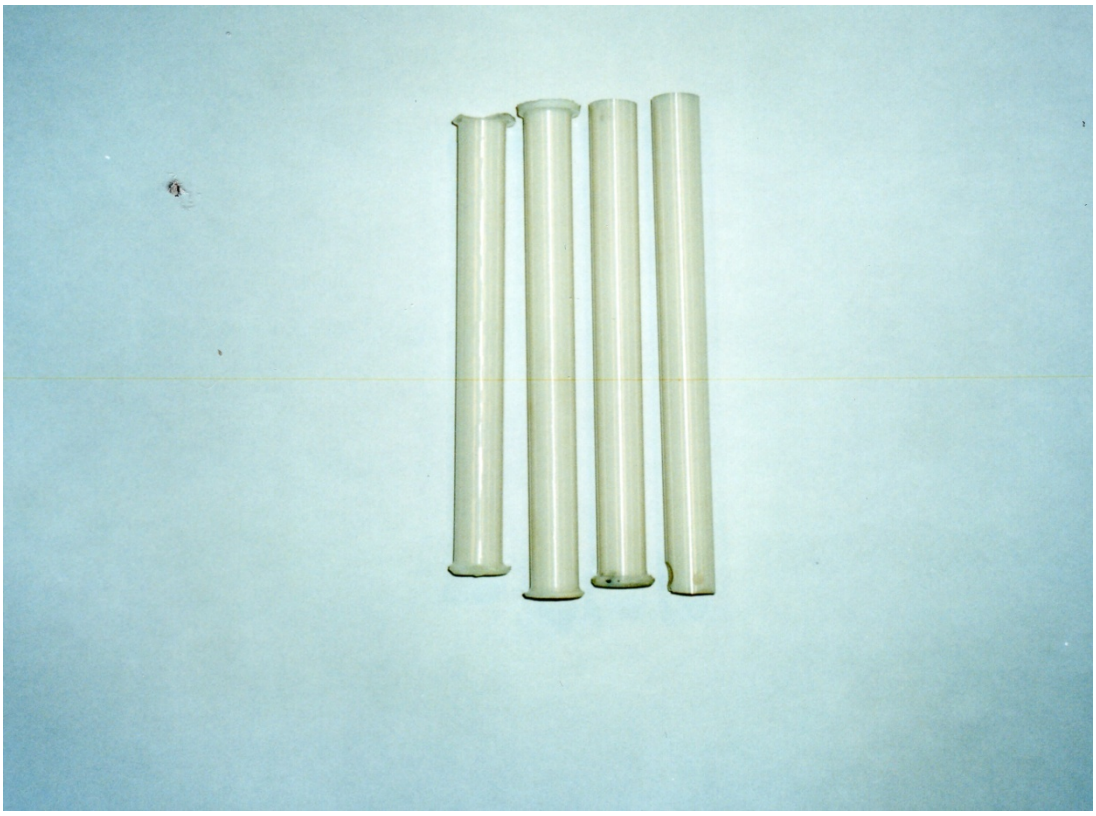

Figure 3.22 Samples Machine Ground to final dimension ready for cutting to final length.

Specimens were cut using cold cutting method. Specimens were cut using a diamond tip circular blade with water as the coolant.

### 3.4 Preparation for Examination – Sub-surface Examination

Specimens were mounted and polished for examination for sub-surface examination. The specimen was mounted using Bakelite thermoplastic. The specimen was placed in a LECO PR-25 mounting press.

The specimen was ground on the 240, 320, 400 and 600 sieve size papers for approximately five minutes. All four papers were lubricated with a stream of water and the specimen was thoroughly washed between each grinding. After the final hand grinding the specimen was washed and air dried before being taken to the polishing wheels. The specimen was polished first on a wheel with 6µm diamond paste and then with 0.5µm diamond paste. The specimen was polished for approximately 15 minutes per wheel. The specimen was washed with water and alcohol and dried with a hair drier after each polishing wheel.

### 3.5 Method of Analysis and Charting Results

A combination of mass loss, profilometer and SEM (Scanning Electron Microscope) measurements are used to charactise the magnitude of the wear profile. Mass loss and wear scar height are plotted for operating variables load and duration. Tests initially start on 52100 bearing steel on 52100 bearing steel and progress to OA-Mg-PSZ (Overaged Partially Stabilised Zirconia) on 52100 bearing steel.

### 3.6 Test Series Description

Below is a description of the test series conducted in this investigation using the new wear test rig.

***Experiment A – Effect of wear on test duration. (Steel sample at 300N load)***

In Experiment A, 52100 steel balls simulating the inner and outer race of a bearing, were loaded against a 12mm diameter 52100 bearing steel rod at 300N. The test rig described in Section 3.2.2 was used for this test.

The purpose of Experiment A was to determine the relationship between wear and test duration at a fixed load and speed. In this test a 300N load was applied to the test sample. Tests were conducted at durations 6.25min, 10min, 15min, 20min, 25min, 30min, 35min, 40min, 45min, 50min, 55min, 60min. Test were repeated 3 times at each duration.

***Experiment B – Effect of wear on load. (Steel sample at 790N load)***

In Experiment B, 52100 steel balls simulating the inner and outer race of a bearing were loaded against a 12mm diameter 52100 bearing steel rod at 790N. The test rig described in Section 3.2.2 was used for this test.

The purpose of Experiment B was to determine the relationship between wear and load at a fixed speed. In this test the load was increased to 790N and applied to the test sample. Tests were conducted at durations 10min, 20min, 30min, 40min, 50min, 60min. Test were repeated 2 times at each duration. Mass Loss (grams) vs. Duration (minutes) at 300N (Experiment A), 790N (experiment B), 450N (Experiment C) are plotted.

***Experiment C – Effect of wear on load and baseline data for project.***
***(Steel sample at 450N load)***

In Experiment C, 52100 steel balls simulating the inner and outer race of a bearing were loaded against a 12mm diameter 52100 bearing steel rod at 450N. The test rig described in Section 3.2.2 was used for this test.

The purpose of Experiment C was to establish baseline data for this investigation. Future experiments that analyze SEM will be checked to ensure data is consistent with that of Experiment C. Experiment C was also conducted at a new load of 450N. This data was used to add data to Experiment B which showed the relationship between wear and load at a fixed speed. Tests were conducted at durations 10min, 15min, 20min, 25min, 30min, 35min, 45min, 50min, 60min. Tests were repeated 3 times at each duration and a fourth time at most durations to establish a good baseline.

***Experiment D – Experiment D was terminated due to an un-calibrated load cell.***

***Experiment E& F – Scanning Electron Micrographs (SEM) Analysis***
***(Steel sample at 450N load)***

In Experiment E, 52100 steel balls simulating the inner and outer race of a bearing were loaded against a 12mm diameter 52100 bearing steel rod at 450N. The test rig described in Section 3.2.2 was used for this test.

The purpose of Experiment E was to conduct SEM investigations of the wear tracks at certain durations. The Micrographs were studied to get an understanding of the wear process with time / increasing cycles. Tests were conducted at durations 1min, 5min, 10min, 15min, 20min, 25min, 30min, 35min, 45min, 50min, 55min 60min. Tests were not repeated as in previous experiments but mass loss and wear depth data were compared to the baseline data established in Experiment C.

***Experiment G – Wear vs. duration and load for Ceramic rod on steel balls.***
***(Ceramic sample at 300N and 750N load)***

In Experiment G, 52100 steel balls simulating the inner and outer race of a bearing were loaded against a 12mm diameter OA-Mg-PSZ ceramic rod at 300N and 790N loads. The test rig described in Section 3.2.2 was used for this test.

The purpose of Experiment G was to establish mass loss and wear depth data for the ceramic rod at various loads. Data was compared to that obtained for steel samples of Experiment A and B. Due to the long duration of the ceramic tests it was not possible to repeat tests several times to confirm error bars thus the data needs to be treated as trends.

# Chapter 4

# Results of the Rolling contact Wear Tests

Rolling wear tests were conducted using the wear test rig detailed in Section 3. Materials under investigation are detailed in Table 4.1. The experiments conducted and their purposes are shown in Table 4.2. Tabulated and graphed data in this section contains mass loss measured in grams (g) and wear depth measured in micro-meters (μm) versus test duration. Scanning Electron Microscope (SEM) figures show the progressive wear of the materials.

Table 4.1 Materials under Investigation

| Material | Elastic Modulus (Gpa) | Density ($g/cm^3$) | Hardness | Fracture Toughness $K_{IC}$ ($Mpa.m^{1/2}$) | Possion Ratio |
|---|---|---|---|---|---|
| 52100 Steel | 207 | 7.8 | 7.85 | 18 to 20 | 0.29 |
| PSZ Ceramic | 205 | 9.1 | 9.1 | 8 to 12 | 0.22 |

Table 4.2 List of Experiments conducted in this Investigation

| | Materials | Purpose | Load | Mass Loss Measurements | Wear Height Measurements (Profilometry Traces) | SEM |
|---|---|---|---|---|---|---|
| **Experiment A** | Metal on Metal | Mass Loss and Wear Depth vs Duration at 300N | 300N | Yes | Yes | Yes |
| **Experiment B** | Metal on Metal | Mass Loss vs Duration at 790N Load. Mass Loss vs Load (300N, 450N, 790N) Plotted | 790N | Yes | Yes | No |
| **Experiment C** | Metal on Metal | Mass Loss and Wear Depth vs Duration at 450N Load. Large sample size data to be used as baseline statistical data at 450N | 450N | Yes | Yes | No |
| **Experiment D** | Metal on Metal | Test Terminated | | | | |
| **Experiment E** | Metal on Metal | To Inspect using SEM the surface wear over time interval of 0-60min at 5 min intervals. Sub-surface SEM Conducted | 450N | Yes | Yes | Yes |
| **Experiment F** | Metal on Metal | To Inspect using detailed SEM at 20-35min range at high magnification. | 450N | Yes | No | Yes |
| **Experiment G** | Metal on Ceramic | To investigate the wear of Metal on Ceramic at 2 loads. Tests durations are 2hrs, 4hrs and 6hrs. SEM Investigations of wear tracks | 300N & 790N | Yes | Yes | Yes |

## 4.1 Experiment A – Effect of Test Duration on Wear of 52100 Steel Samples at 300N load.

In Experiment A, 52100 steel balls simulating the inner and outer race of a bearing, were loaded against a 12mm diameter 52100 bearing steel rod at 300N. The test rig described in Section 3 was used for this test.

The purpose of Experiment A was to determine the relationship between wear and test duration at a fixed load and speed. In this test a 300N load was applied to the test sample. Tests were conducted at durations 6.25min, 10min, 15min, 20min, 25min, 30min, 35min, 40min, 45min, 50min, 55min, 60min. Test were repeated 3 times at each duration. Figure 4.1 shows the wear tracks produced for this experiment.

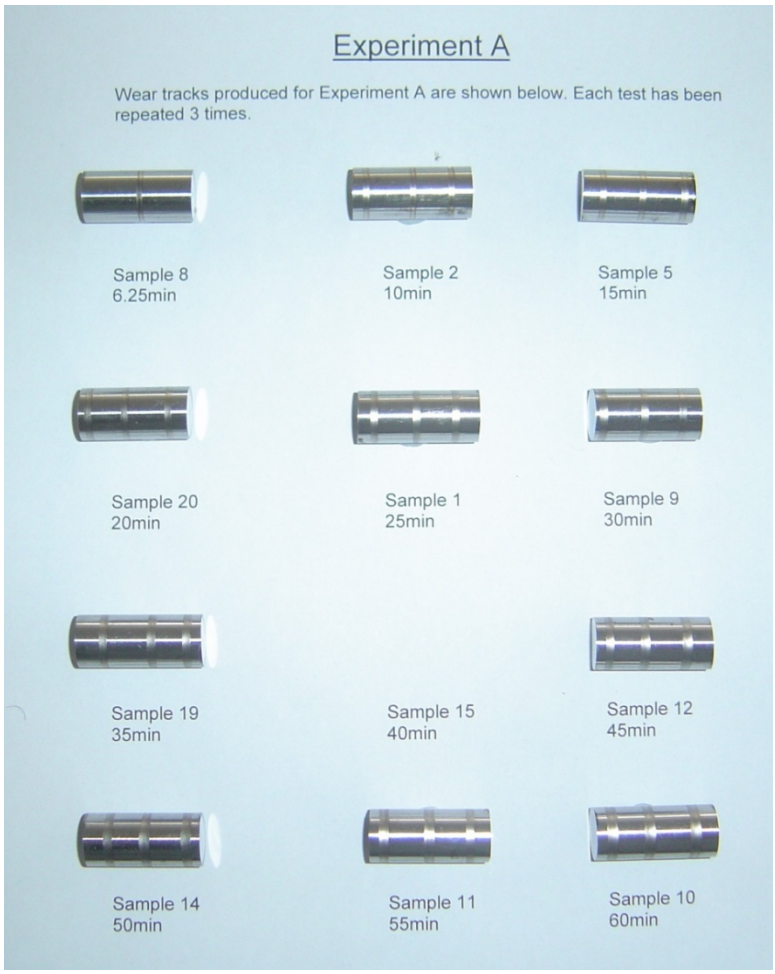


Figure 4.1 Wear tracks on Test Samples for Experiment A

### 4.1.1 Mass Loss – Experiment A

For each test the mass of the sample before and after the test was measured. The mass data for each test is recorded in Tables 4.3 – 4.5 for Experiment A.

| TABLE 4.3 | | | | | | | | | |
|---|---|---|---|---|---|---|---|---|---|
| Test 1 - Experiment A | | | | | | | | | |
| | | | | | | | | | |
| | | | | | BEFORE | | | AFTER | |
| Sample No | Duration (Min) | Speed (Hz) | Load (N) | Mass Specimen | Mass Ball 1 | Mass Ball 2 | Mass Specimen | Mass Ball 1 | Mass Ball 2 |
| 2 | 10 | 7.5/7.2 | 300 | 51.8825 | 66.7909 | 66.7874 | 51.8817 | Not Recorded | Not Recorded |
| 5 | 15 | 7.5/7.2 | 300 | 52.6318 | 66.7883 | 66.7718 | 52.6314 | Not Recorded | Not Recorded |
| 20 | 20 | 7.5/7.2 | 300 | 52.0342 | 66.7883 | 66.7685 | 52.033 | Not Recorded | Not Recorded |
| 1 | 25 | 7.5/7.2 | 300 | 51.0124 | 66.7669 | 66.7882 | 51.0113 | Not Recorded | Not Recorded |
| 9 | 30 | 7.5/7.2 | 300 | 52.1539 | 66.7824 | 66.7709 | 52.1521 | Not Recorded | Not Recorded |
| 19 | 35 | 7.5/7.2 | 300 | 53.1681 | 66.7856 | 66.7856 | 53.1639 | Not Recorded | Not Recorded |
| 15 | 40 | 7.5/7.2 | 300 | 51.9205 | 66.7852 | 66.7836 | 51.9173 | Not Recorded | Not Recorded |
| 12 | 45 | 7.5/7.2 | 300 | 52.3999 | 66.7858 | 66.7873 | 52.3943 | Not Recorded | Not Recorded |
| 14 | 50 | 7.5/7.2 | 300 | 52.1264 | 66.7747 | 66.7836 | 52.1196 | Not Recorded | Not Recorded |
| 11 | 55 | 7.5/7.2 | 300 | 52.7071 | 66.7874 | 66.7846 | 52.6978 | Not Recorded | Not Recorded |
| 10 | 60 | 7.5/7.2 | 300 | 52.224 | 66.7916 | 66.7894 | 52.2142 | Not Recorded | Not Recorded |

TABLE 4.4

Test 2 - Experiment A

| | | | | | BEFORE | | | AFTER | |
|---|---|---|---|---|---|---|---|---|---|
| Sample No | Duration (Min) | Speed (Hz) | Load (N) | Mass Specimen | Mass Ball 1 | Mass Ball 2 | Mass Specimen | Mass Ball 1 | Mass Ball 2 |
| 2 | 10 | 7.5/7.2 | 300 | 51.8817 | 66.7898 | 66.7851 | 51.8817 | 66.7908 | 66.7853 |
| 5 | 15 | 7.5/7.2 | 300 | 52.6309 | 66.7864 | 66.7664 | 52.631 | 66.7672 | 66.7846 |
| 20 | 20 | 7.5/7.2 | 300 | 52.0342 | 66.7815 | 66.7739 | 52.032 | 66.7707 | 66.7817 |
| 1 | 25 | 7.5/7.2 | 300 | 52.0111 | 66.7874 | 66.7749 | 52.0088 | 66.7884 | 66.7709 |
| 9 | 30 | 7.5/7.2 | 300 | 52.152 | 66.7833 | 66.7868 | 52.149 | 66.7822 | 66.7824 |
| 19 | 35 | 7.5/7.2 | 300 | 53.1635 | 66.7824 | 66.7737 | 53.1603 | 66.7776 | 66.7741 |
| 15 | 40 | 7.5/7.2 | 300 | 51.9168 | 66.7928 | 66.7696 | 51.9149 | 66.7871 | 66.7701 |
| 12 | 45 | 7.5/7.2 | 300 | 52.3938 | 66.7729 | 66.7742 | 52.3869 | 66.7688 | 66.765 |
| 14 | 50 | 7.5/7.2 | 300 | 52.1192 | 66.7863 | 66.7853 | 52.1127 | 66.7819 | 66.7725 |
| 11 | 55 | 7.5/7.2 | 300 | 52.6977 | 66.7673 | 66.7842 | 52.6899 | 66.7526 | 66.7798 |
| 10 | 60 | 7.5/7.2 | 300 | 52.2143 | 66.7844 | 66.769 | 52.2046 | 66.778 | 66.7534 |

| Table 4.5 | | | | | | | | | |
|---|---|---|---|---|---|---|---|---|---|
| Test 3 - Experiment A | | | | | | | | | |
| | | | | | BEFORE | | | AFTER | |
| Sample No | Duration (Min) | Speed (Hz) | Load (N) | Mass Specimen | Mass Ball 1 | Mass Ball 2 | Mass Specimen | Mass Ball 1 | Mass Ball 2 |
| 2 | 10 | 7.5/7.2 | 300 | 51.8816 | 66.7871 | 66.7711 | 51.8814 | 66.7719 | 66.7877 |
| 5 | 15 | 7.5/7.2 | 300 | 52.6307 | 66.7882 | 66.7764 | 52.6308 | 66.7763 | 66.789 |
| 20 | 20 | 7.5/7.2 | 300 | 52.0317 | 66.7851 | 66.775 | 52.031 | 66.7754 | 66.7829 |
| 1 | 25 | 7.5/7.2 | 300 | 52.0089 | 66.7742 | 66.7871 | 52.0079 | 66.7866 | 66.7713 |
| 9 | 30 | 7.5/7.2 | 300 | 52.1489 | 66.7731 | 66.7873 | 52.148 | 66.7699 | 66.7885 |
| 19 | 35 | 7.5/7.2 | 300 | 53.1605 | 66.7879 | 66.7863 | 53.1575 | 66.7887 | 66.7821 |
| 15 | 40 | 7.5/7.2 | 300 | 51.915 | 66.785 | 66.7895 | 51.9112 | 66.7783 | 66.7894 |
| 12 | 45 | 7.5/7.2 | 300 | 52.3871 | 66.7872 | 66.7708 | 52.3832 | 66.7717 | 66.7815 |
| 14 | 50 | 7.5/7.2 | 300 | 52.1125 | 66.7663 | 66.7862 | 52.1089 | 66.7808 | 66.7654 |
| 11 | 55 | 7.5/7.2 | 300 | 52.6897 | 66.768 | 66.7841 | 52.687 | 66.7797 | 66.7678 |
| 10 | 60 | 7.5/7.2 | 300 | 52.2043 | 66.7829 | 66.7717 | 52.1948 | 66.7792 | 66.7602 |

Table 4.6 shows the mass loss results for Experiment A.

| Sample | Duration | Test 1 | Test 2 | Test 3 |
|---|---|---|---|---|
| 2 | 10 | 0.0008 | 0 | 0.0002 |
| 5 | 15 | 0.0004 | 0 | 0 |
| 20 | 20 | 0.0012 | 0.0022 | 0.0007 |
| 1 | 25 | 0.0011 | 0.0023 | 0.001 |
| 9 | 30 | 0.0018 | 0.003 | 0.0009 |
| 19 | 35 | 0.0042 | 0.0032 | 0.003 |
| 15 | 40 | 0.0032 | 0.0019 | 0.0038 |
| 12 | 45 | 0.0056 | 0.0069 | 0.0039 |
| 14 | 50 | 0.0068 | 0.0065 | 0.0036 |
| 11 | 55 | 0.0093 | 0.0078 | Test Failed |
| 10 | 60 | 0.0098 | 0.0097 | 0.0095 |

Table 4.6 – Mass Loss of 12mm rod vs. duration for Test 1, 2, 3, Experiment A

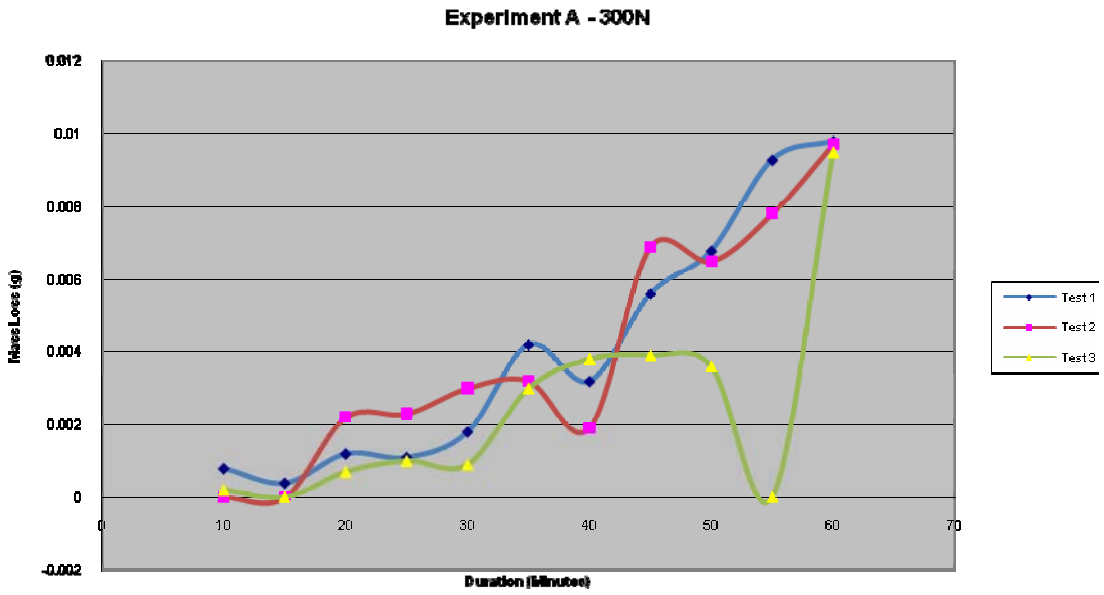


Graph 4.1 Plot of the data in Table 4.6. Mass Loss (grams) vs. Duration (minutes) for Test 1,2,3 Experiment A at 300N load.

The data shows that as duration / no of cycle's increases mass loss increases. It is noted that data point 50 min in Test 3 is outside values of Test 1 and 2 and that 55min Test 3 was interrupted.

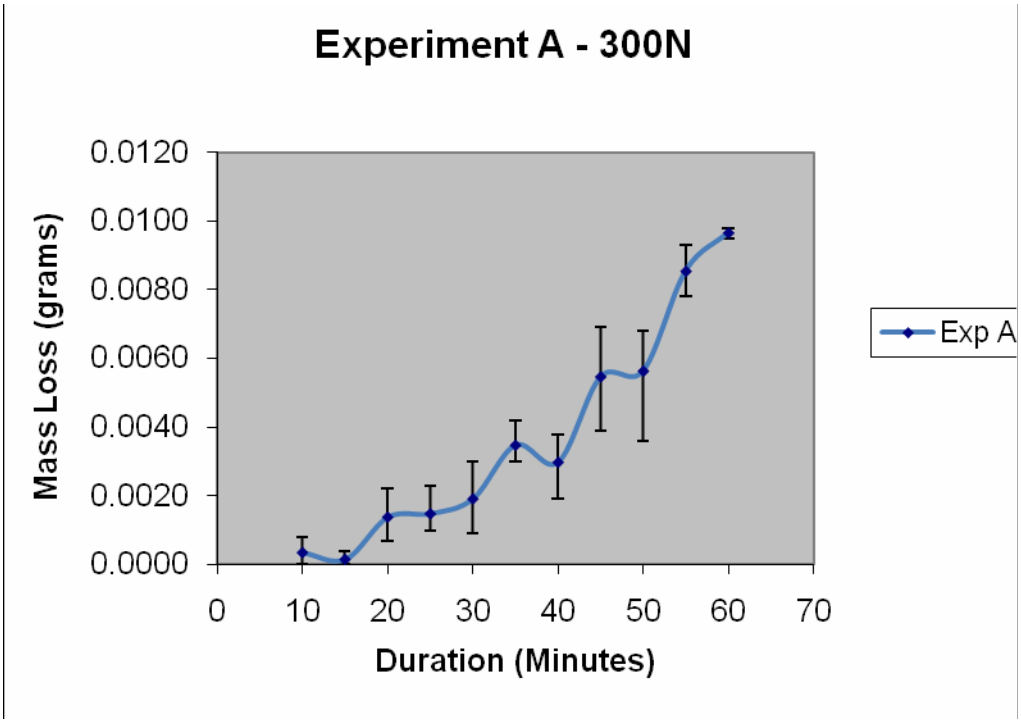


Graph 4.2 Plot of Average Mass Loss (grams) for Test 1–3 vs. Duration (Minutes) with Error Bars.

| Sample | Duration | Average | Error Max | Error Min |
|---|---|---|---|---|
| 2 | 10 | 0.0003 | 0.0005 | 0.0003 |
| 5 | 15 | 0.0001 | 0.0003 | 0.0001 |
| 20 | 20 | 0.0014 | 0.0008 | 0.0007 |
| 1 | 25 | 0.0015 | 0.0008 | 0.0005 |
| 9 | 30 | 0.0019 | 0.0011 | 0.0010 |
| 19 | 35 | 0.0035 | 0.0007 | 0.0005 |
| 15 | 40 | 0.0030 | 0.0008 | 0.0011 |
| 12 | 45 | 0.0055 | 0.0014 | 0.0016 |
| 14 | 50 | 0.0056 | 0.0012 | 0.0020 |
| 11 | 55 | 0.0085 | 0.0008 | 0.0008 |
| 10 | 60 | 0.0097 | 0.0001 | 0.0002 |

Table 4.7 – Average Mass Loss and Error bar Data for Graph 4.2

### 4.1.2 Wear Depth – Experiment A

A profilometer was used to measure the wear depth for the wear tracks produced in Experiment A. The method used is detailed in Section 3. The profilometer traces are shown in Figures 4.2 – 4.11 for each of the tests conducted. Table 4.8 is a summary of the wear depth results. The data is plotted in Graph 4.3.

| Sample | Duration | Test 1 | Test 2 | Test 3 |
|---|---|---|---|---|
| 2 | 10 | Not Recorded | Not Recorded | Not Recorded |
| 5 | 15 | 3.6 | 2.5 | 0.0 |
| 20 | 20 | 5.1 | 5.1 | 5.1 |
| 1 | 25 | 7.1 | 8.6 | 6.1 |
| 9 | 30 | 10.2 | 10.2 | 6.4 |
| 19 | 35 | 11.4 | 14.0 | 10.2 |
| 15 | 40 | 11.4 | 14.0 | 16.5 |
| 12 | 45 | 20.3 | 19.1 | 14.0 |
| 14 | 50 | 19.1 | 17.8 | 14.0 |
| 11 | 55 | 22.9 | 24.1 | Failed Test |
| 10 | 60 | 24.8 | 24.1 | 24.1 |

Table 4.8 – Wear Depth (um) vs. Duration for Tests 1 – 3, Experiment A, 300N

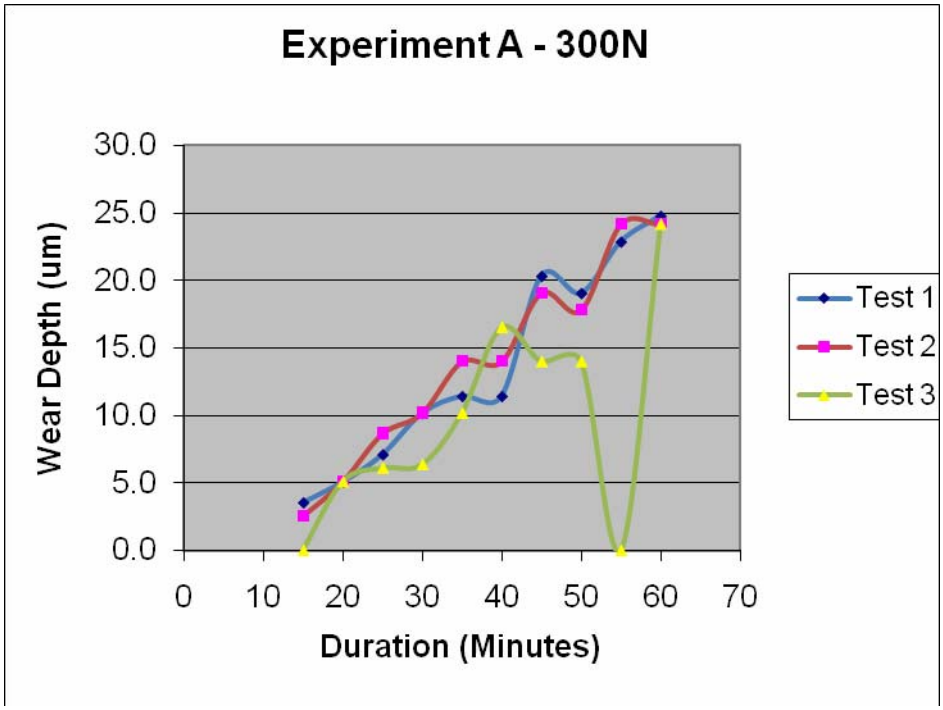

Graph 4.3 Wear depth (µm) vs. Duration for Tests 1 – 3, Experiment A, 300N

Graph 4.3 shows as duration / number cycles increases the wear depth increases. Figures 4.2 to 4.11 show the profilometer traces for Test 1-3 for each duration conducted in Experiment A.

**Experiment A – Profilometer Traces**

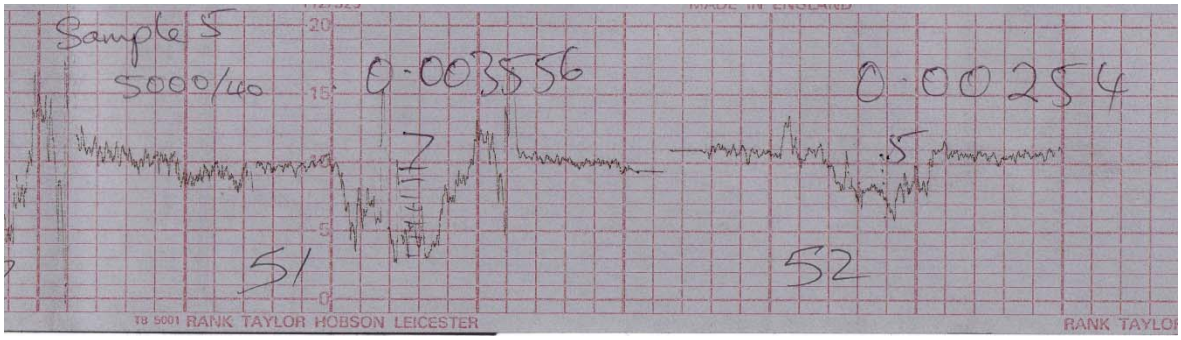


Figure 4.2 - Profilometer Trace Sample 5, 10 minute Duration, Tests 1 & 2

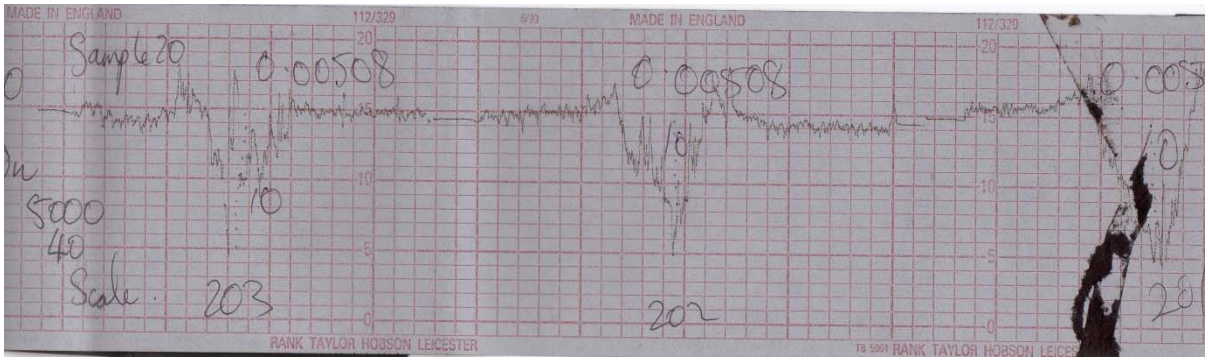


Figure 4.3 - Profilometer Trace Sample 20, 15 minute Duration, Tests 1, 2 & 3


Figure 4.4 - Profilometer Trace Sample 1, 25 minute Duration, Tests 1, 2 & 3

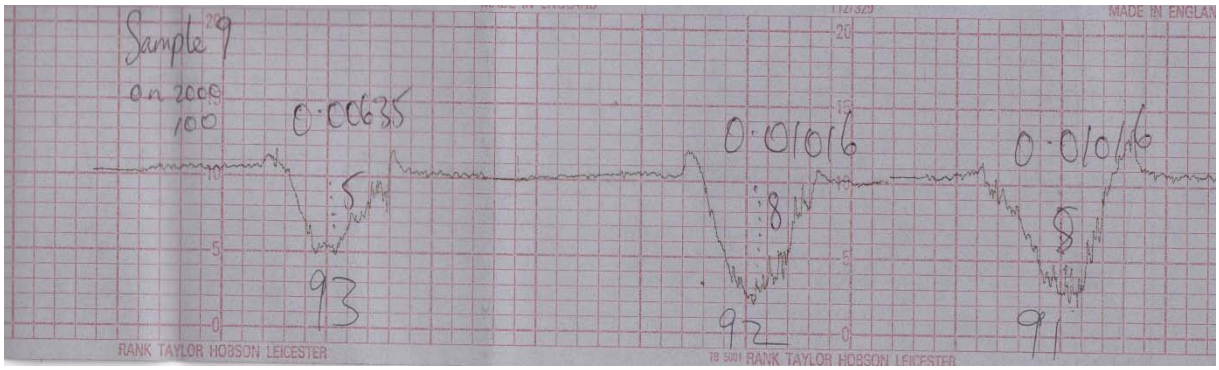


Figure 4.5 - Profilometer Trace Sample 9, 30 minute Duration, Tests 1, 2 & 3

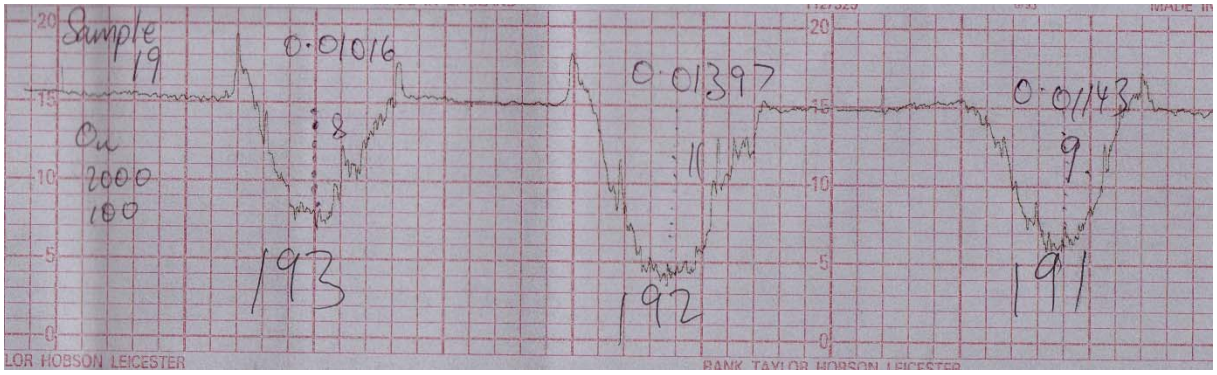


Figure 4.6 - Profilometer Trace Sample 19, 35 minute Duration, Tests 1, 2 & 3

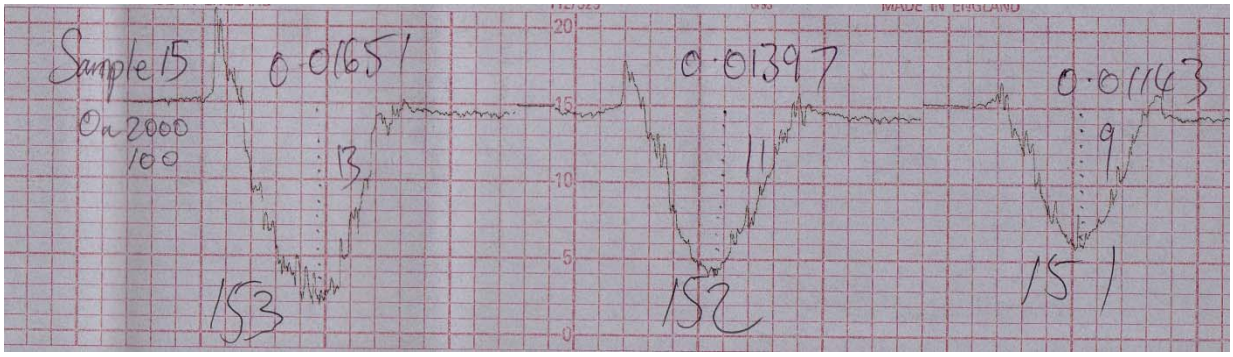


Figure 4.7 - Profilometer Trace Sample 15, 40 minute Duration, Tests 1, 2 & 3

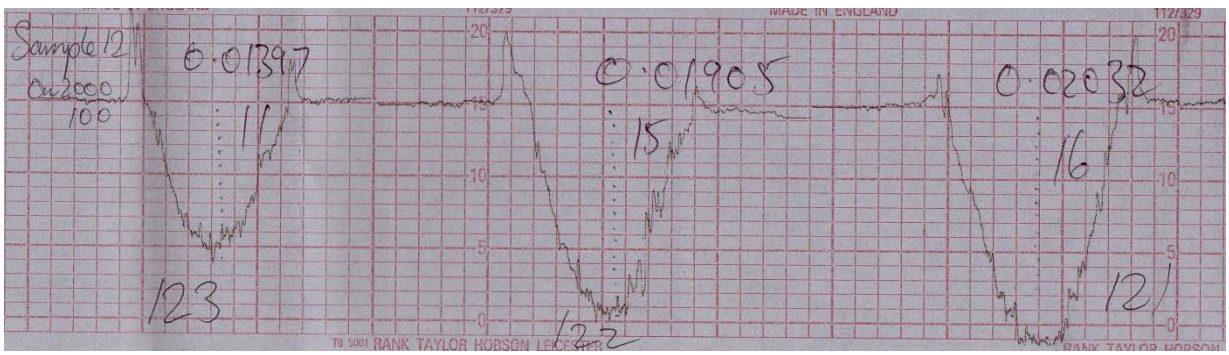

Figure 4.8 - Profilometer Trace Sample 12, 45 minute Duration, Tests 1, 2 & 3

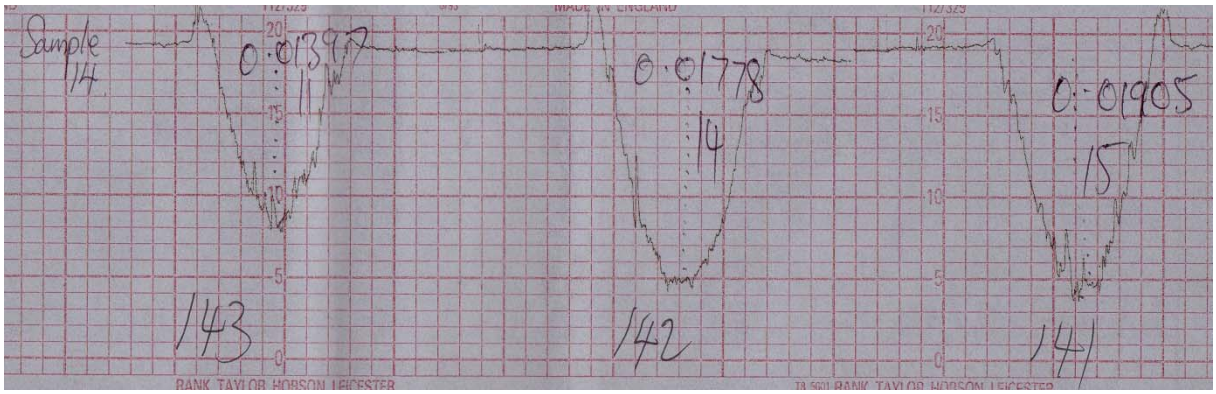


Figure 4.9 - Profilometer Trace Sample 14, 50 minute Duration, Tests 1, 2 & 3

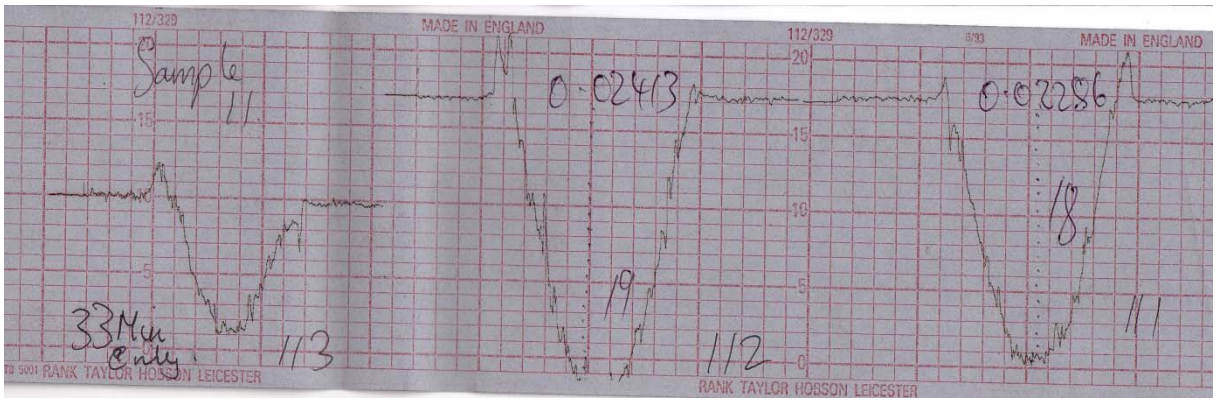


Figure 4.10 - Profilometer Trace Sample 11, 55 minute Duration, Tests 1, 2 & 3

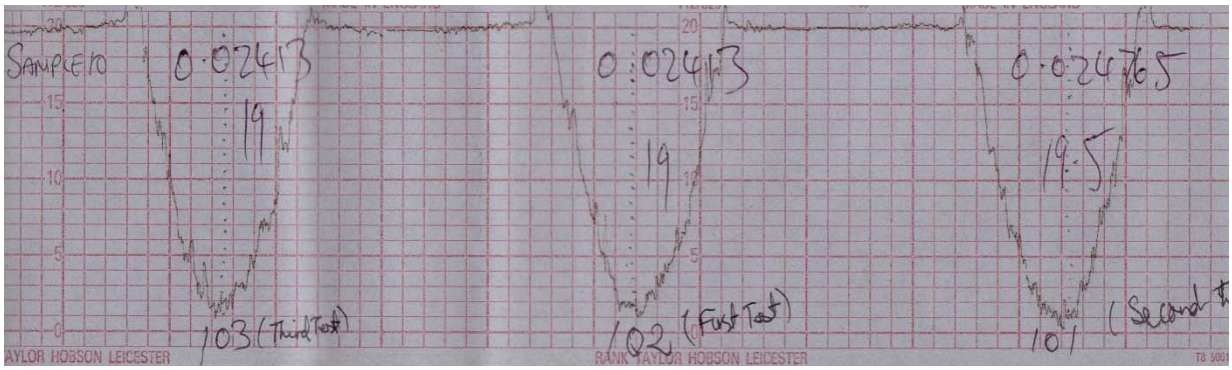


Figure 4.11 - Profilometer Trace Sample 10, 60 minute Duration, Tests 1, 2 & 3

## 4.2 Experiment B – Effect of load on Wear (Steel Sample at 790N Load)

In Experiment B, 52100 steel balls simulating the inner and outer race of a bearing were loaded against a 12mm diameter 52100 bearing steel rod at 790N. The test rig described in Section 3 was used for this test.

The purpose of Experiment B was to determine the relationship between wear and load at a fixed speed. In this test the load was increased to 790N and applied to the test sample. Tests were conducted at durations 10min, 20min, 30min, 40min, 50min, 60min. Test were repeated 2 times at each duration. Mass Loss (grams) vs. Duration (minutes) at 300N (Experiment A), 790N (experiment B), 450N (Experiment C) are plotted in Graph 4.4. Figure 4.1 shows the wear tracks produced for this experiment.

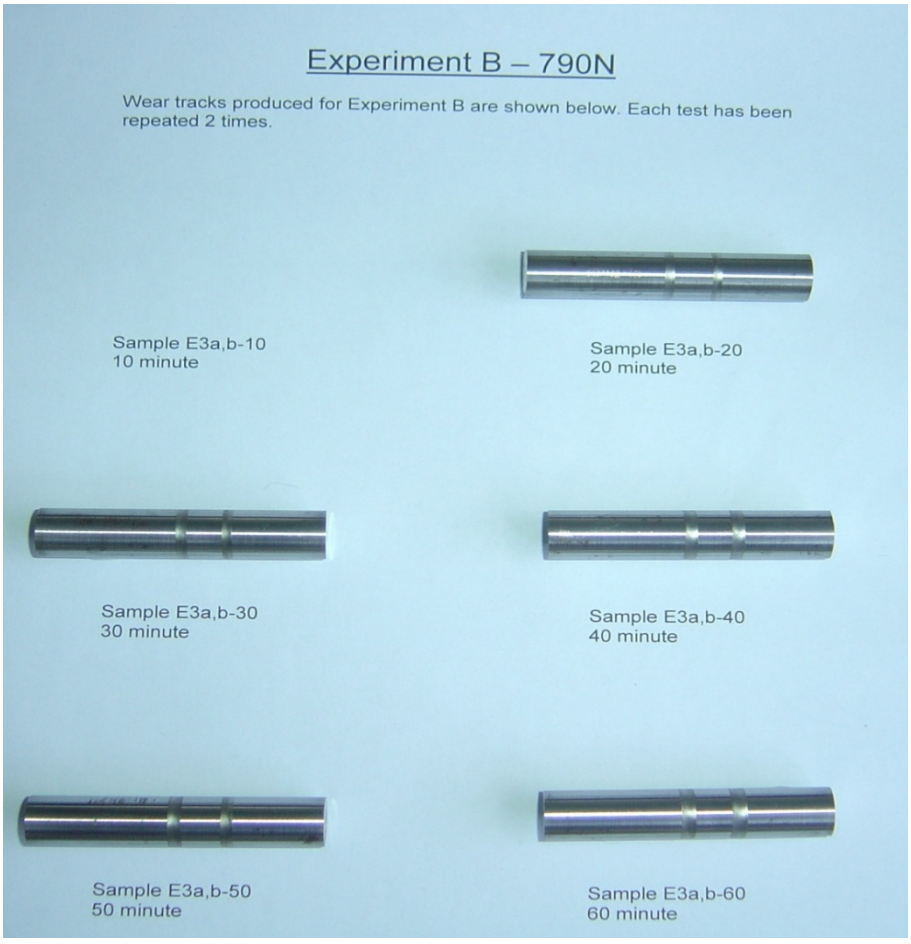


Figure 4.12 Wear Tracks on test samples for Experiment B

### 4.2.1 Mass Loss – Experiment B

For each test the mass of the sample before and after the test was measured. The mass data for each test is recorded in Tables 4.10 – 4.11 for Experiment B.

| Experiment B - Results 790N | | | | | |
|---|---|---|---|---|---|
| Test 1 | | | | Before Test | After Test |
| Sample No | Duration (min) | Speed (Hz) | Load (N) | Mass Rod (g) | Mass Rod (g) |
| E3a-10 | 10 | 7.5/7.2 | 790 | Not Tested | Not Tested |
| E3a-20 | 20 | 7.5/7.2 | 790 | 52.9143 | 52.9106 |
| E3a-30 | 30 | 7.5/7.2 | 790 | 51.8832 | 51.8765 |
| E3a-40 | 40 | 7.5/7.2 | 790 | 51.477 | 51.4618 |
| E3a-50 | 50 | 7.5/7.2 | 790 | 52.4117 | 52.3957 |
| E3a-60 | 60 | 7.5/7.2 | 790 | 51.6327 | 51.6064 |
| E3a-120 | 120 | 7.5/7.2 | 790 | 53.0292 | 52.9447 |

Table 4.10 – Mass Loss Data for Experiment B, Test 1, 790N Load

| Test 2 | | | | Before Test | After Test |
|---|---|---|---|---|---|
| Sample No | Duration (min) | Speed (Hz) | Load (N) | Mass Rod (g) | Mass Rod (g) |
| E3b-10 | 10 | 7.5/7.2 | 790 | Not Tested | Not Tested |
| E3b-20 | 20 | 7.5/7.2 | 790 | 52.9106 | 52.9065 |
| E3b-30 | 30 | 7.5/7.2 | 790 | 51.8765 | 51.8696 |
| E3b-40 | 40 | 7.5/7.2 | 790 | 51.4618 | 51.4448 |
| E3b-50 | 50 | 7.5/7.2 | 790 | 52.3957 | 52.3839 |
| E3b-60 | 60 | 7.5/7.2 | 790 | 51.6064 | 51.5759 |
| E3b-120 | 120 | 7.5/7.2 | 790 | Not Tested | Not Tested |

Table 4.11 – Mass Loss Data for Experiment B, Test 2, 790N Load

Table 4.12 shows the Mass Loss results for Experiment B.

| | Test 3a | Test 3b | |
|---|---|---|---|
| Duration (min) | Mass Loss (g) | Mass Loss (g) | Average |
| 20 | 0.0037 | 0.0041 | 0.0039 |
| 30 | 0.0067 | 0.0069 | 0.0068 |
| 40 | 0.0152 | 0.017 | 0.0161 |
| 50 | 0.016 | 0.0118 | 0.0139 |
| 60 | 0.0263 | 0.0305 | 0.0284 |
| 120 | 0.0845 | Not tested | 0.0845 |

Table 4.12: Mass Loss data for Experiment B, 790N

Graph 4.4 shows the Mass Loss (grams) vs. Duration (Minutes) at 300N, 450N & 790N. The 300N data is from Experiment A, 790N data from Experiment B and 450N data from Experiment C (discussed in next section but shown here). Graph 4.4 shows that as the load is increased the wear rate is increased. Note data point 50min in Test 2 was significantly lower than the trend data.

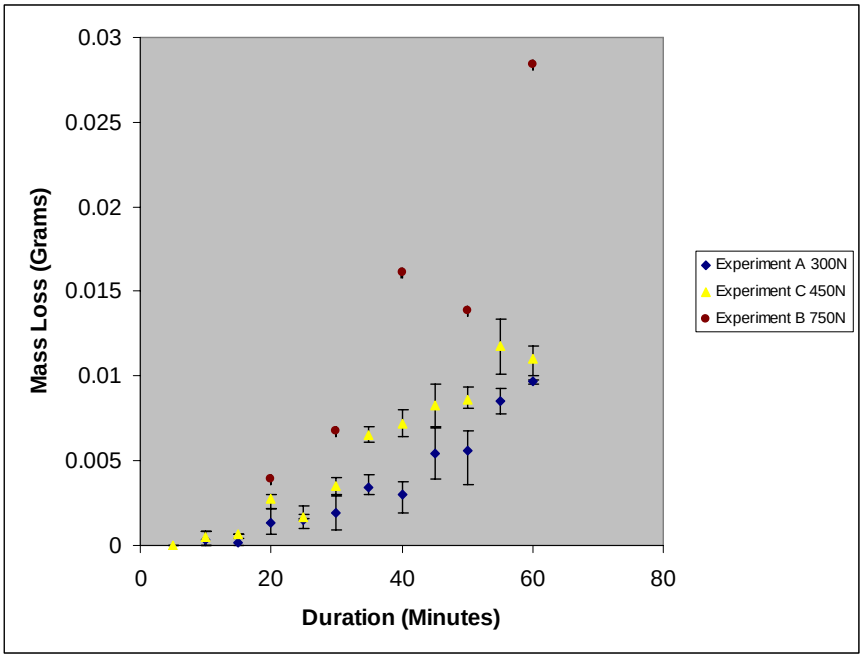

Graph 4.4 - Mass Loss (grams) vs. Duration (Minutes) at 300N, 450N & 790N.

### 4.2.2 Wear Volume Shape Profilometer Results – Experiment B.

For Experiment B, the load was increased to 790N. It was observed that the mass loss increase significantly to 0.0284g at 60min vs. 0.0097g for 300N at 60min duration. Figure 4.11a shows the profilometer trace of the 790N sample vs. the 300N sample as previously shown in Figure 4.11. The width of the groove is significantly larger in the 790N load sample vs. 300N load sample, however the maximum wear depth height is larger in the 300N load sample.


Figure 4.11a – Profilometer trace of Sample 3a and 3b, 790N load, 60min Duration

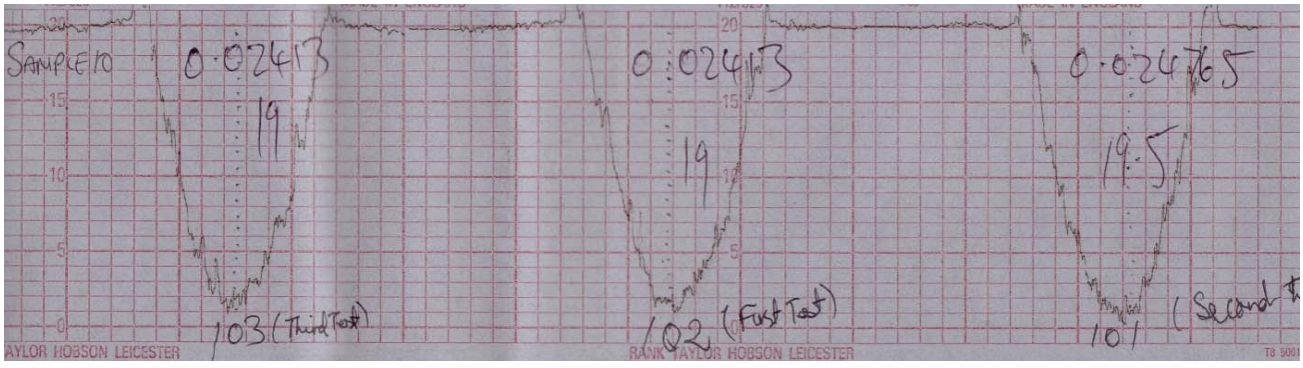


Figure 4.11 (previously shown) - Profilometer Trace Sample 10, 60 minute Duration, Tests 1, 2 & 3 at 300N load

## 4.3 Experiment C – Effect of Load on Wear and Baseline Data for Project.

## (Steel Sample at 450N Load)

In Experiment C, 52100 steel balls simulating the inner and outer race of a bearing were loaded against a 12mm diameter 52100 bearing steel rod at 450N. The test rig described in Section 3 was used for this test.

The purpose of Experiment C was to establish baseline data for this investigation. Future experiments that analyze SEM will be checked to ensure data is consistent with that of Experiment C. Experiment C was also conducted at a new load of 450N. This data was used to add data to Experiment B which showed the relationship between wear and load at a fixed speed. Tests were conducted at durations 10min, 15min, 20min, 25min, 30min, 35min, 45min, 50min, 60min. Tests were repeated 3 times at each duration and a fourth time at most durations to establish a good baseline. Figures 4.13 - 4.14 shows the wear tracks produced for this experiment.


Figure 4.13 Wear Tracks on test samples for Experiment C (10 – 35 minutes)

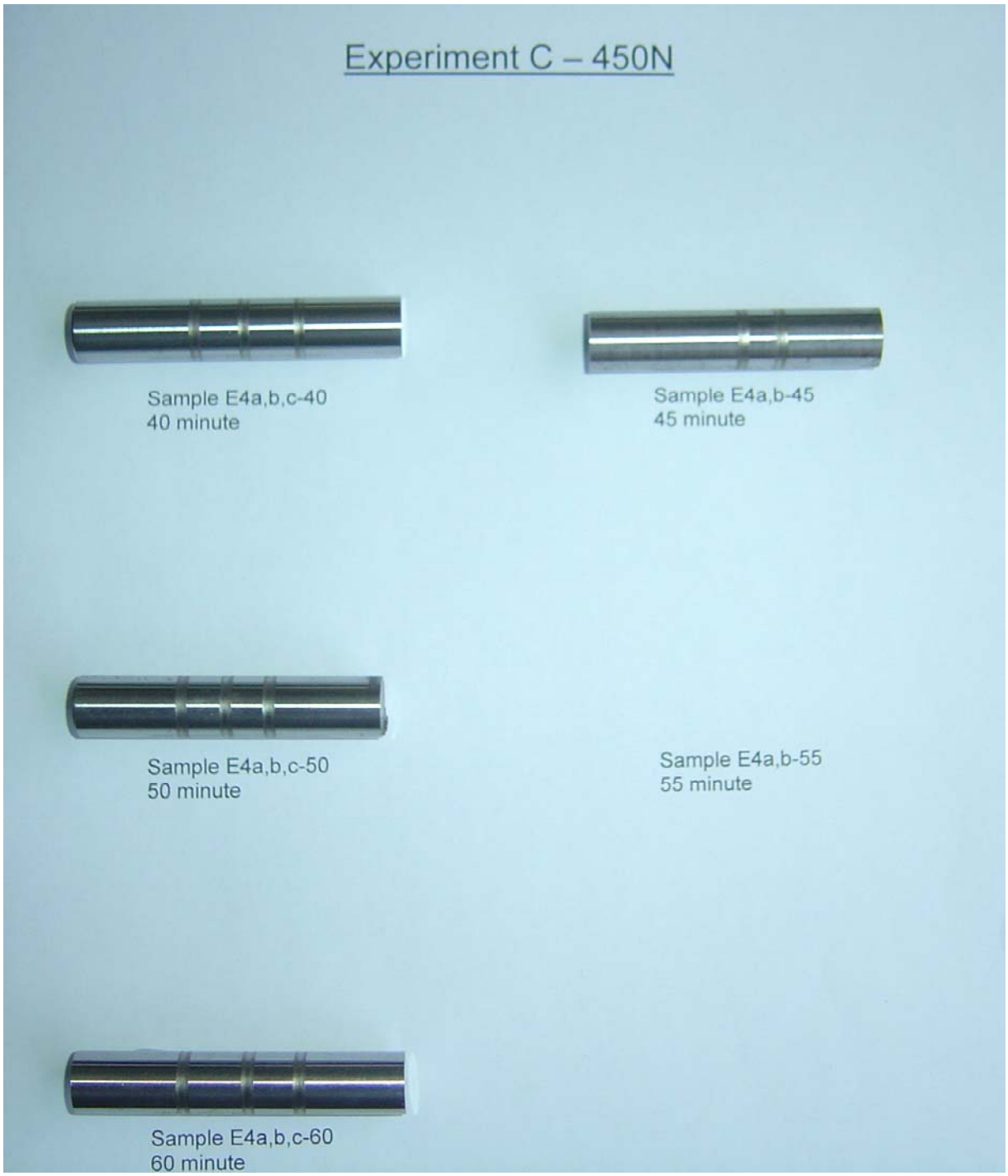


Figure 4.14 Wear Tracks on test samples for Experiment C (40 – 60 minutes). Some samples are not shown as they have been sectioned for Subsurface Analysis. They are shown in later sections.

### 4.3.1 Mass Loss – Experiment C

For each test the mass of the sample before and after the test was measured. The mass data for each test is recorded in Tables 4.13 – 4.15 for Experiment C. Table 4.16 summarises the mass loss data for Experiment C and is graphed in Graph 4.6.

| Test 1 | | | | BEFORE | AFTER |
|---|---|---|---|---|---|
| Sample No | Duration | Speed | Load | Mass Specimen | Mass Specimen |
| E4a-5 | 5 | 7.5/7.2 | Cover | 51.6183 | 51.6187 |
| E4a-10 | 10 | 7.5/7.2 | Cover | 54.9578 | 54.957 |
| E4a-15 | 15 | 7.5/7.2 | Cover | 52.7873 | Not Tested |
| E4a-20 | 20 | 7.5/7.2 | Cover | 55.494 | 55.4918 |
| E4a-25 | 25 | 7.5/7.2 | Cover | 55.431 | 55.4294 |
| E4a-30 | 30 | 7.5/7.2 | Cover | 56.1292 | 56.1256 |
| E4a-35 | 35 | 7.5/7.2 | Cover | 59.0769 | 59.0708 |
| E4a-40 | 40 | 7.5/7.2 | Cover | 56.3429 | 56.3357 |
| E4a-45 | 45 | 7.5/7.2 | Cover | 51.0512 | 51.0442 |
| E4a-50 | 50 | 7.5/7.2 | Cover | 52.1246 | 52.1164 |
| E4a-55 | 55 | 7.5/7.2 | Cover | 52.2126 | 52.2025 |
| E4a-60 | 60 | 7.5/7.2 | Cover | 56.0017 | 55.9899 |

Table 4.13 – Mass Data for Experiment C, Test 1, 450N Load

| Test 2 | | | | BEFORE | AFTER |
|---|---|---|---|---|---|
| Sample No | Duration | Speed | Load | Mass Specimen | Mass Specimen |
| E4b-5 | 5 | 7.5/7.2 | Cover | Not Tested | Not Tested |
| E4b-10 | 10 | 7.5/7.2 | Cover | 54.957 | 54.9571 |
| E4b-15 | 15 | 7.5/7.2 | Cover | 52.7868 | 52.7861 |
| E4b-20 | 20 | 7.5/7.2 | Cover | 55.4918 | 55.4888 |
| E4b-25 | 25 | 7.5/7.2 | Cover | 55.4294 | 55.4276 |
| E4b-30 | 30 | 7.5/7.2 | Cover | 56.1256 | 56.1227 |
| E4b-35 | 35 | 7.5/7.2 | Cover | 59.0708 | 59.0638 |
| E4b-40 | 40 | 7.5/7.2 | Cover | 56.3357 | 56.3277 |
| E4b-45 | 45 | 7.5/7.2 | Cover | 51.0442 | 51.0347 |
| E4b-50 | 50 | 7.5/7.2 | Cover | 52.1164 | 52.107 |
| E4b-55 | 55 | 7.5/7.2 | Cover | 52.2025 | 52.1891 |
| E4b-60 | 60 | 7.5/7.2 | Cover | 55.9899 | 55.9799 |

Table 4.14 – Mass Data for Experiment C, Test 2, 450N Load

| Test 3 | | | | BEFORE | AFTER |
|---|---|---|---|---|---|
| Sample No | Duration | Speed | Load | Mass Specimen | Mass Specimen |
| E4c-10 | 10 | 7.5/7.2 | Cover | 54.9572 | 54.9565 |
| E4c-20 | 20 | 7.5/7.2 | Cover | 55.489 | 55.486 |
| E4c-30 | 30 | 7.5/7.2 | Cover | 56.1228 | 56.1188 |
| E4c-40 | 40 | 7.5/7.2 | Cover | 56.3278 | 56.3214 |
| E4c-50 | 50 | 7.5/7.2 | Cover | 52.107 | 52.0989 |
| E4c-60 | 60 | 7.5/7.2 | Cover | 55.9802 | 55.9689 |

Table 4.15 – Mass Data for Experiment C, Test 3, 450N Load

| Duration | Test 1 | Test 2 | Test 3 |
|---|---|---|---|
| | Mass Loss (grams) | Mass Loss (grams) | Mass Loss (grams) |
| 5 | 0 | Not tested | Not tested |
| 10 | 0.0008 | 0 | 0.0007 |
| 15 | Not tested | 0.0007 | Not tested |
| 20 | 0.0022 | 0.003 | 0.003 |
| 25 | 0.0016 | 0.0018 | Not tested |
| 30 | 0.0036 | 0.0029 | 0.004 |
| 35 | 0.0061 | 0.007 | Not tested |
| 40 | 0.0072 | 0.008 | 0.0064 |
| 45 | 0.007 | 0.0095 | Not tested |
| 50 | 0.0082 | 0.0094 | 0.0081 |
| 55 | 0.0101 | 0.0134 | Not tested |
| 60 | 0.0118 | 0.01 | 0.0113 |

Table 4.16 – Mass Loss of 12mm rod vs. duration for Test 1, 2, 3, Experiment C

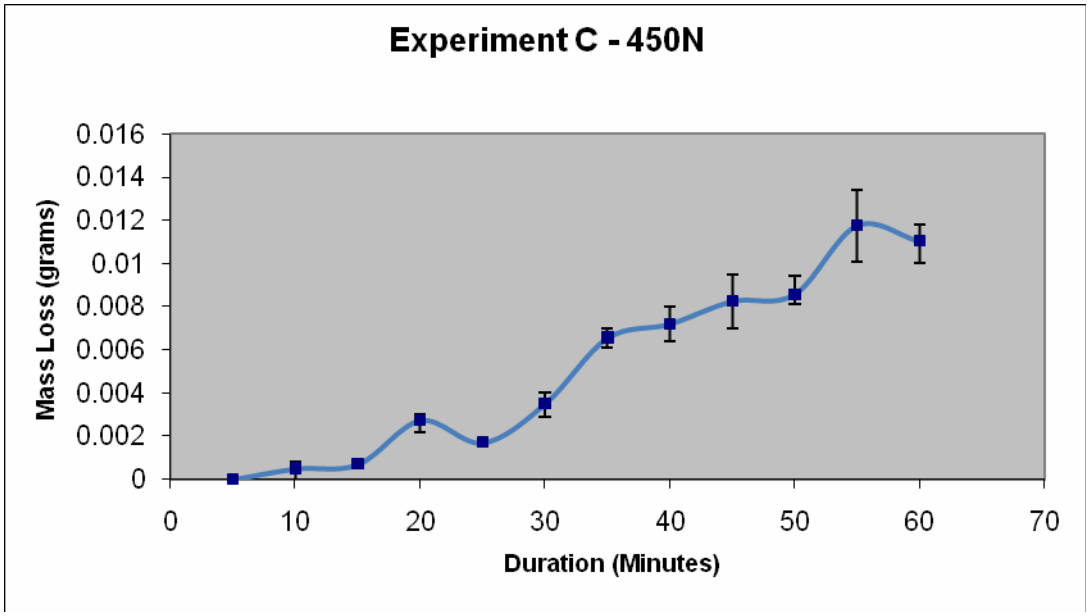


Graph 4.6 Plot of Average Mass Loss (grams) for Test 1–3 vs. Duration (Minutes) with Error Bars

### 4.3.2 Wear Depth – Experiment C

A profilometer was used to measure the wear depth for the wear tracks produced in Experiment C. The method used is detailed in Section 3. The profilometer traces are shown in Figures 4.15 – 4.24 for each of the tests conducted. Table 4.17 is a summary of the wear depth results. The data is plotted in Graph 4.7.

| | Experiment C - 450N Wear Depth (um) | | | | |
|---|---|---|---|---|---|
| Duration (Minutes) | Test 1 | Test 2 | Test 3 | Test 4 | Additonal |
| 5 | 0.0 | Not Tested | Not Tested | Not Tested | Not Tested |
| 10 | 3.3 | 3.6 | 4.1 | Not Tested | Not Tested |
| 15 | 5.2 | 0.5 | 3.6 | 3.2 | Not Tested |
| 20 | 14.0 | 12.1 | 12.7 | Not Tested | Not Tested |
| 25 | 8.9 | 10.8 | 11.4 | 11.4 | 10.2 |
| 30 | 12.7 | 11.4 | 10.8 | Not Tested | Not Tested |
| 35 | 18.4 | 19.3 | Not Tested | Not Tested | Not Tested |
| 40 | 17.8 | 18.4 | 19.7 | Not Tested | Not Tested |
| 45 | 21.0 | 22.2 | 25.4 | 20.3 | Not Tested |
| 50 | 22.9 | 22.9 | 24.1 | Not Tested | Not Tested |
| 55 | 27.9 | 27.9 | 29.2 | 22.9 | Not Tested |
| 60 | 26.4 | 22.9 | 26.7 | Not Tested | Not Tested |

Table 4.17 – Wear Depth (µm) vs. Duration for Tests 1 – 4, Experiment C, 450N

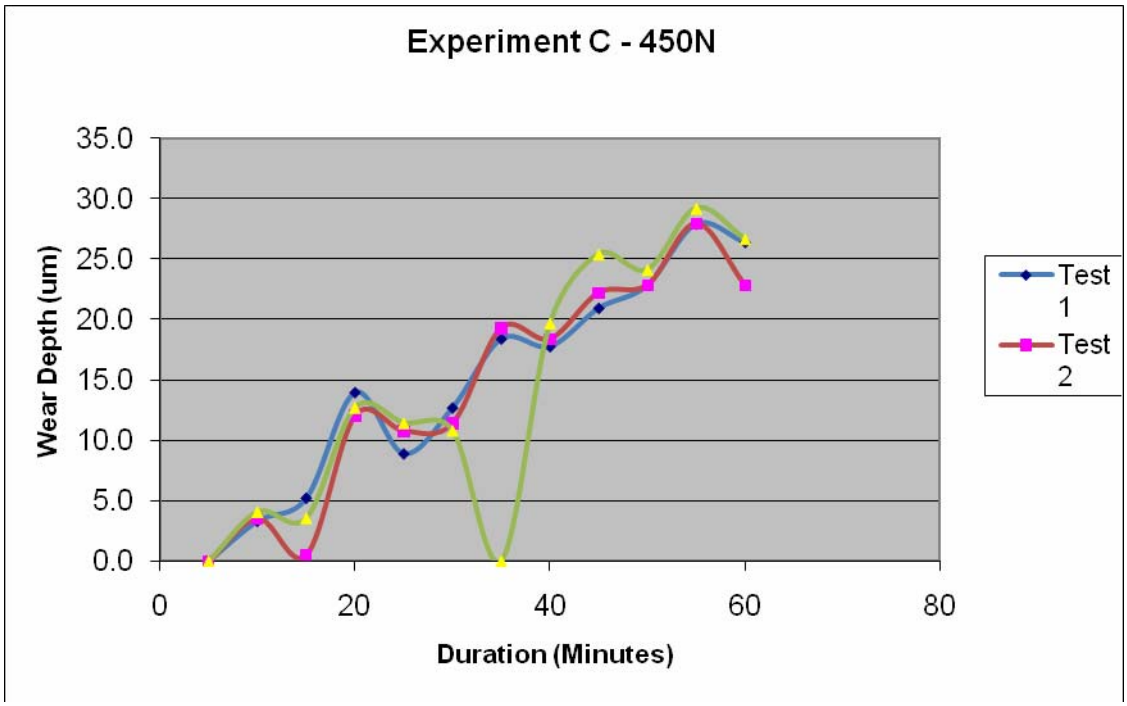


Graph 4.7 – Wear Depth (µm) vs. Duration for Tests 1 – 3, Experiment A, 450N

Graph 4.7 shows as duration / number of cycles increases the wear depth increases. Figures 4.15 to 4.24 show the profilometer traces for Test 1-3 for each duration conducted in Experiment C.

**Experiment C – Profilometer Traces**

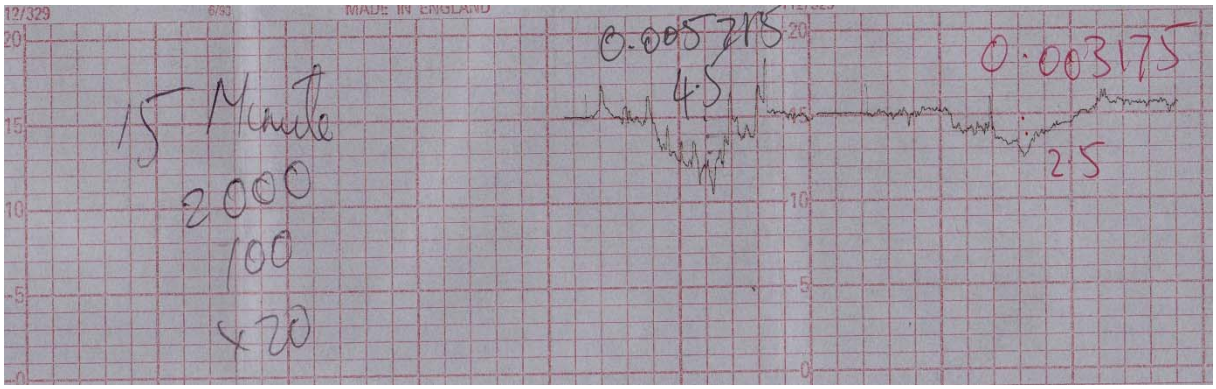


Figure 4.15 - Profilometer 15 minute Duration, Tests 1, 2

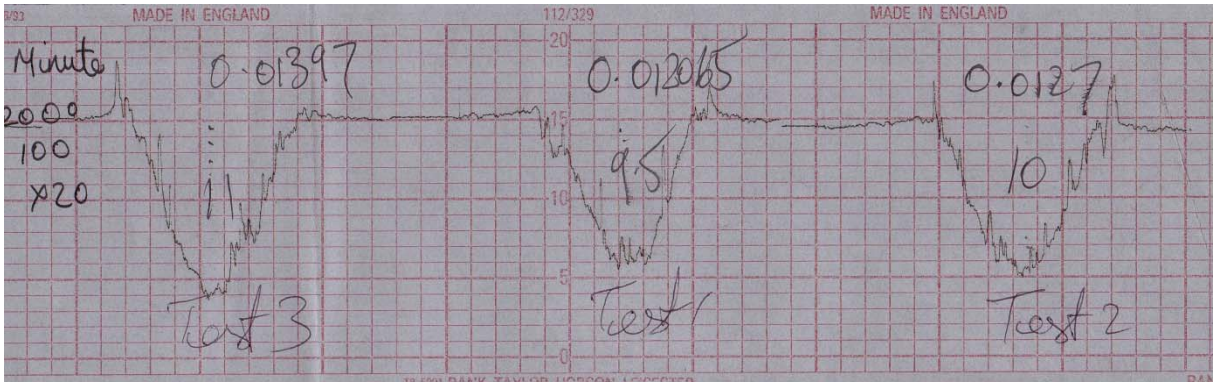


Figure 4.16 - Profilometer 20 minute Duration, Tests 1, 2 & 3

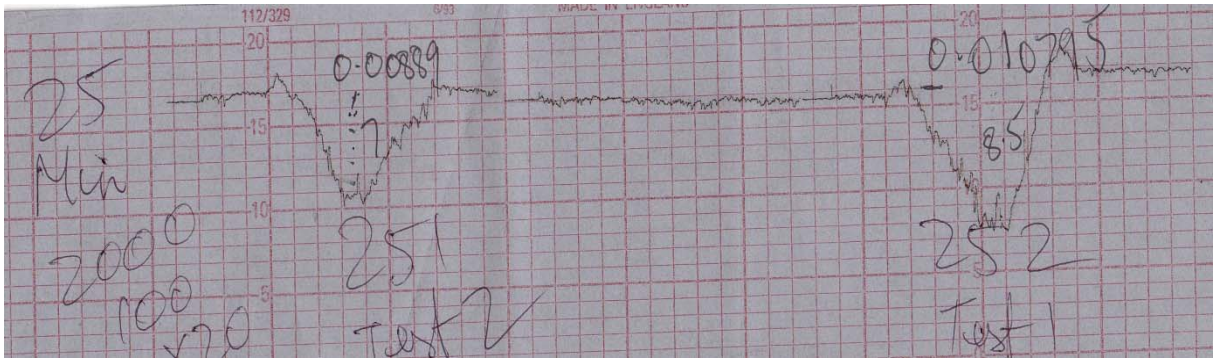


Figure 4.17 - Profilometer 25 minute Duration, Tests 1, 2 & 3

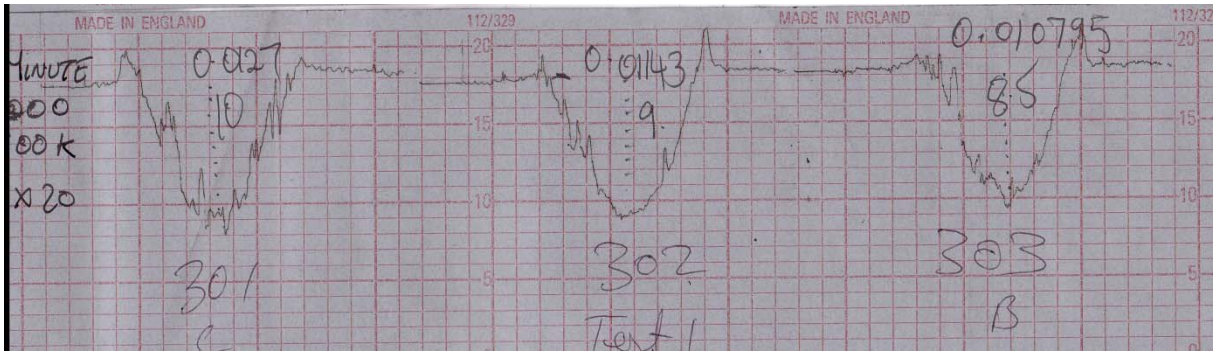


Figure 4.18 - Profilometer 30 minute Duration, Tests 1, 2 & 3

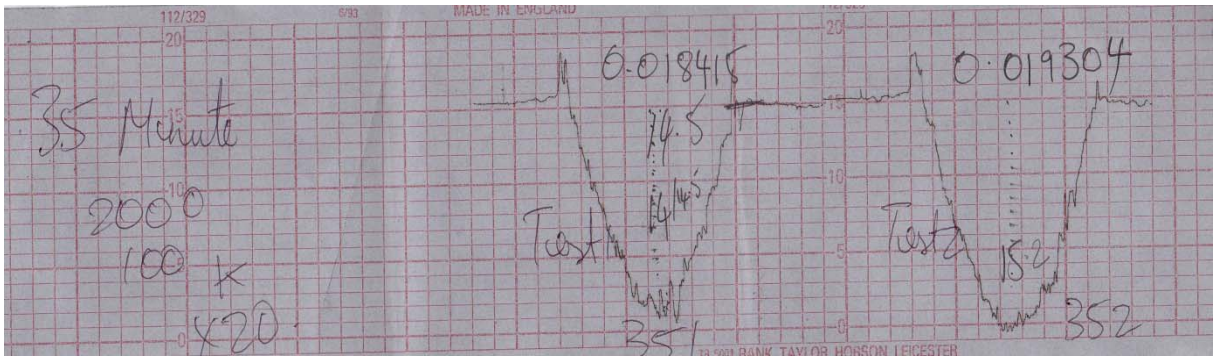


Figure 4.19 - Profilometer 35 minute Duration, Tests 1, 2

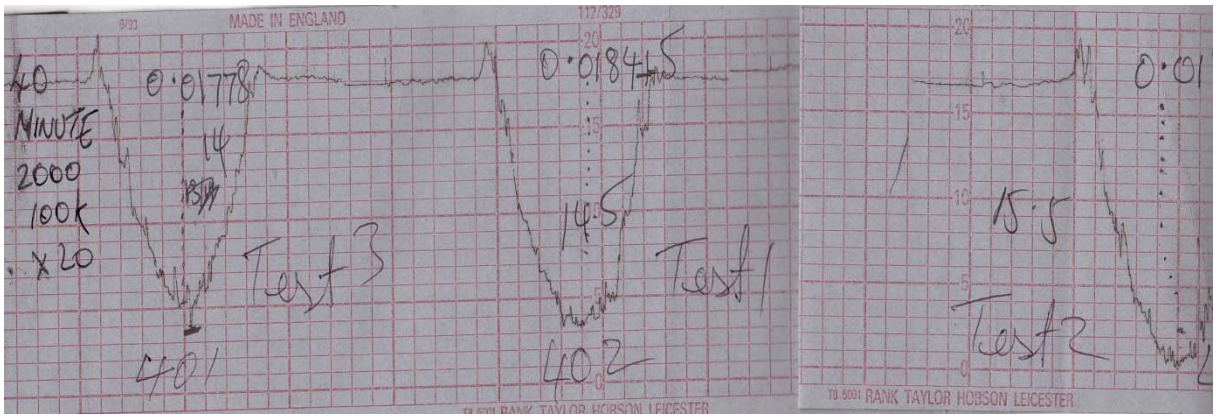


Figure 4.20 - Profilometer 40 minute Duration, Tests 1, 2 & 3

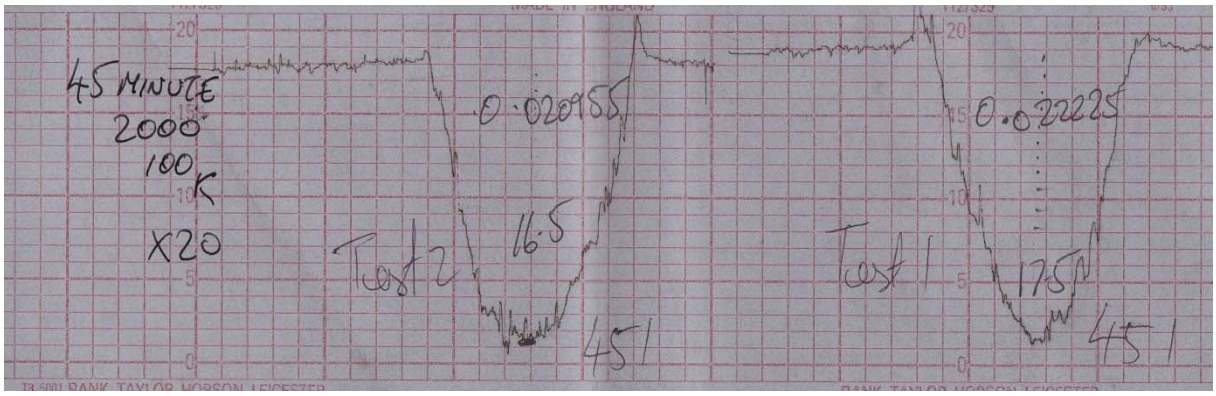


Figure 4.21 - Profilometer 45 minute Duration, Tests 1, 2

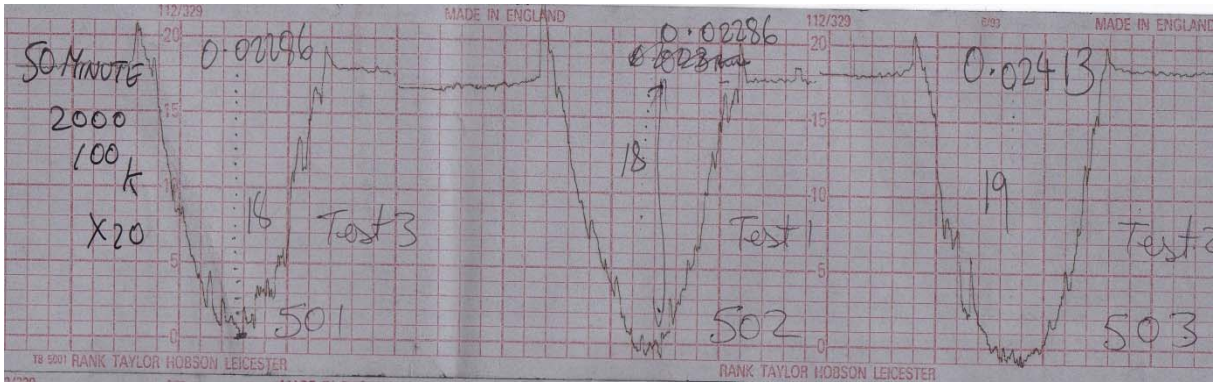


Figure 4.22 - Profilometer 50 minute Duration, Tests 1, 2 & 3

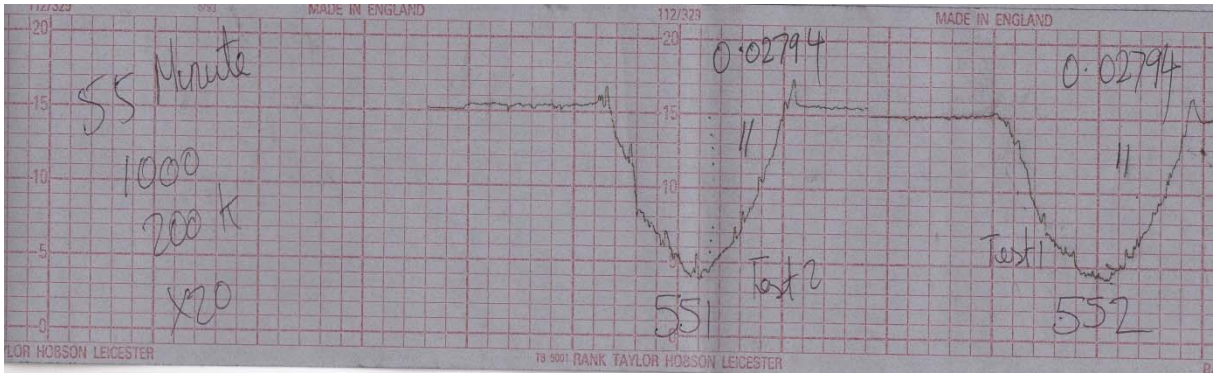


Figure 4.23 - Profilometer 55 minute Duration, Tests 1, 2

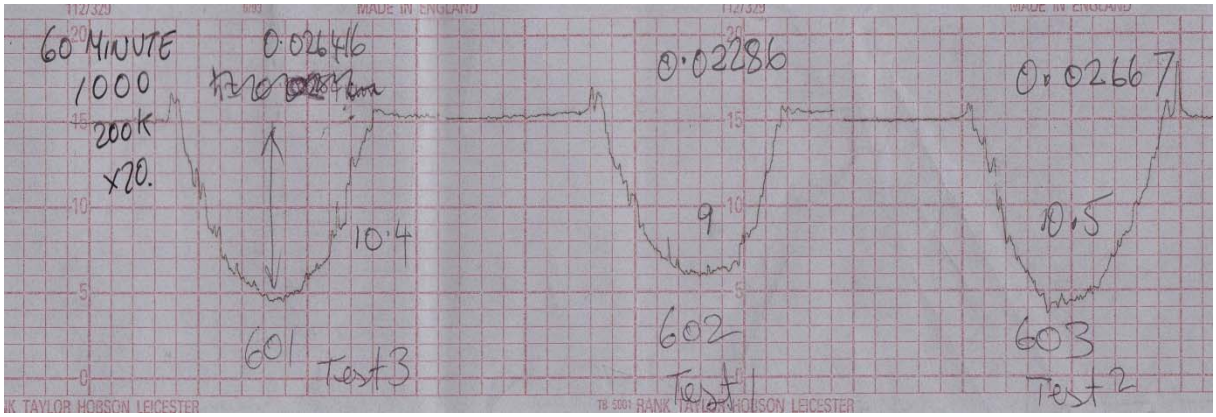


Figure 4.24 - Profilometer  60 minute Duration, Tests 1, 2 & 3

## 4.4 Experiment E – Scanning Electron Microscope (SEM) Analysis for 52100 Steel Wear Tracks produced at 450N Load.

In Experiment E, 52100 steel balls simulating the inner and outer race of a bearing were loaded against a 12mm diameter 52100 bearing steel rod at 450N. The test rig described in Section 3 was used for this test.

The purpose of Experiment E was to conduct SEM investigations of the wear tracks at certain durations. The Micrographs were studied to get an understanding of the wear process with time / increasing cycles. Tests were conducted at durations 1min, 5min, 10min, 15min, 20min, 25min, 30min, 35min, 45min, 50min, 55min 60min. Tests were not repeated as in previous experiments but mass loss and wear depth data compared to the baseline data established in Experiment C. Mass data is shown in Table 4.18. Mass loss data is presented in Table 4.19 and graphed in Graph 4.8. Mass loss data correlates well within the error bars of Experiment C with the exception of the 30 and 35 min samples which have lower wear than the baseline. Wear depth data is shown in Table 4.20 and graphed in Graph 4.9. Again, only the 30 and 35min samples have a lower wear depth value than the baseline Experiment C data. Samples at 30 and 35 min will not be used for the SEM analysis

| Table 4.18 | | | | | | | | | |
|---|---|---|---|---|---|---|---|---|---|
| Experiment E - Results | | | | | | | | | |
| | | | | BEFORE TEST | | | AFTER TEST | | |
| Sample No | Duration (Min) | Speed (Hz) | Load (N) | Mass Rod (g) | Mass Ball 1 (g) | Mass Ball 2 (g) | Mass Rod (g) | Mass Ball 1 (g) | Mass Ball 2 (g) |
| a1 | 1 | 7.5/7.2 | 450 | 51.7136 | 66.8196 | 66.8155 | 51.7136 | Not Recorded | Not Recorded |
| a2 | 5 | 7.5/7.2 | 450 | 51.7136 | 66.8379 | 66.8161 | 51.7139 | Not Recorded | Not Recorded |
| a3 | 10 | 7.5/7.2 | 450 | 51.7139 | 66.7842 | 66.8115 | 51.7137 | Not Recorded | Not Recorded |
| b1 | 15 | 7.5/7.2 | 450 | 52.4638 | 66.8139 | 66.817 | 52.4629 | Not Recorded | Not Recorded |
| b2 | 20 | 7.5/7.2 | 450 | 52.4629 | 66.8199 | 66.8177 | 52.4609 | Not Recorded | Not Recorded |
| b3 | 25 | 7.5/7.2 | 450 | 52.4609 | 66.8175 | 66.8264 | 52.458 | Not Recorded | Not Recorded |
| c1 | 30 | 7.5/7.2 | 450 | 51.9076 | 66.8502 | 66.8165 | 51.9057 | Not Recorded | Not Recorded |
| c2 | 35 | 7.5/7.2 | 450 | 51.9057 | 66.8141 | 66.8132 | 51.9014 | Not Recorded | Not Recorded |
| c3 | 40 | 7.5/7.2 | 450 | 51.9014 | 66.8177 | 66.8164 | 51.8951 | Not Recorded | Not Recorded |
| d1 | 45 | 7.5/7.2 | 450 | 50.4009 | 66.8157 | 66.8179 | 50.3931 | Not Recorded | Not Recorded |
| d2 | 50 | 7.5/7.2 | 450 | 50.3931 | 66.7826 | 66.813 | 50.3836 | Not Recorded | Not Recorded |
| d3 | 55 | 7.5/7.2 | 450 | 50.3836 | 66.8194 | 66.8204 | 50.3707 | Not Recorded | Not Recorded |

### 4.4.1 Mass Loss – Experiment E

| Sample No | Duration (Min) | Mass Loss of Rod (g) |
|---|---|---|
| a1 | 1 | 0 |
| a2 | 5 | 0 |
| a3 | 10 | 0.0002 |
| b1 | 15 | 0.0009 |
| b2 | 20 | 0.002 |
| b3 | 25 | 0.0029 |
| c1 | 30 | 0.0019 |
| c2 | 35 | 0.0043 |
| c3 | 40 | 0.0063 |
| d1 | 45 | 0.0078 |
| d2 | 50 | 0.0095 |
| d3 | 55 | 0.0129 |

Table 4.19 - Mass Loss of test sample vs. Duration for Experiment E (450N)

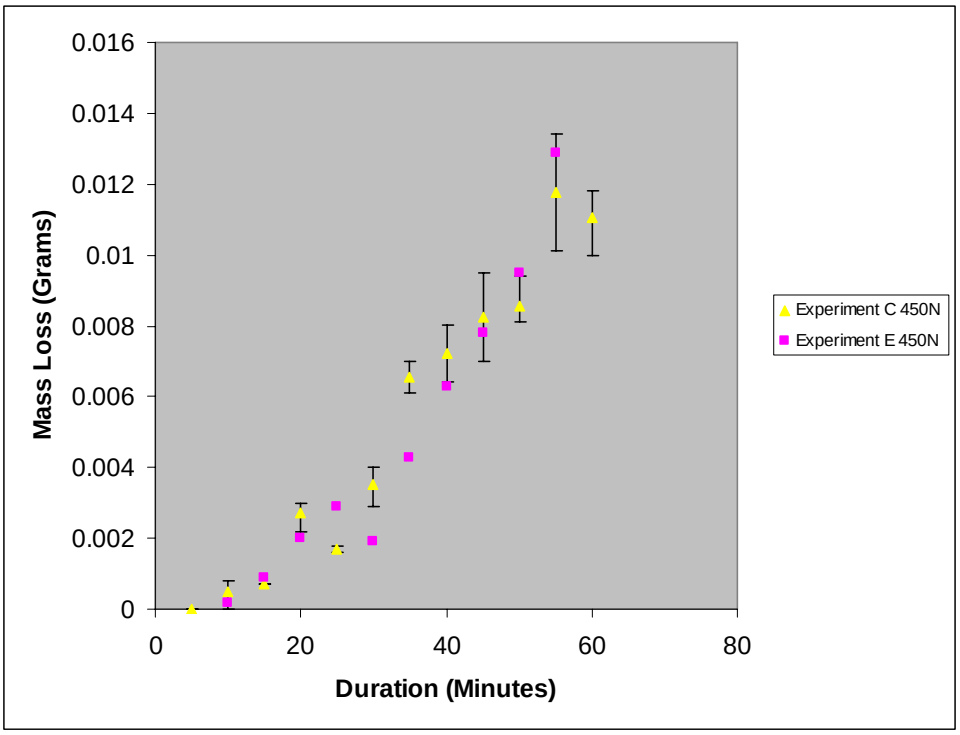


Graph 4.8 - Mass Loss vs. Duration for Experiment E (450N). Data compared to Experiment C and error bars.

### 4.4.2 Wear Depth – Experiment E

A profilometer was used to measure the wear depth for the wear tracks produced in Experiment E. The method used is detailed in Section 3. The profilometer traces are shown in Figures 4.25 – 4.27 for each of the tests conducted. Table 4.20 is a summary of the wear depth results. The data is plotted in Graph 4.9.

| Sample No | Duration (Min) | Wear height (µm) |
|---|---|---|
| a1 | 1 | Not measureable |
| a2 | 5 | Not measureable |
| a3 | 10 | Not measureable |
| b1 | 15 | 6.35 |
| b2 | 20 | 9.652 |
| b3 | 25 | 12.7 |
| c1 | 30 | 7.62 |
| c2 | 35 | 13.97 |
| c3 | 40 | 16.51 |
| d1 | 45 | 19.05 |
| d2 | 50 | 22.86 |
| d3 | 55 | 29.21 |

Table 4.20 - Wear depth vs. Duration for Experiment E

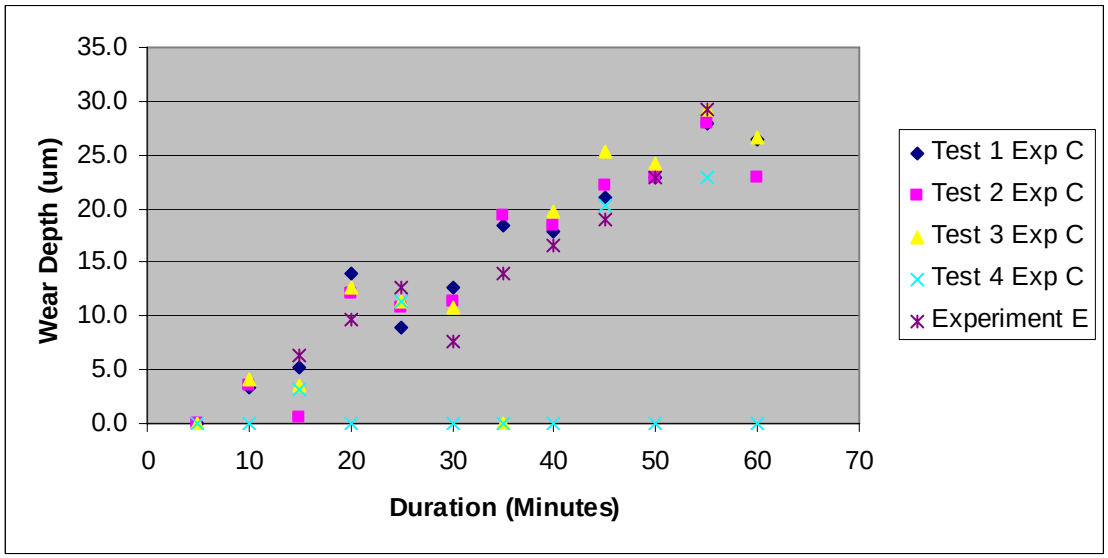


Graph 4.9 Wear depth vs. Time for Experiment E. Data compared to Experiment C

**Experiment E – Profilometer Traces**

Figures 4.25 to 4.27 show the profilometer traces for Experiment E.

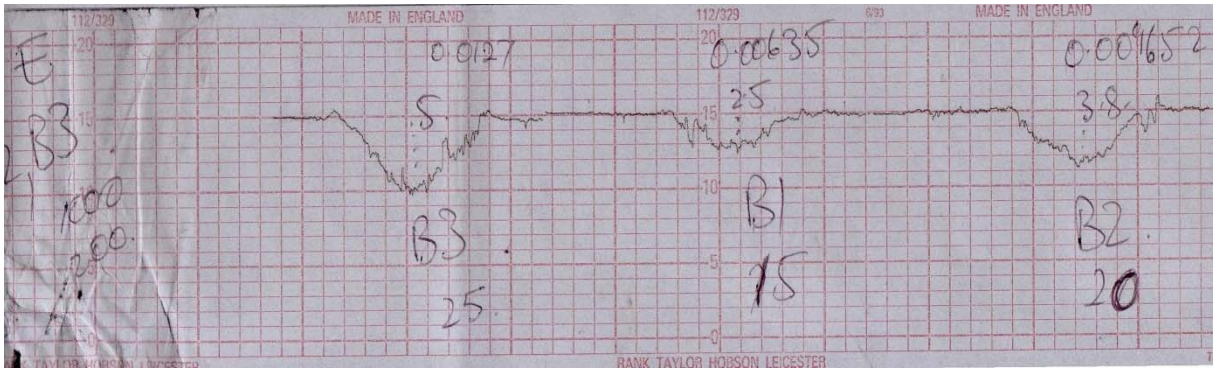


Figure 4.25 - Profilometer 15, 20, 25 minute Duration

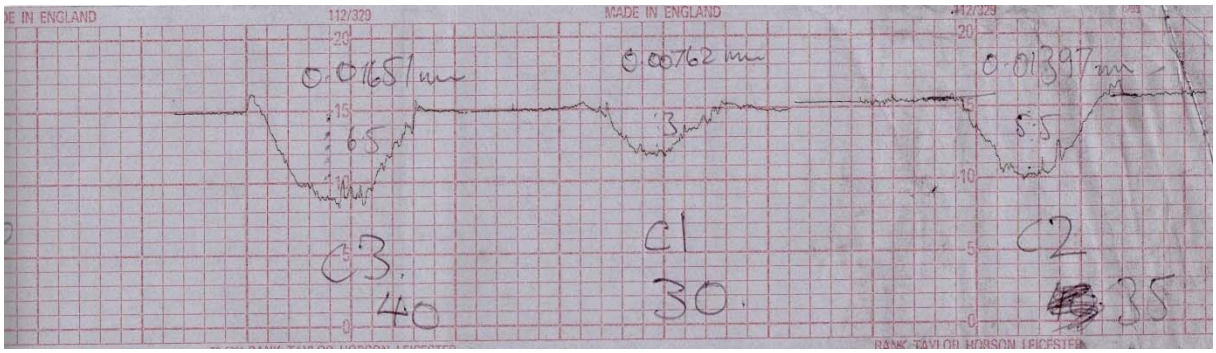


Figure 4.26 - Profilometer 30, 35, 40 minute Duration

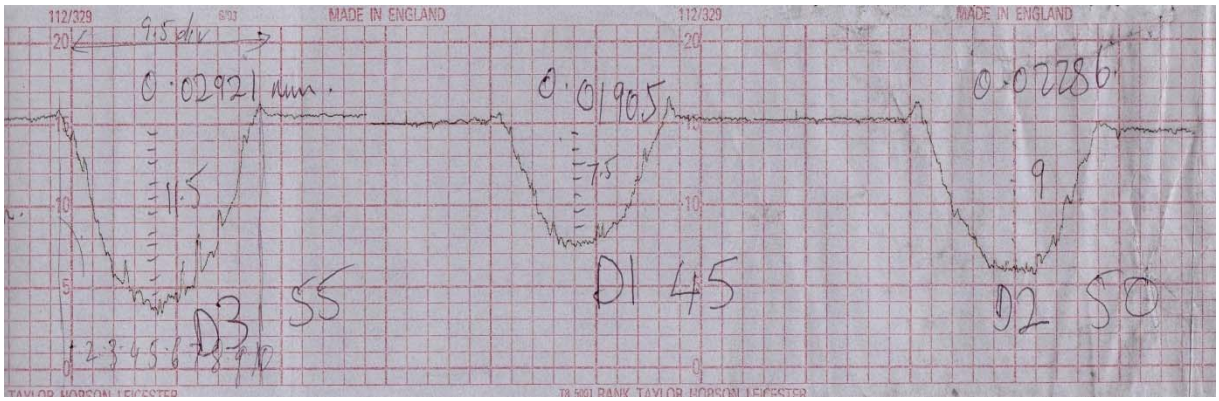


Figure 4.27 - Profilometer 45, 50, 55 minute Duration

### 4.4.3 Scanning Electron Microscope Observations for Experiment E & F Wear Tracks. 52100 Bearing Steel at 450N Load.

#### 4.4.3.1 SEM Results: Experiment E Steel on Steel 450N

Observations – Wear Track Surface

Figures 4.28 to 4.47 show the progressive increase in wear for steel on steel under rolling contact at 450N load. Figure 4.28 and 4.29 show the original surface of the specimen. The parallel markings are the original grinding marks of the 52100 bearing steel surface. At 1 minute (Figure 4.30 and 4.31) there is evidence of smearing and polishing out of the grinding marks leaving a smoother surface. The asperity peaks have been smoothed out during the rolling process. At 5 minutes (Figure 4.32 and 4.33) shows the wear mode has changed from asperity polishing to surface cracking. Cracking is visible on the surface and smearing. Figure 4.35 at 10 minutes shows cracks orientated at 45 deg to the direction of rolling. Cracks have grown in length and smearing has almost completely disappeared. Figures 4.36 and 4.37 at 15 minutes illustrates that the cracks have extended to form thin like flakes. During the period 20 minutes through to 55 minutes, Figures 4.38 – 4.47 show that as rolling continues crack networks increase in size and thin flat flake like sheets are produced. The area of wear increases as time / number of cycles increases.

**Experiment E - SEM**

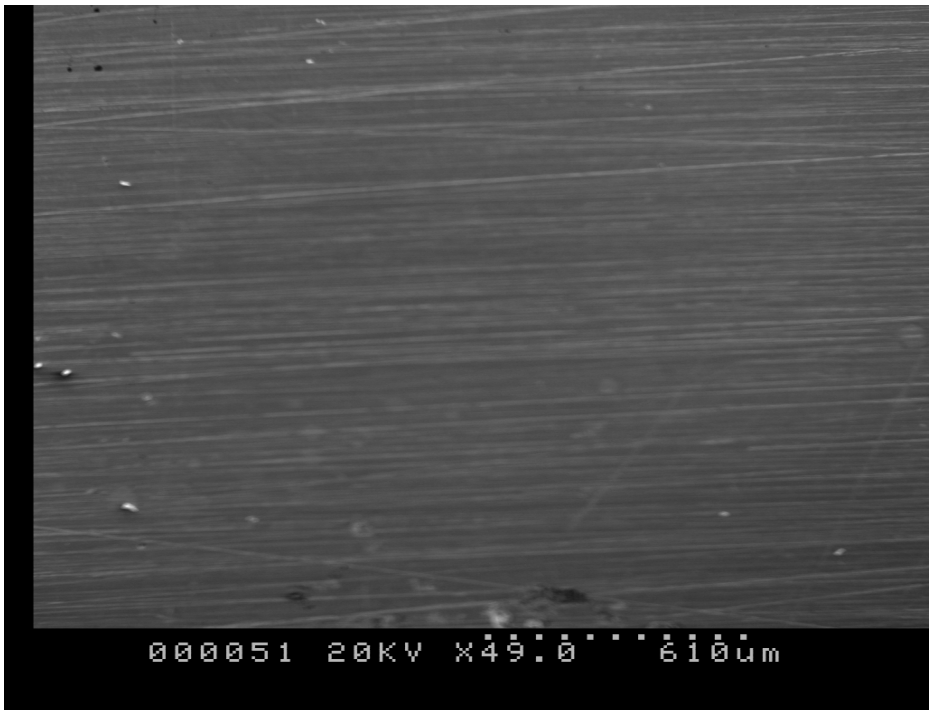


Figure 4.28: Original Surface of 52100 rod showing Grinding Marks. Mag. X49

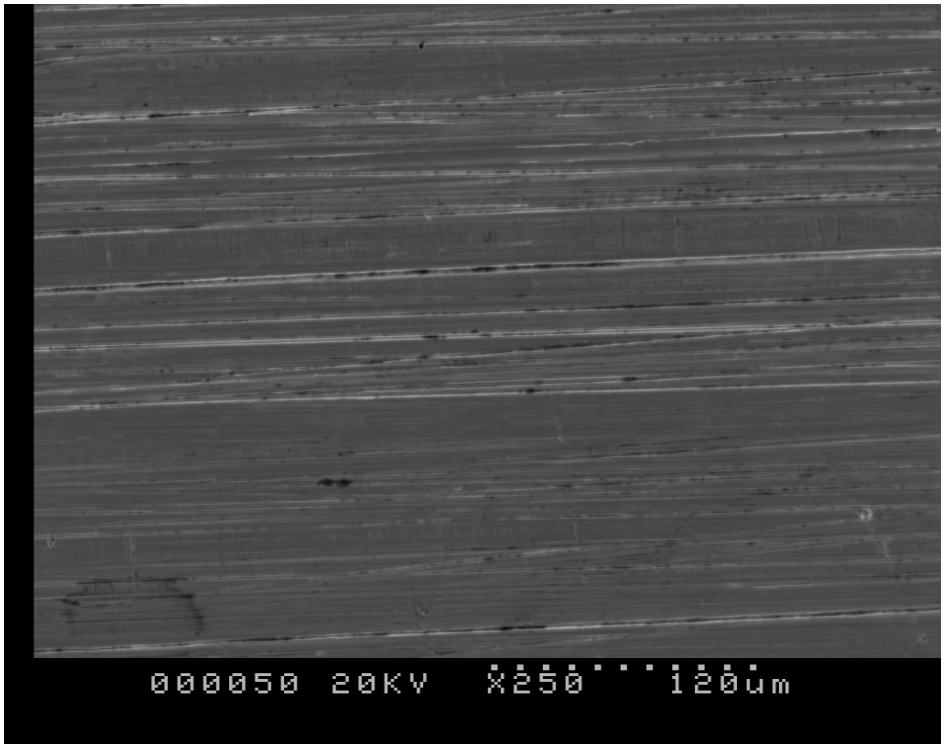


Figure 4.29: Original Surface of 52100 rod showing Grinding Marks. Magnification X250


Figure 4.30: Sample A1, 1 minute Duration. There is smearing on the Wear Track and removal of the original Grinding Marks. Magnification X50

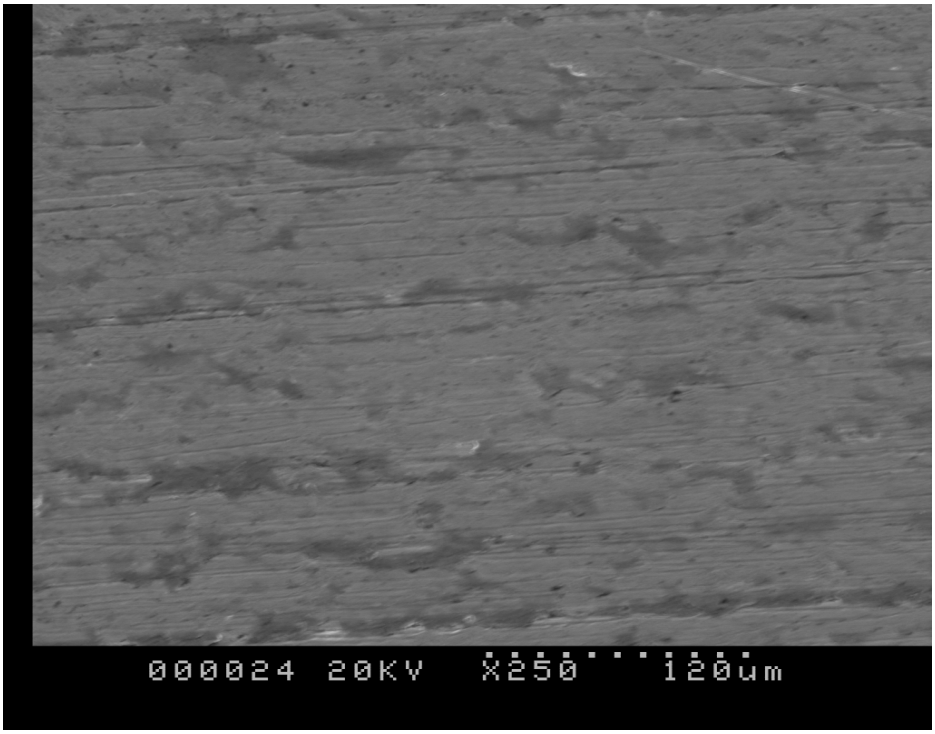


Figure 4.31: Sample A1, 1 minute Duration. Smoothing of Surface as compared to original Grinding Marks for Figure 4.30.


Figure 4.32 Sample A2: 5 minute Duration, X50

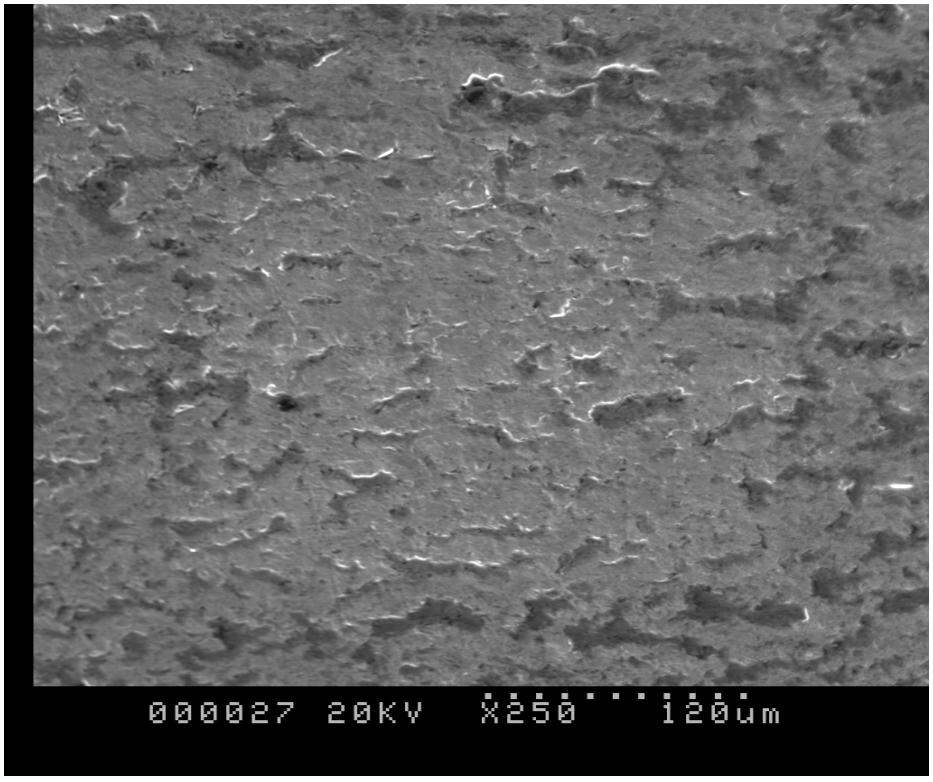


Figure 4.33 Sample A2: 5 minute Duration X250

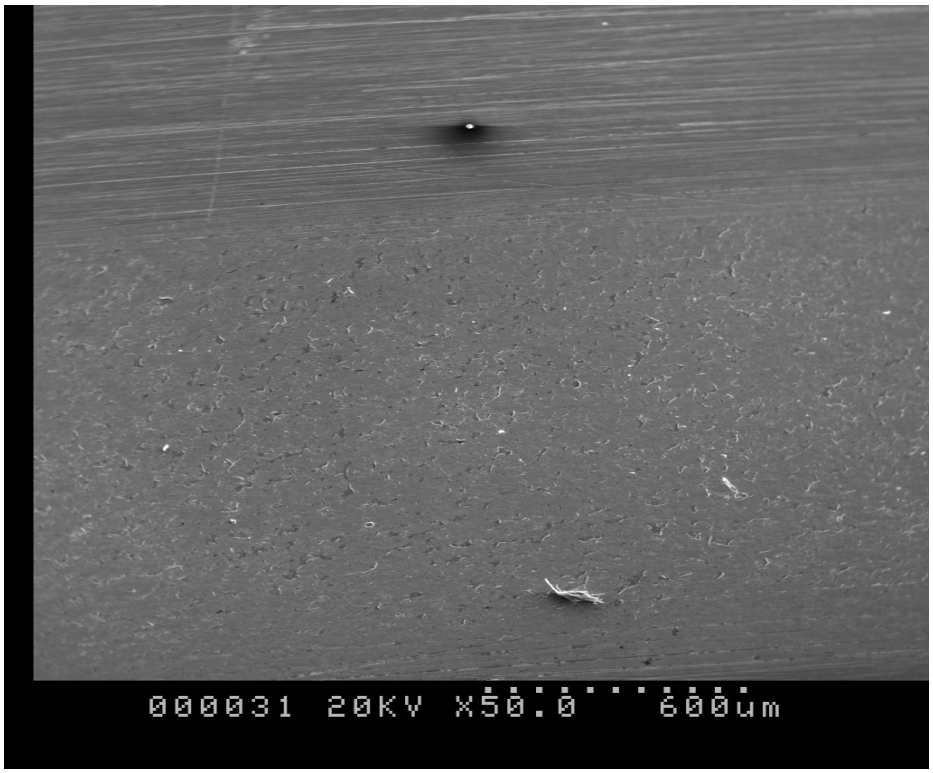


Figure 4.34: Sample A3: 10 minute Duration X50

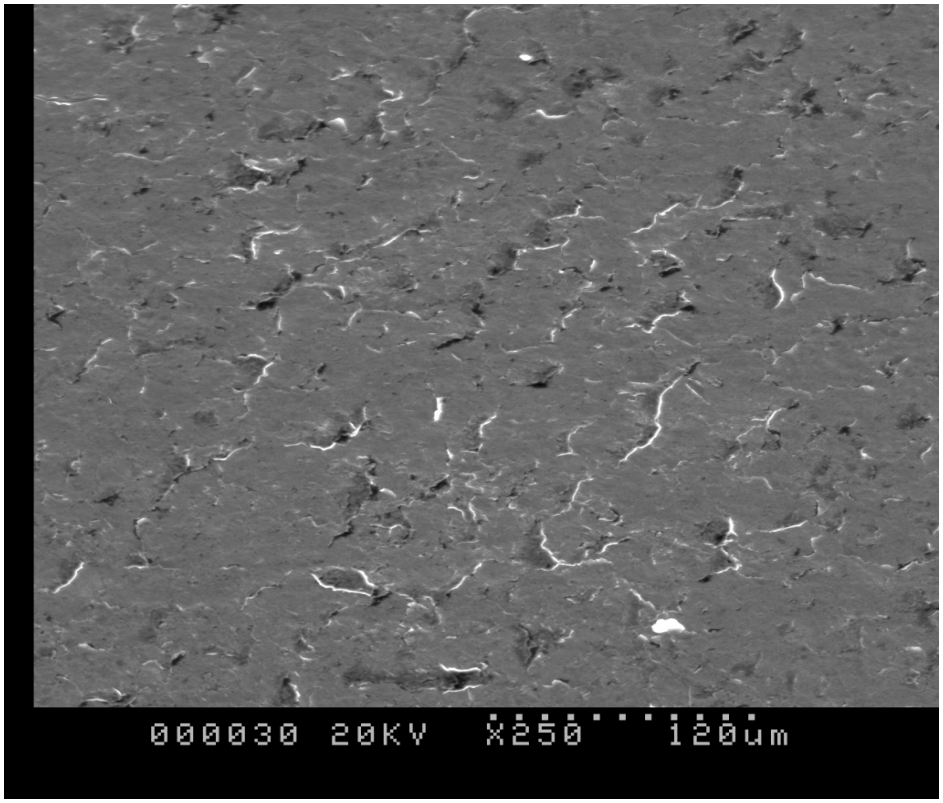


Figure 4.35 Sample A3: 10 minute Duration X250

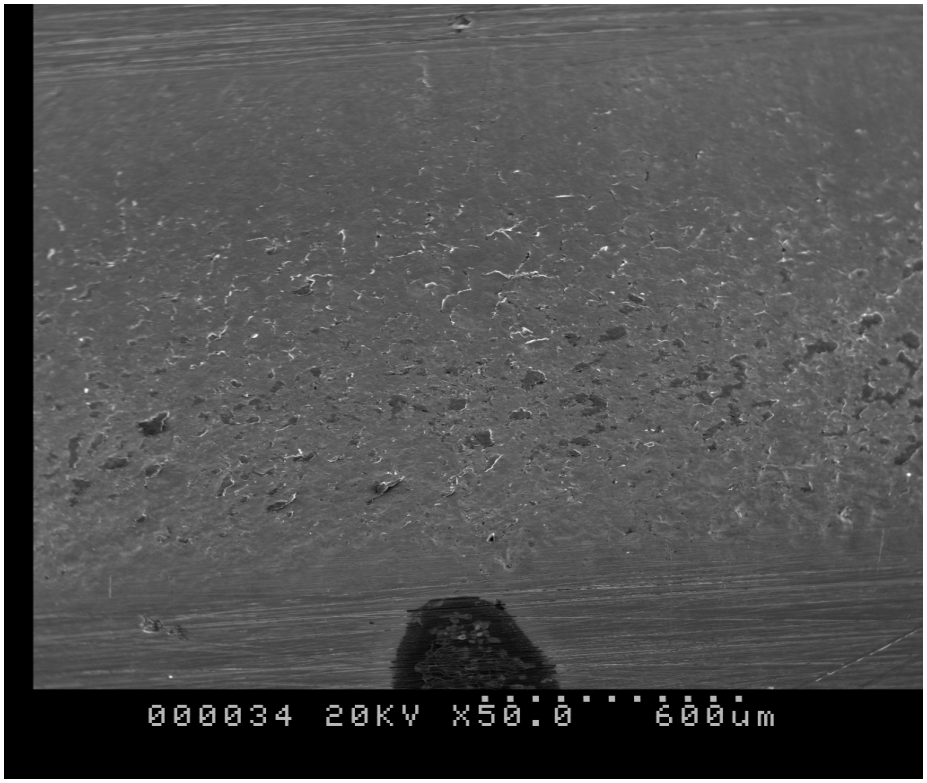


Figure 4.36 Sample B1: 15 minute Duration X50

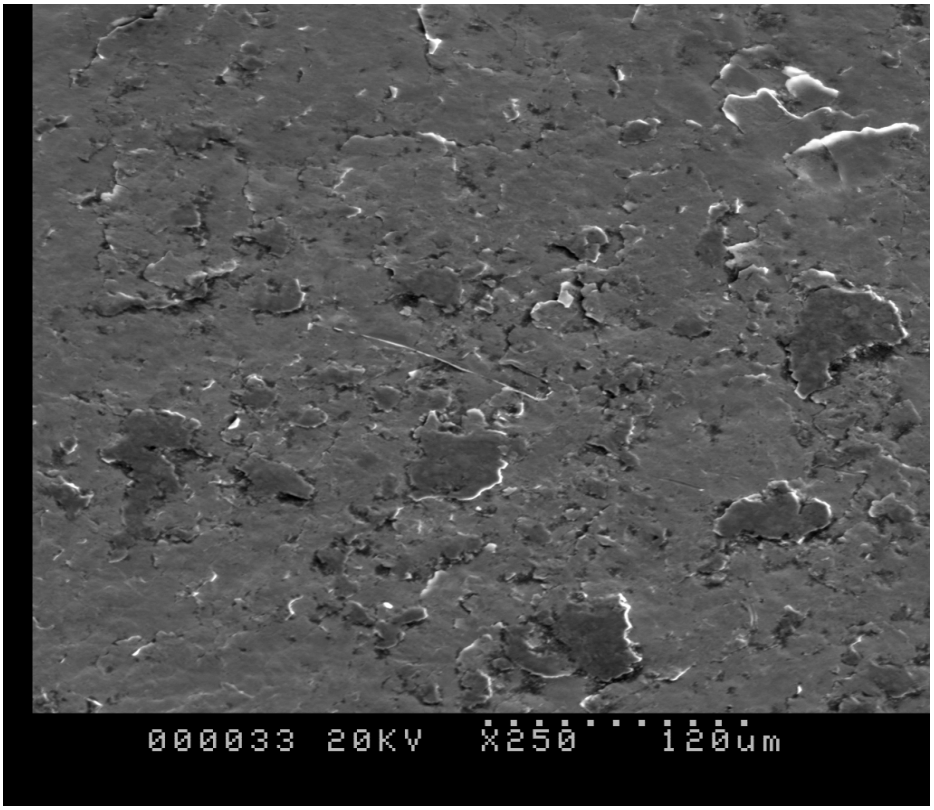


Figure 4.37 Sample B1: 15 minute Duration X250

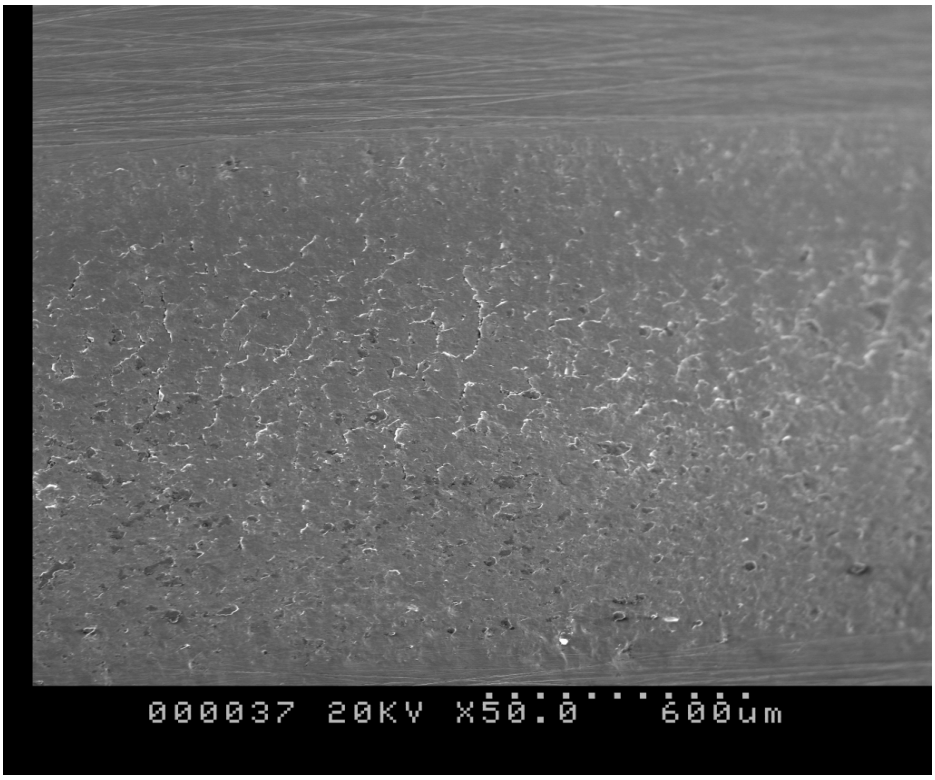


Figure 4.38 Sample B2: 20 minute Duration X50

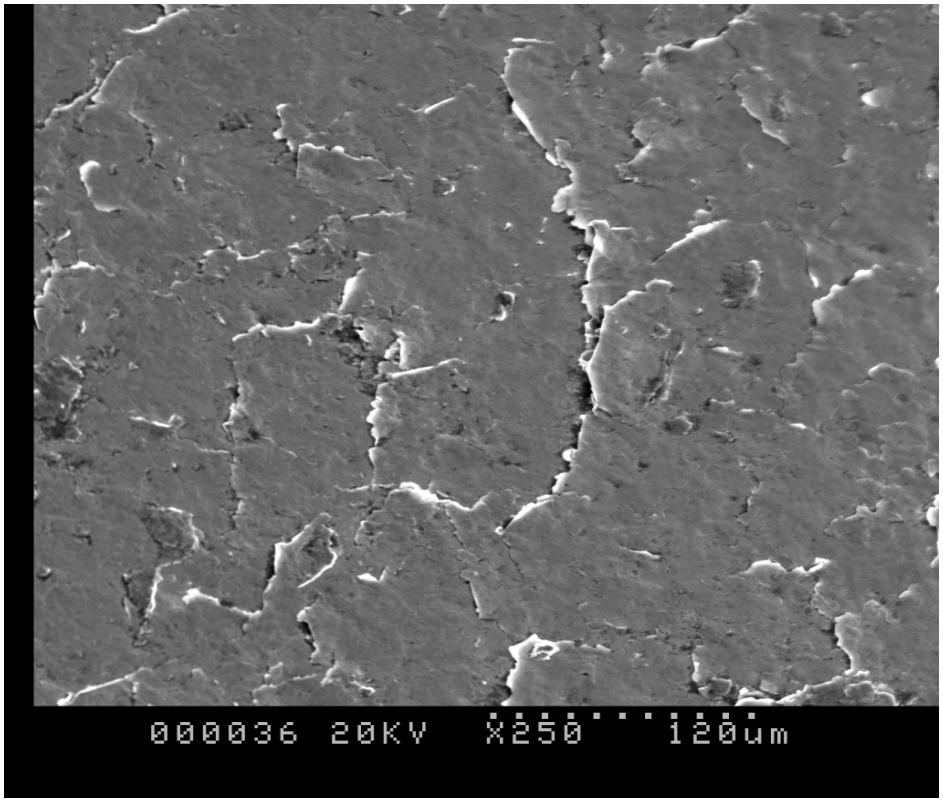


Figure 4.39 Sample B2: 20 minute Duration X250

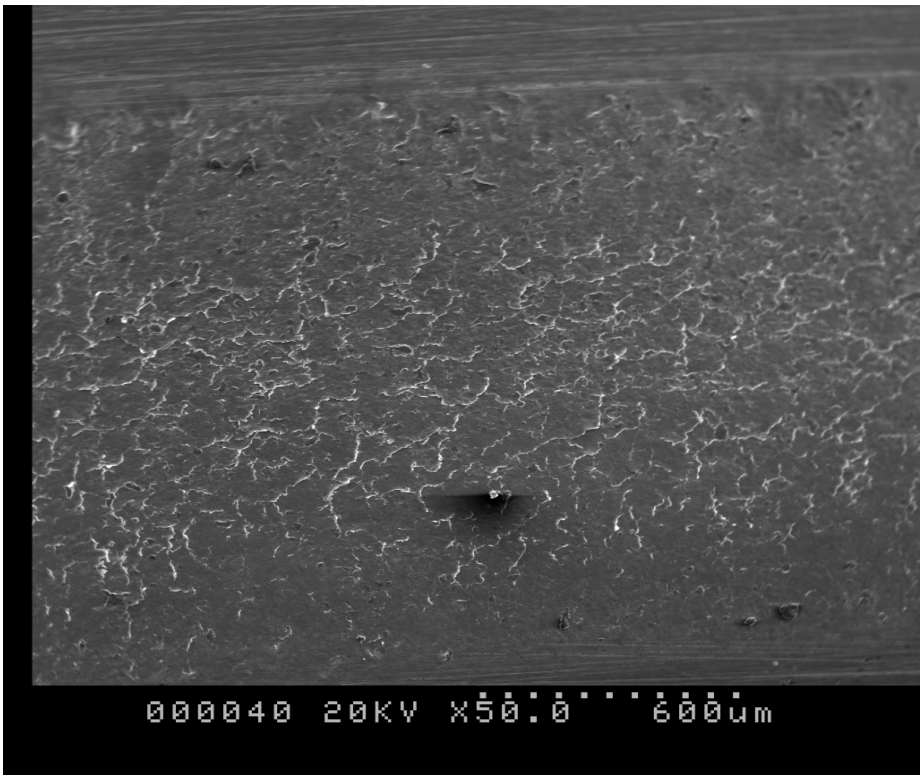


Figure 4.40 Sample B3: 25 minute Duration X50

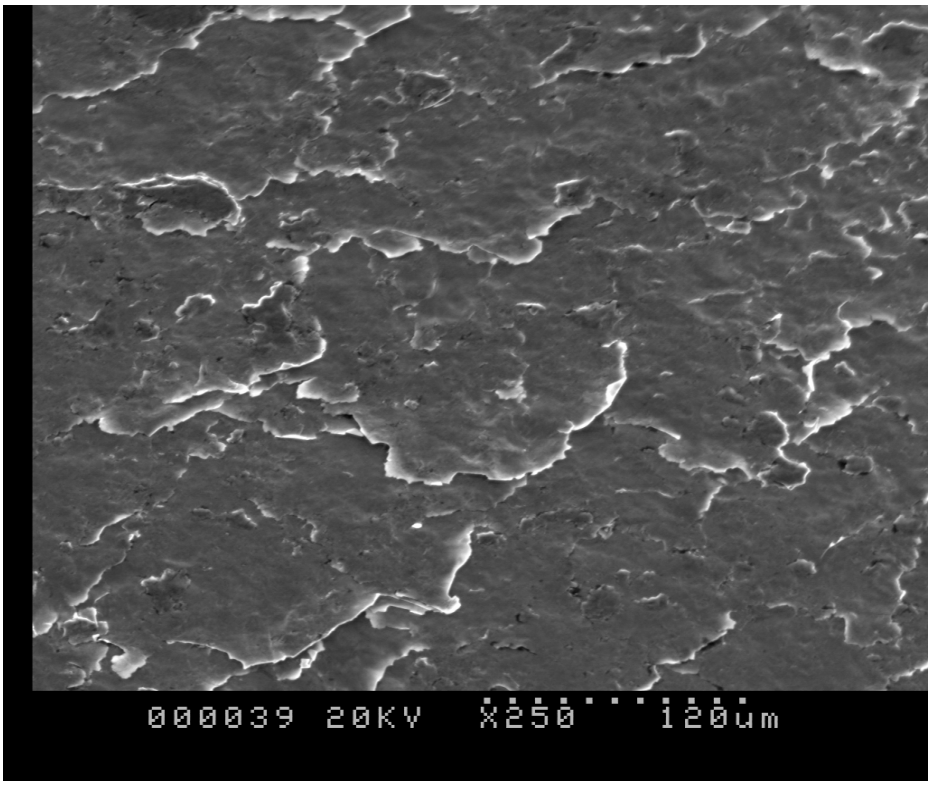


Figure 4.41 Sample B3: 25 minute Duration X250

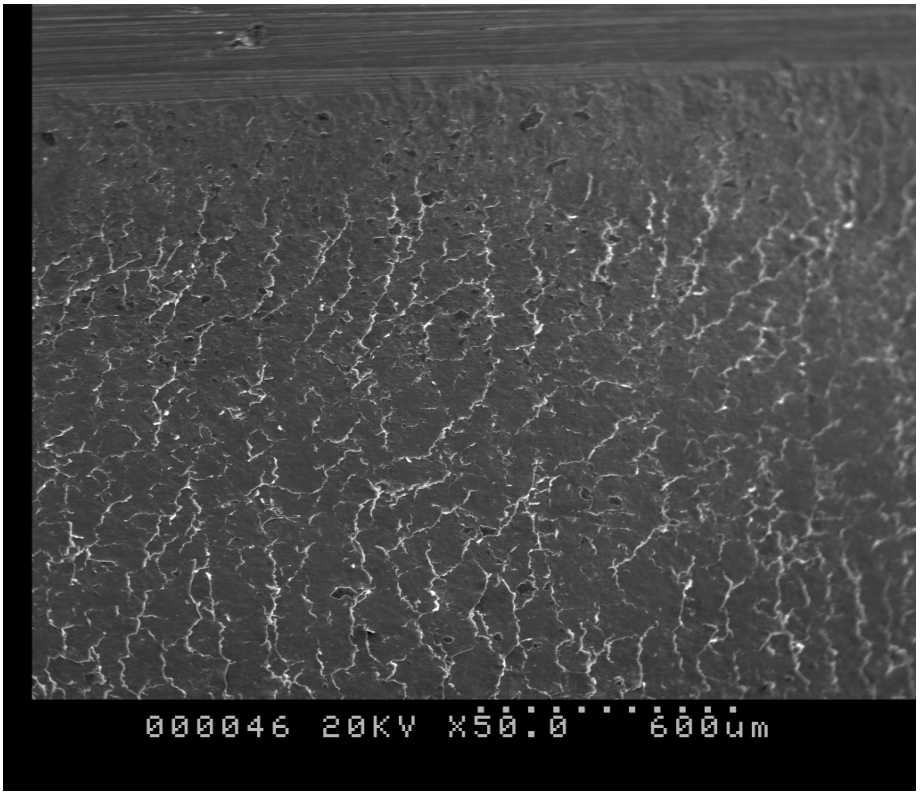


Figure 4.42 Sample D1: 45 minute Duration X50

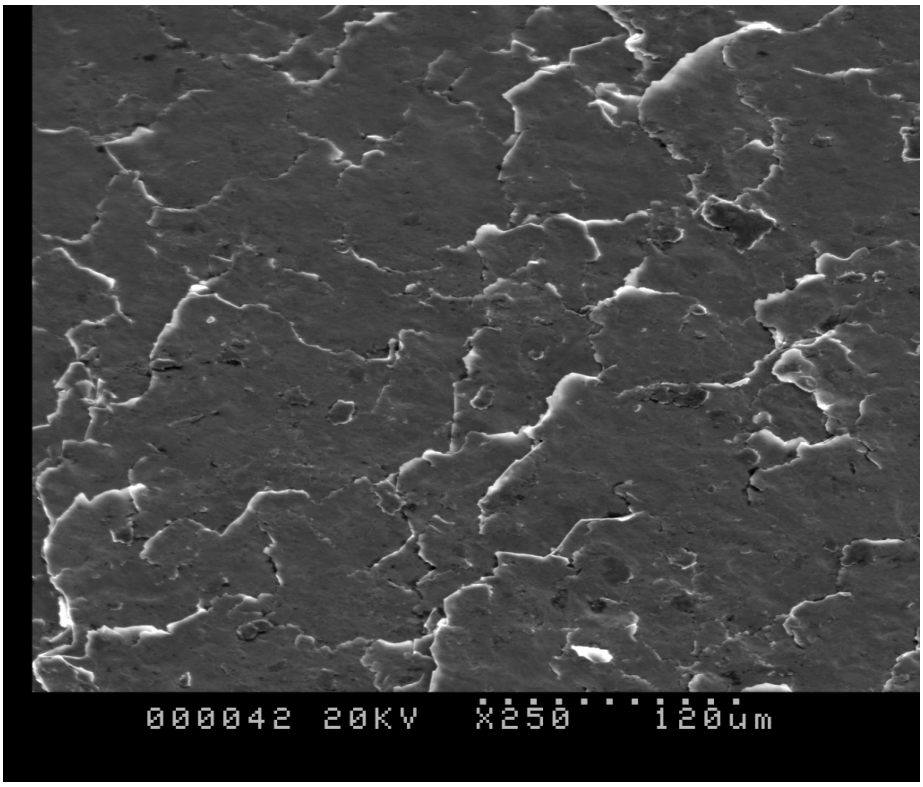


Figure 4.43 Sample D1: 45 minute Duration X250

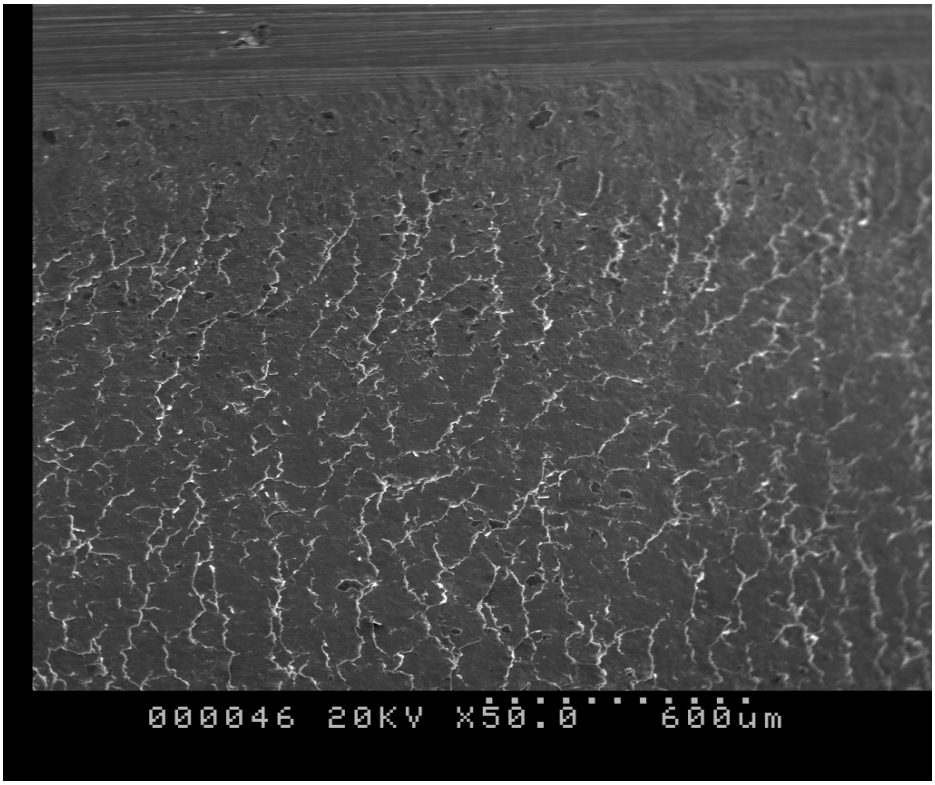


Figure 4.44 Sample D2: 50 minute Duration X50

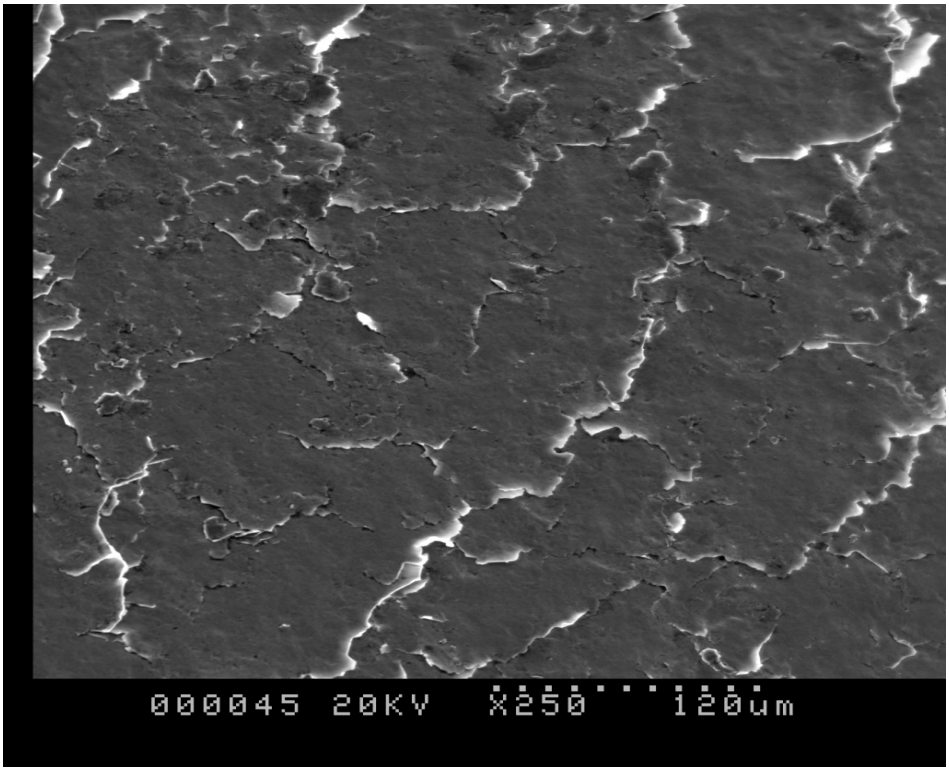


Figure 4.45 Sample D2: 50 minute Duration X250

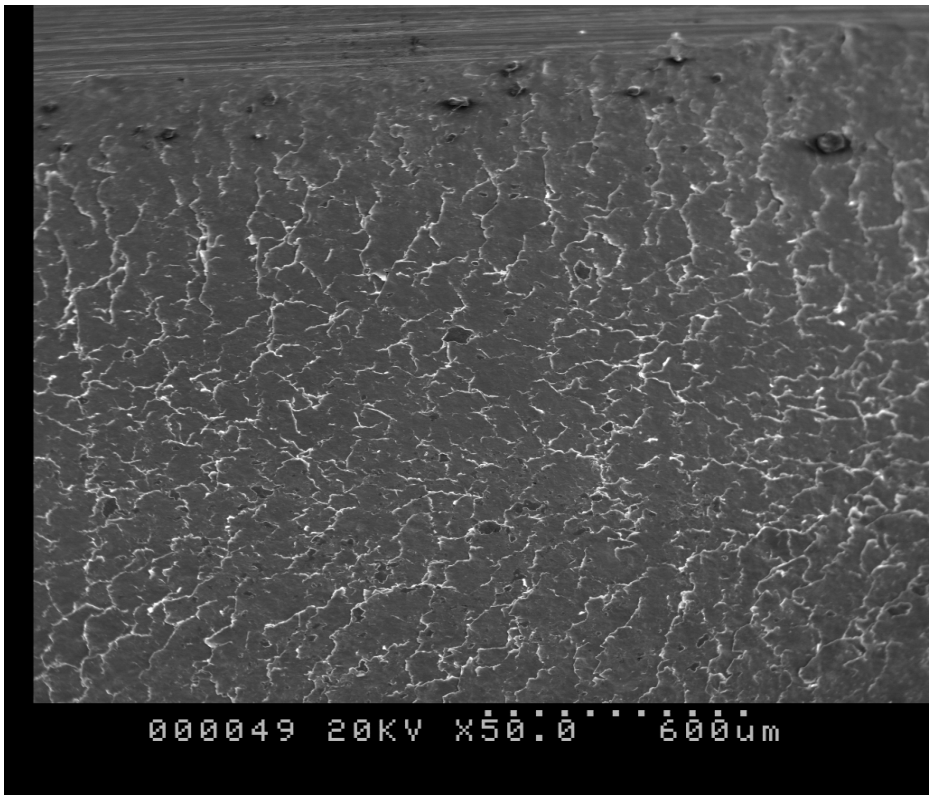


Figure 4.46 Sample D3: 55 minute Duration X50

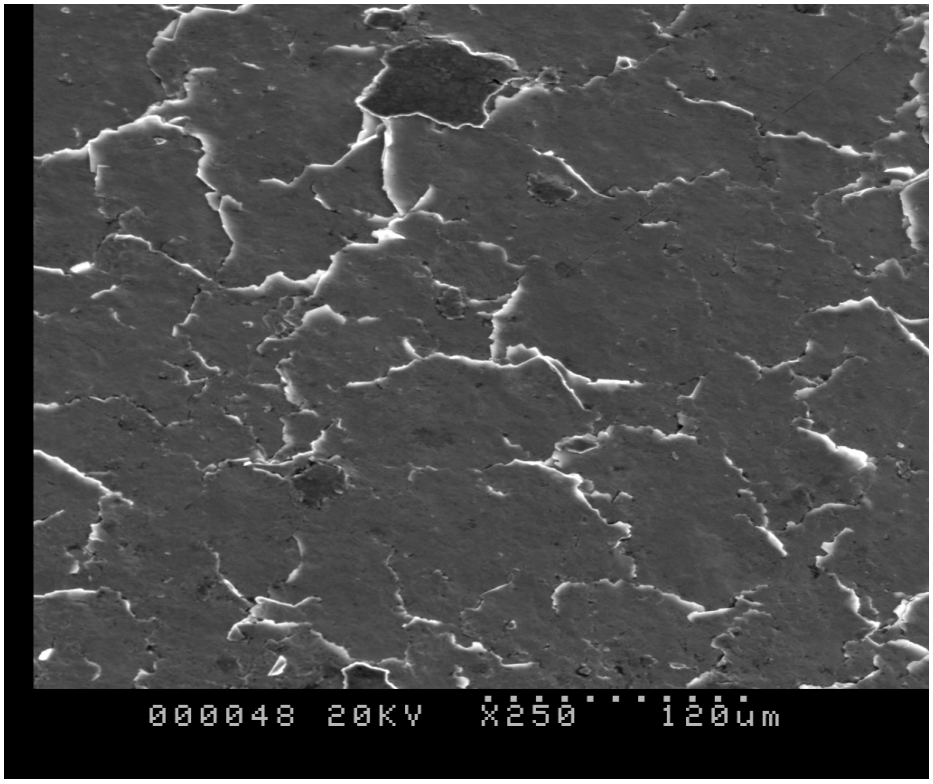


Figure 4.47 Sample D3: 55 minute Duration X250

#### 4.4.3.2 SEM Results: Experiment F, 52100 Steel on Steel at 450N load.

Observations – Wear Track Surface

In Experiment F, SEM investigations focused in the 20 – 35min duration range. As the 30 – 35min range in Experiment E was not observed due to wear data being out of range of the Experiment C baseline data. Experiment F repeated the wear tests in this region. SEM was also done at higher magnifications (X500 – X2000) to get a better picture of the thin flakes seen in Experiment E SEM. Figures 4.48 to 4.54 show the micrographs for Experiment F. Figure 4.48 and 4.49 at 5 minute shows thin flakes on surface. Figures 4.53 and 4.54 at 35min shows the thin flat flakes in detail.

**Experiment F – SEM**

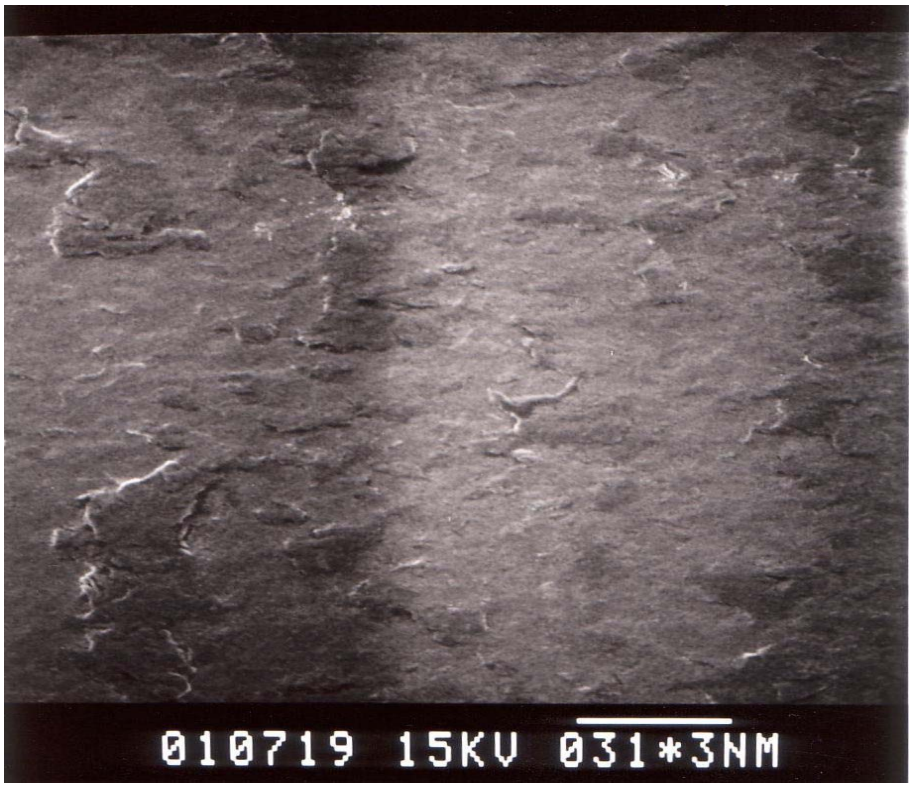


Figure 4.48 Sample A2: 5 minute X2000

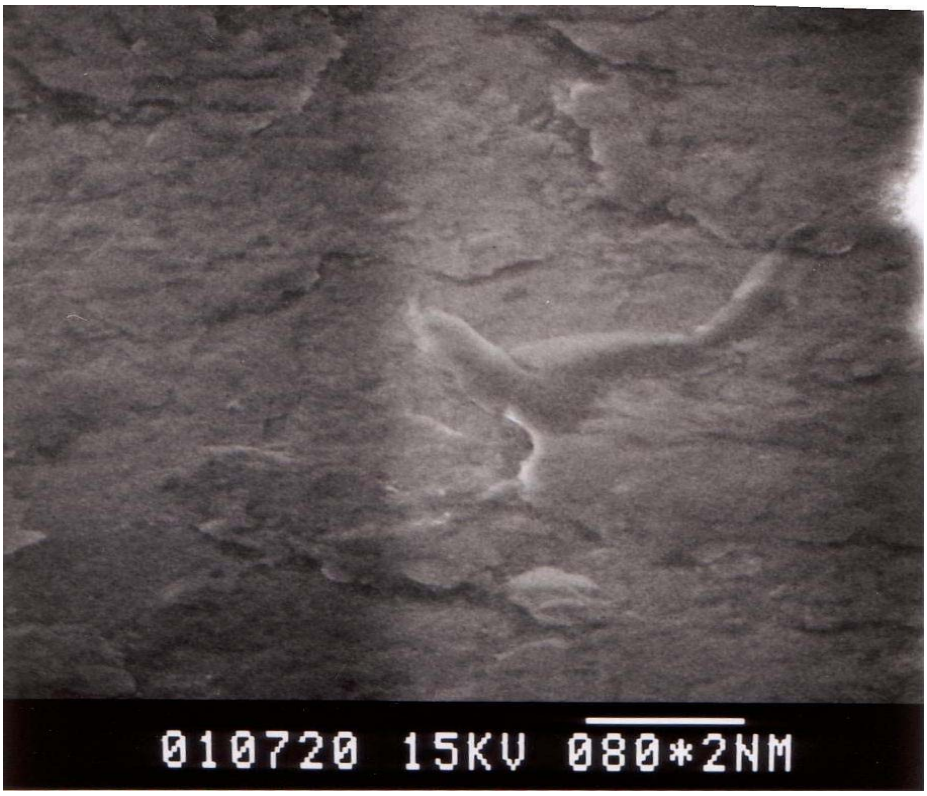


Figure 4.49 Sample A2: 5 minute X2000

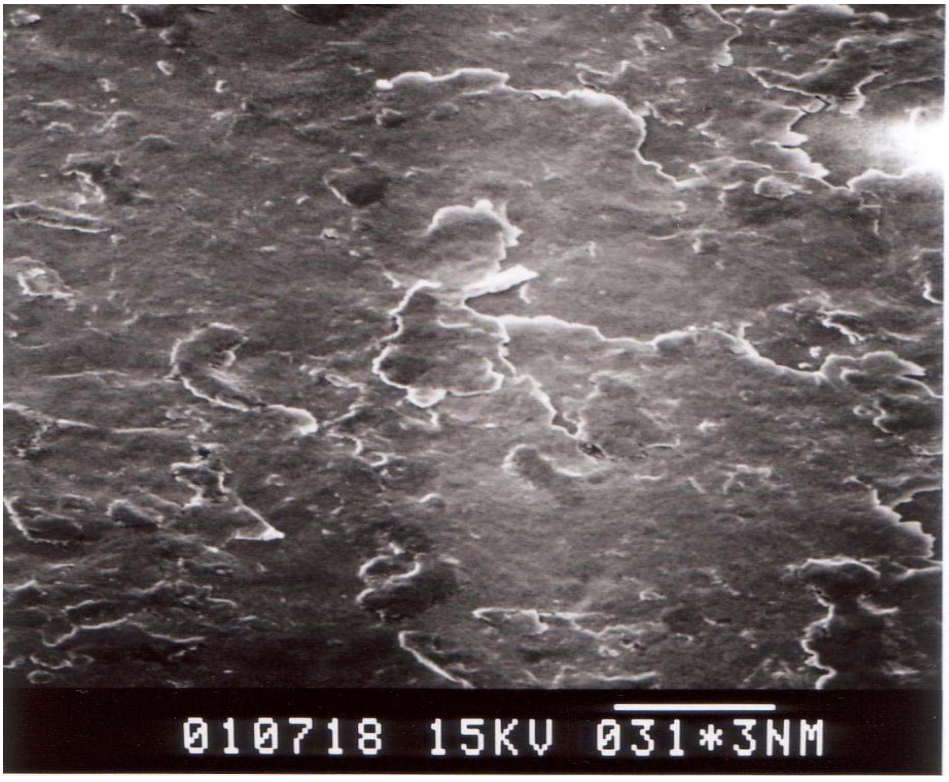


Figure 4.50 Sample 2b: 20 minute X500

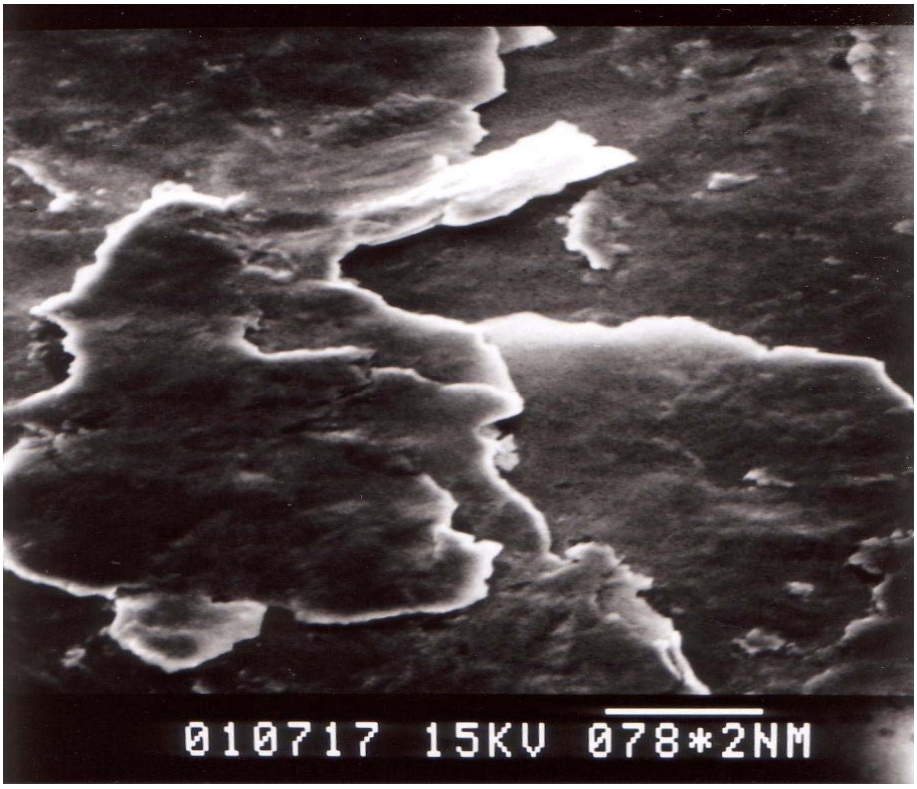


Figure 4.51 Sample 2b: 20 minute X2000

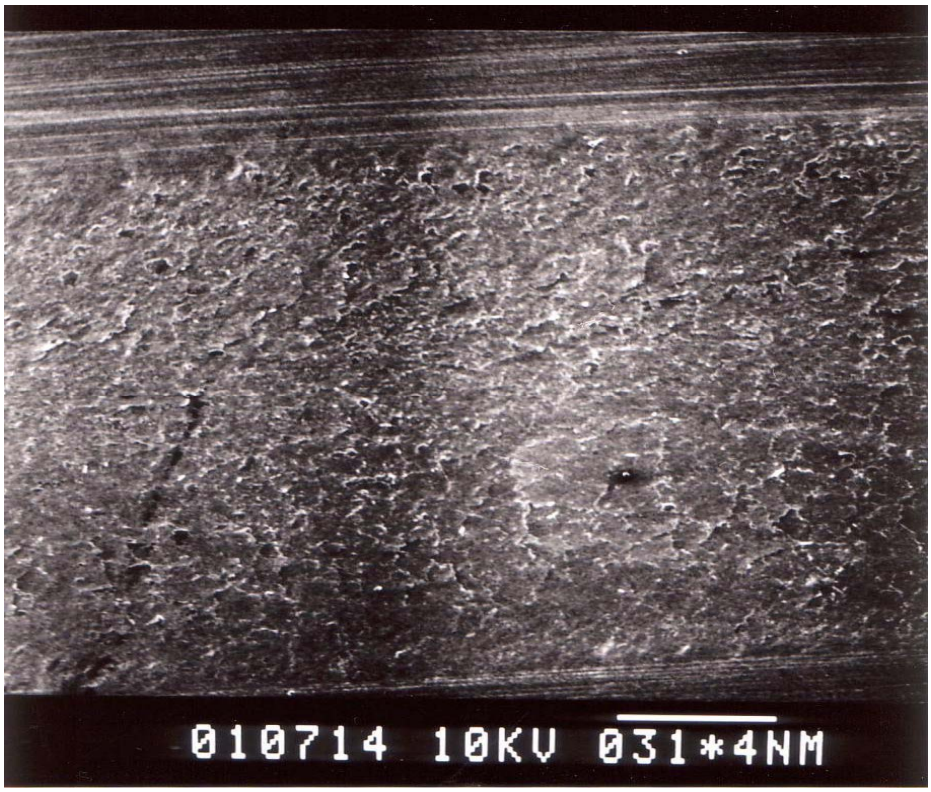


Figure 4.52 Sample 2c: 35 minute X50

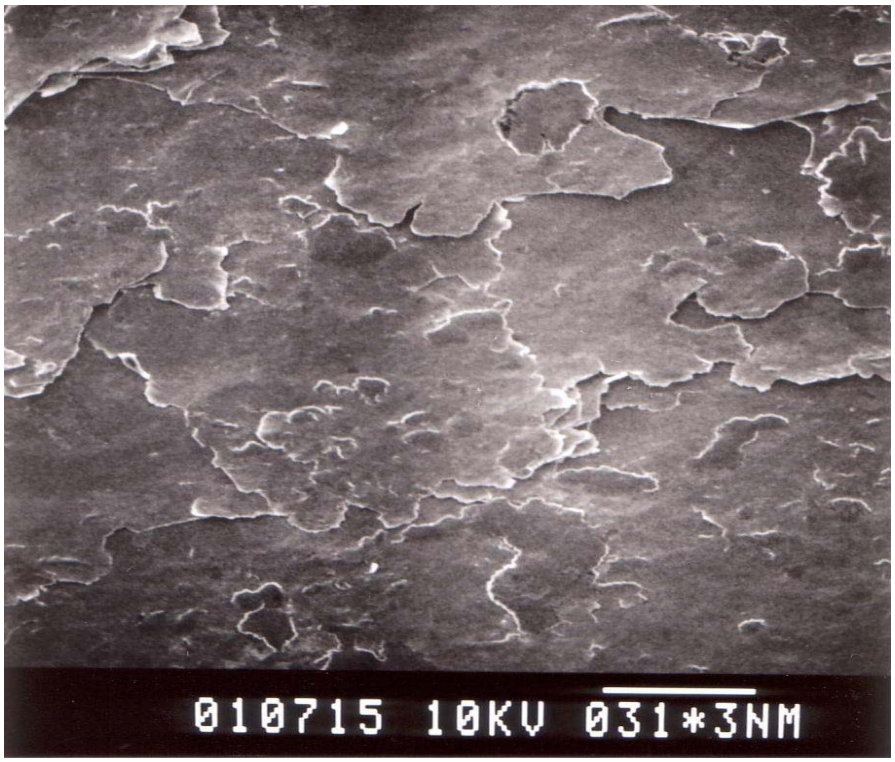


Figure 4.53 Sample 2c: 35 minute X500

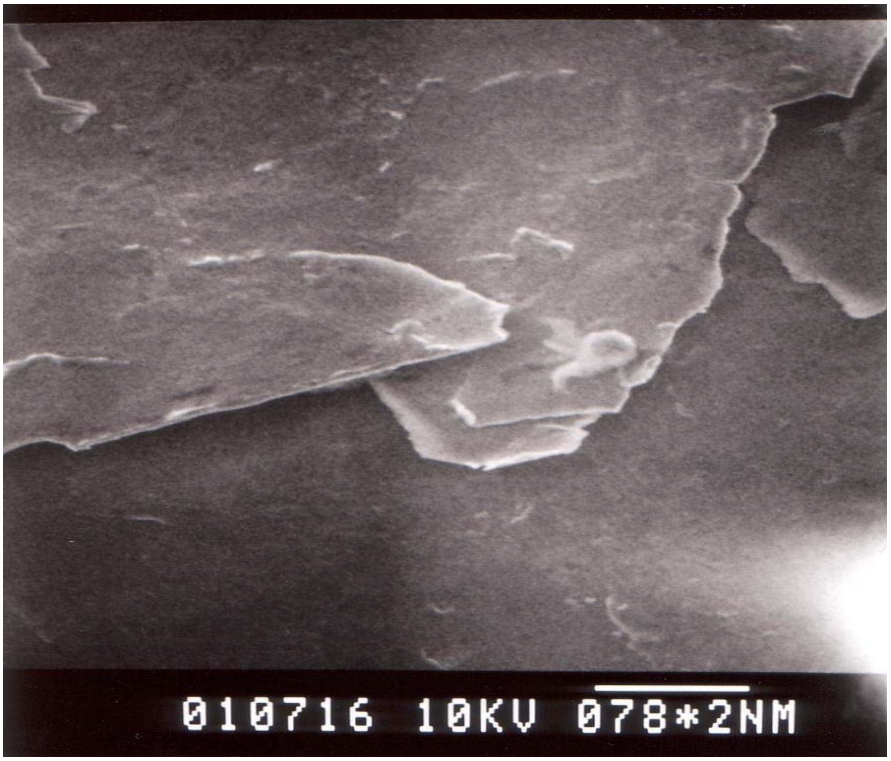


Figure 4.54 Sample 2c: 35 minute X2000. High magnification view of the Thin Flat Flakes developed during wear.

Tables 4.21 and 4.22 are the Mass Loss and Mass data for Experiment F.

| Sample No | Duration (Min) | Mass Loss of Rod (g) |
|---|---|---|
| a1 | 1 | 0 |
| a2 | 5 | 0 |
| a3 | 10 | 0.0007 |
| b1 | 15 | 0.0002 |
| b2 | 20 | 0.001 |
| b3 | 25 | 0.0021 |
| c1 | 30 | 0.0044 |
| c2 | 35 | 0.0059 |
| c3 | 40 | 0.0097 |
| d1 | 45 | 0.004 |
| d2 | 50 | 0.0079 |
| d3 | 55 | N/A |

Table 4.21 - Mass loss vs. time for Experiment F (450N)

Table 4.2.2 Experiment F Mass Loss Data

| EXPERIMENT F - Results | | | | | | | | | |
|---|---|---|---|---|---|---|---|---|---|
| | | | | | | | | | |
| | | | | BEFORE TEST | | | AFTER TEST | | |
| Sample No | Duration (Min) | Speed (Hz) | Load (N) | Mass Rod (g) | Mass Ball 1 (g) | Mass Ball 2 (g) | Mass Rod (g) | Mass Ball 1 (g) | Mass Ball 2 (g) |
| a1 | 1 | 7.5/7.2 | 450 | 52.2942 | 66.8161 | 66.8212 | 52.2946 | Not Recorded | Not Recorded |
| a2 | 5 | 7.5/7.2 | 450 | 52.2946 | 66.8129 | 66.8176 | 52.2947 | Not Recorded | Not Recorded |
| a3 | 10 | 7.5/7.2 | 450 | 52.2947 | 66.8176 | 66.8177 | 52.294 | Not Recorded | Not Recorded |
| b1 | 15 | 7.5/7.2 | 450 | 52.9898 | 66.8153 | 66.7888 | 52.9896 | Not Recorded | Not Recorded |
| b2 | 20 | 7.5/7.2 | 450 | 52.9896 | 66.818 | 66.7898 | 52.9886 | Not Recorded | Not Recorded |
| b3 | 25 | 7.5/7.2 | 450 | 52.9886 | 66.8333 | 66.8171 | 52.9865 | Not Recorded | Not Recorded |
| c1 | 30 | 7.5/7.2 | 450 | 51.8005 | 66.8176 | 66.8165 | 51.7961 | Not Recorded | Not Recorded |
| c2 | 35 | 7.5/7.2 | 450 | 51.7961 | 66.787 | 66.8123 | 51.7902 | Not Recorded | Not Recorded |
| c3 | 40 | 7.5/7.2 | 450 | 51.7902 | 66.8138 | 66.8134 | 51.7805 | Not Recorded | Not Recorded |
| d1 | 45 | 7.5/7.2 | 450 | 52.5749 | 66.791 | 66.8146 | 52.5709 | Not Recorded | Not Recorded |
| d2 | 50 | 7.5/7.2 | 450 | 52.5709 | 66.8147 | 66.8281 | 52.563 | Not Recorded | Not Recorded |
| d3 | 55 | 7.5/7.2 | 450 | 52.563 | 66.8205 | 66.8237 | Not completed | Not Recorded | Not Recorded |

### 4.4.4 Subsurface SEM Scanning Electron Microscope Observations for 52100 Bearing Steel Wear Track.

To obtain an understanding of the origin of the flat flake - like sheets observed in the SEM micrographs of the wear surface, Sub-surface SEM was performed. Sample 55 minutes of Experiment E was sectioned at the wear track and studied in detail. Figure 4.55 shows the SEM micrograph at low magnification for the section though the wear track of 55 minute sample from Experiment E.

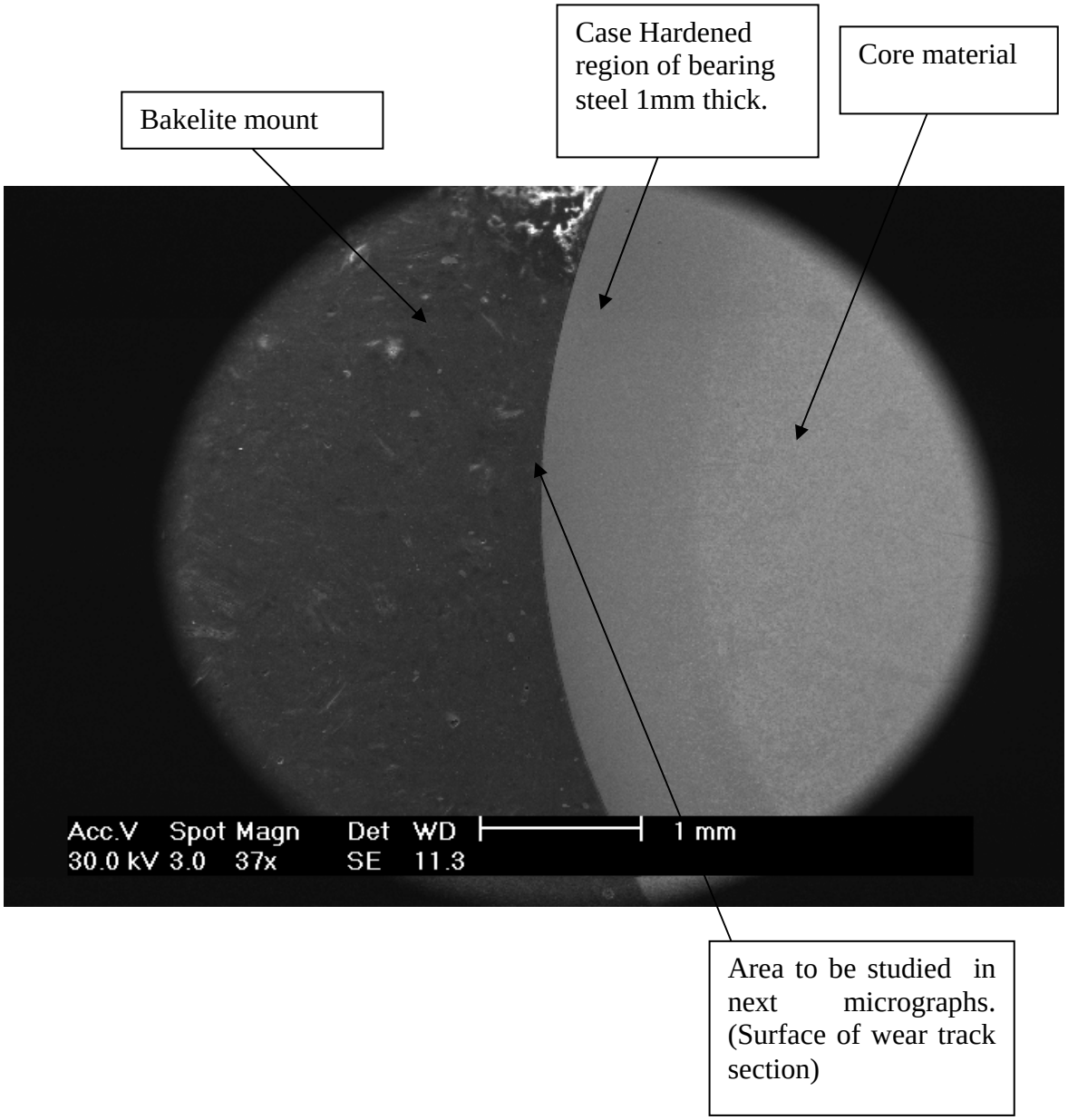


Figure 4.55 - SEM Micrograph of section through Wear Track in 55 minute sample of Experiment E.

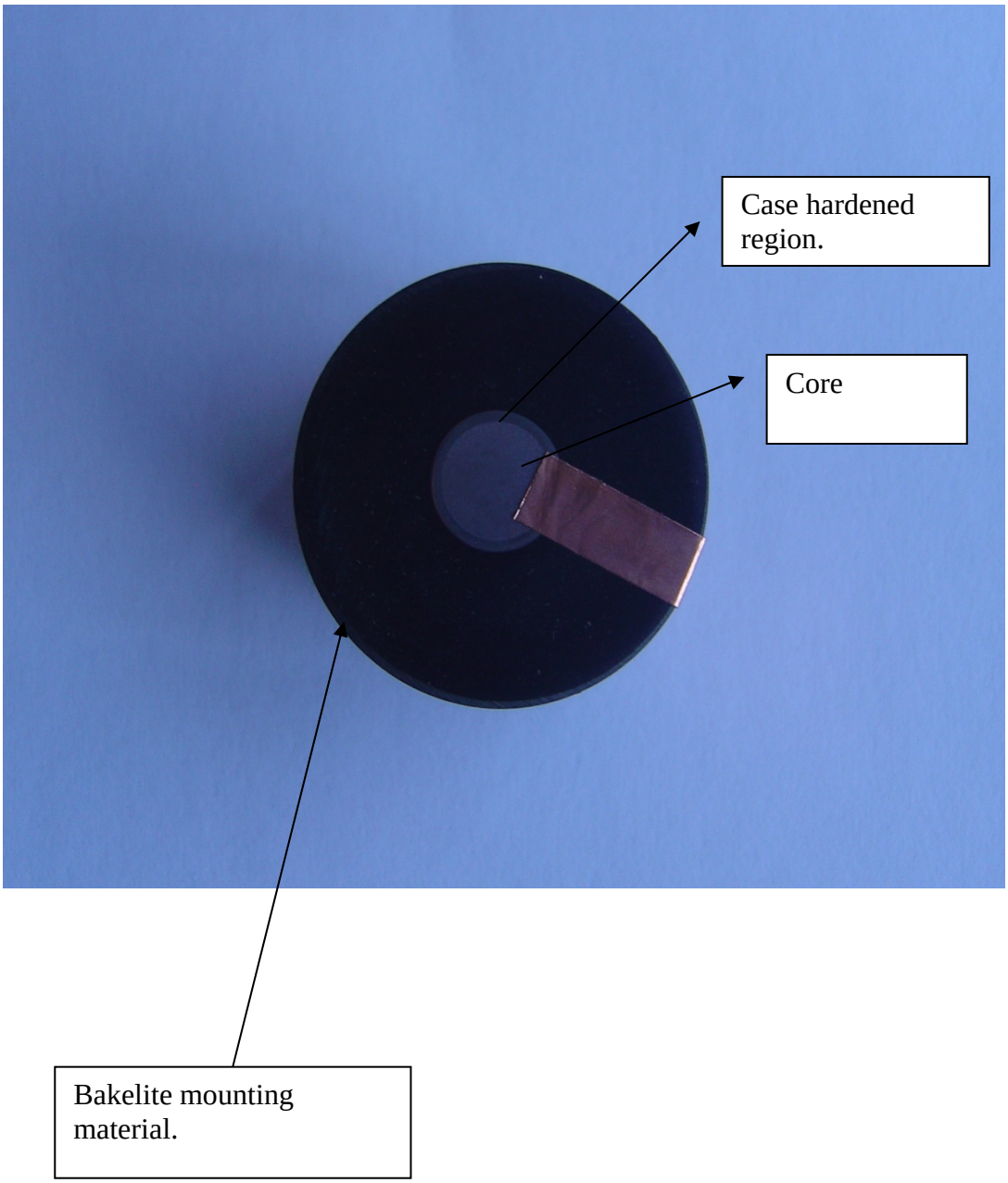


Figure 4.56 - Polished and Mounted Section through Wear Track in 55 minute sample of Experiment E

#### 4.4.4.1 Sub-Surface Examination

Figures 4.57 shows that the cracks originate at a distance below the surface in the case hardened part of the structure. They are typically 10µm below the surface and once they reach the surface produce thin flat sheets as seen in wear track SEM observations of Figure 4.54 Section 4.4.3.2. Hard inclusions below the surface can also become the preferred site for crack initiation as shown in Figures 4.60 and 4.61. Figures 4.58 and 4.59 show magnified views of the flat flakes to be dislodged and the size of the plastically deformed region of the material.

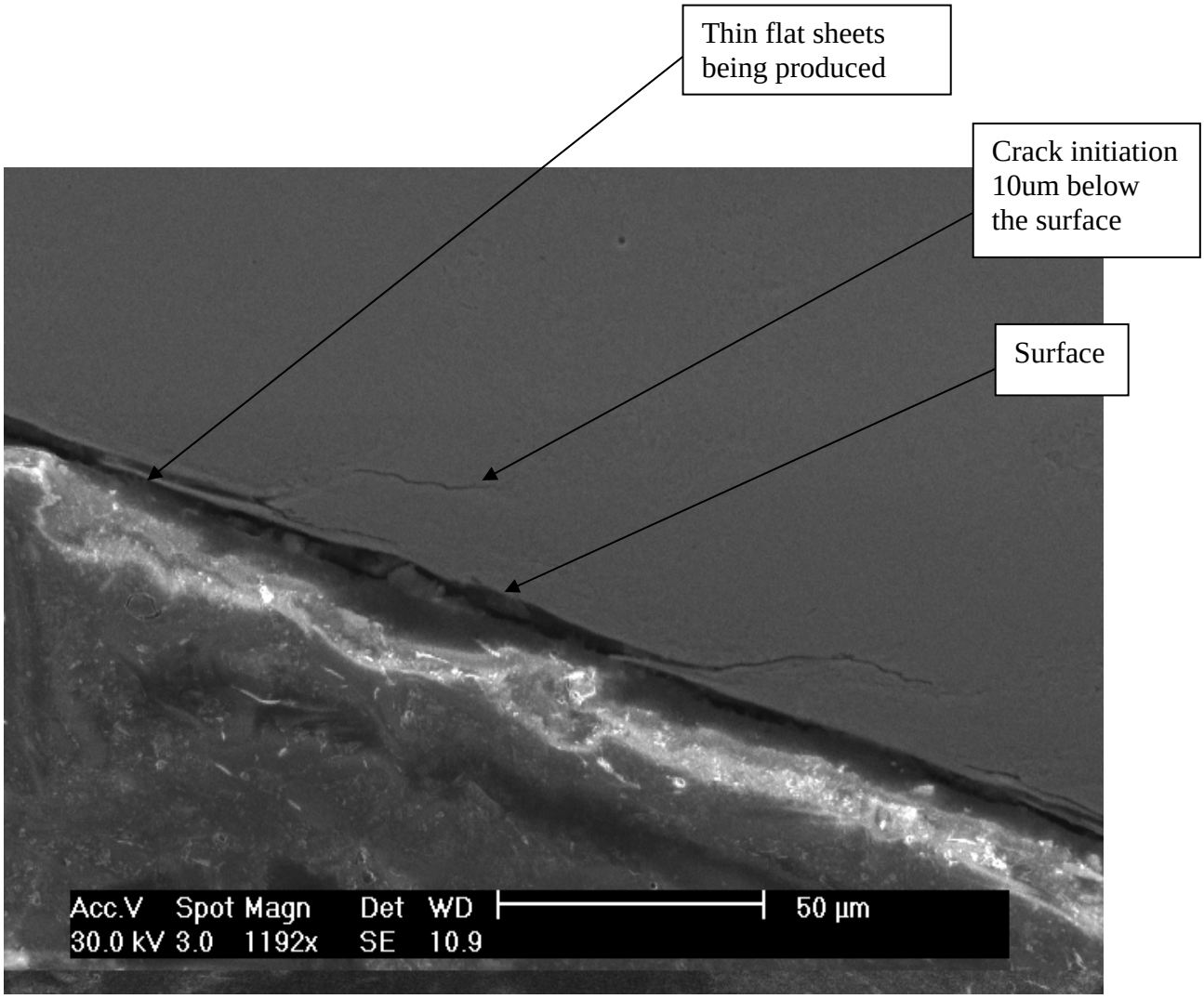


Figure 4.57- Micrograph of 55 minute sample Sub-Surface of Experiment E. Cracks originate 10µm below the surface in the 55 minute sample.

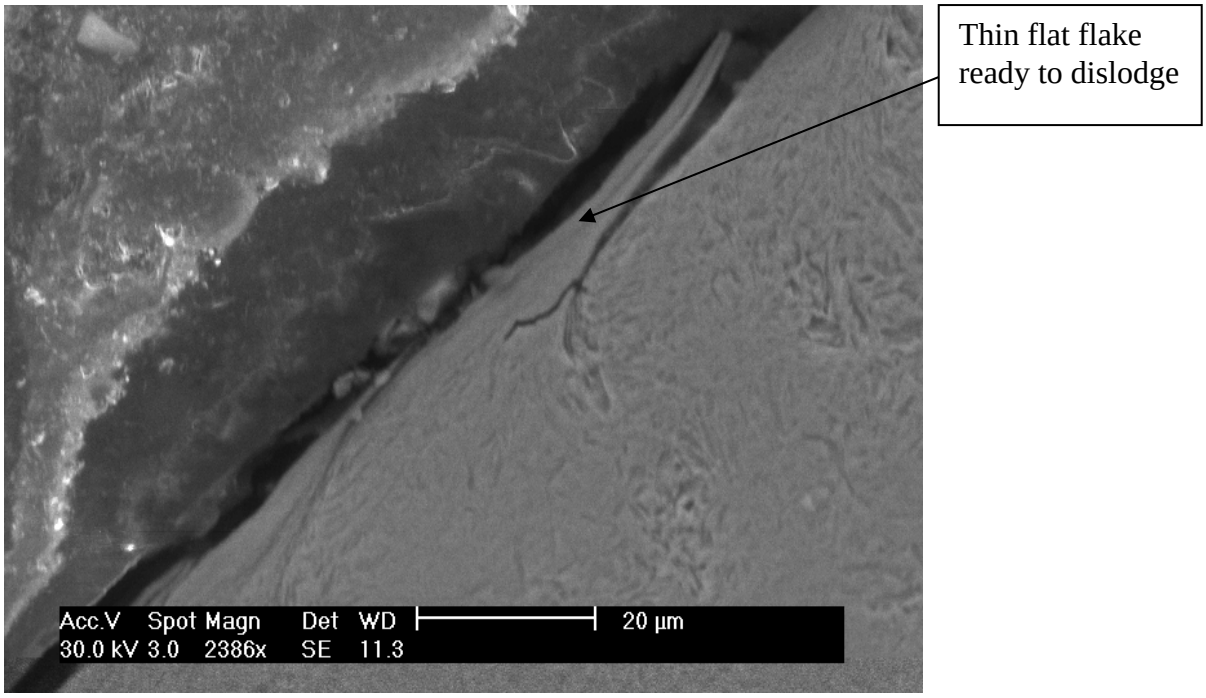


Figure 4.58 - Thin Flat Flake ready to be dislodged. Dimension of Flake is 40µm in length, 5µm in height.

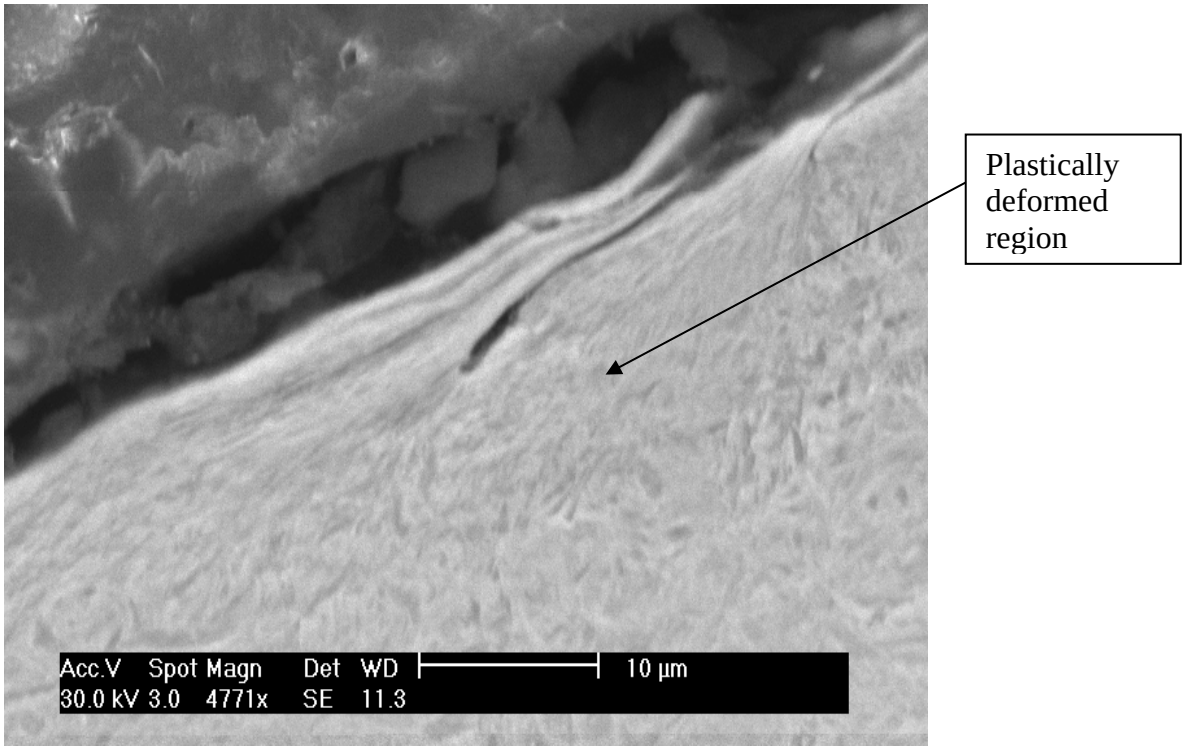


Figure 4.59 Magnified view of Thin Flake. Micrograph also shows plastically deformed zone of material extends 37µm below the surface.

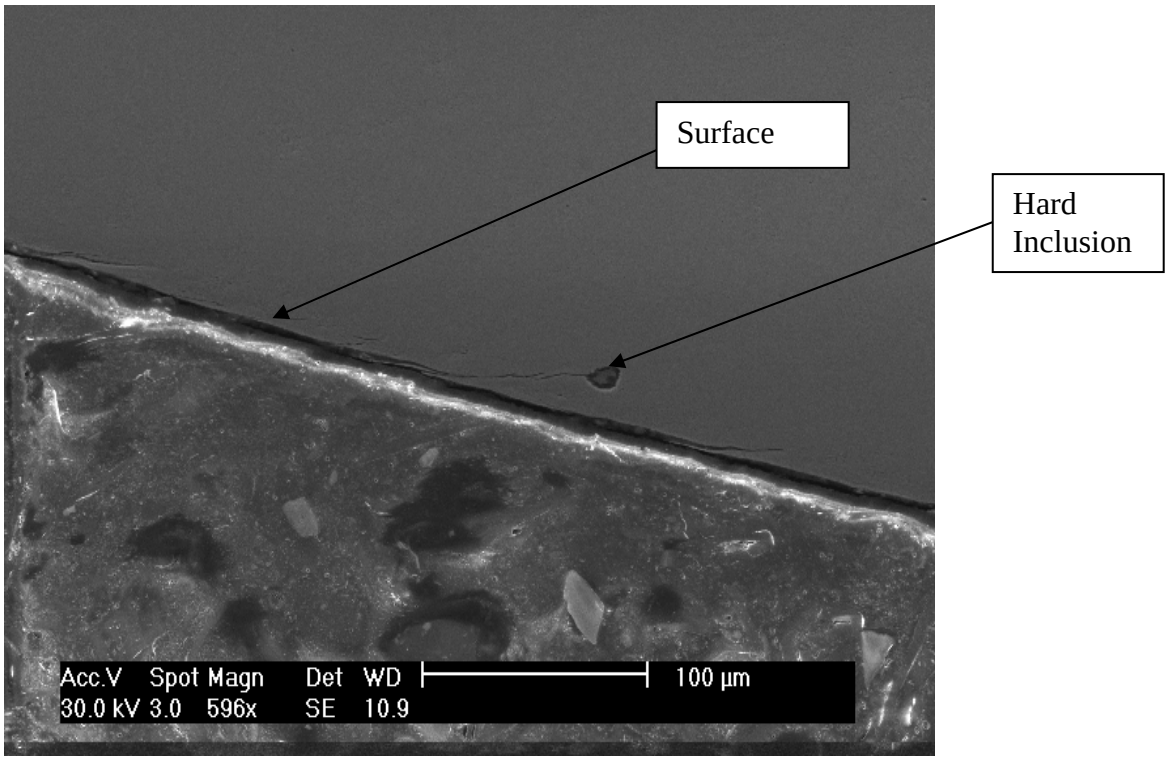


Figure 4.60 Hard Inclusion 10µm-15µm below the surface becomes the preferred site for crack initiation.

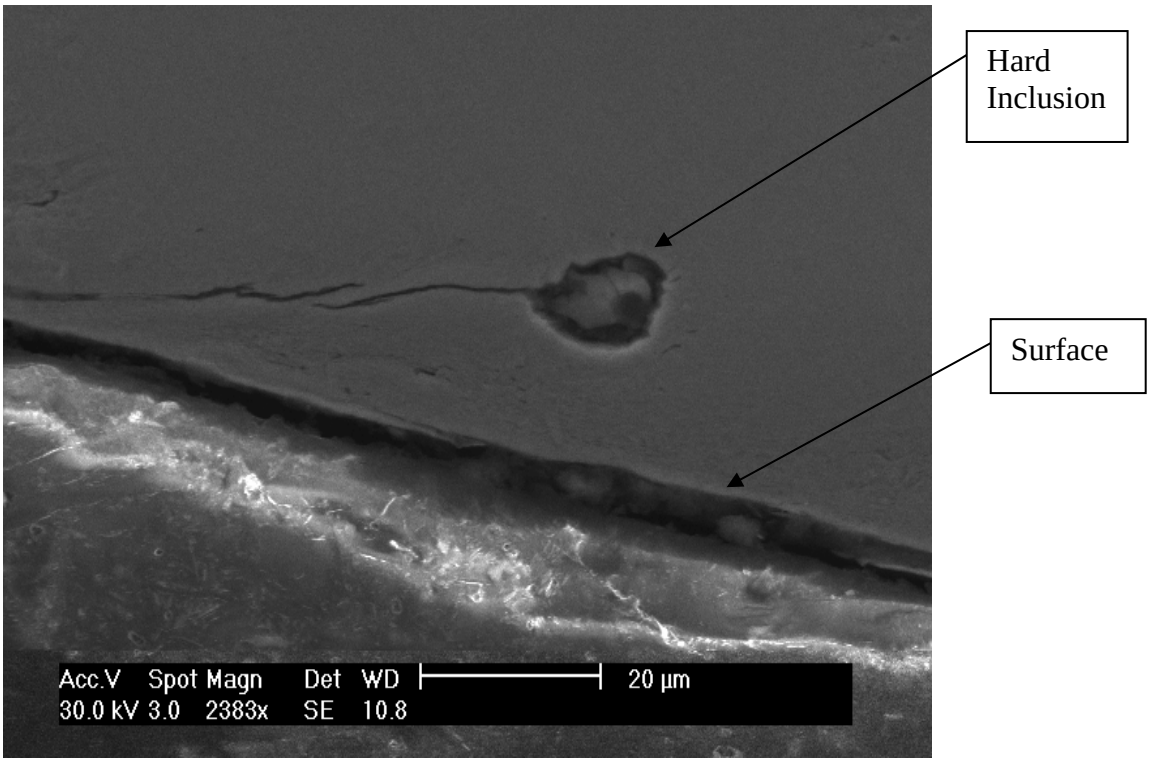


Figure 4.61 Magnified view of Hard Inclusion and location of crack initiation below the surface.

## 4.5 Experiment G – Wear vs. Duration and Load for Ceramic Rod on Steel Balls.
## (OA-Mg-PSZ Ceramic Sample at 300N and 750N Load)

In Experiment G, 52100 steel balls simulating the inner and outer race of a bearing were loaded against a 12mm diameter Partially Stabilized Zirconia (PSZ) ceramic rod at 300N and 790N loads. The test rig described in Section 3 was used for this test.

The purpose of Experiment G was to establish mass loss and wear depth data for the ceramic rod at various loads. Wear tracks on the PSZ ceramic rods are shown in Figure 4.62. Data was compared to that obtained for steel samples of Experiment A and B. The wear values for ceramic rods were an order of magnitude lower than that obtained for steel rods. The comparison is shown in Graph 4.12. Due to the long duration of the ceramic tests it was not possible to repeat tests several times to confirm error bars thus the data needs to be treated as trends. The trend shows that mass loss and wear depth increase with duration and load. The profilometer traces show that the wear scar for PSZ ceramic is smoother than that for the steels. The wear as seen in the SEM micrographs shows highly polished surface with material being removed in fatigue spallations.

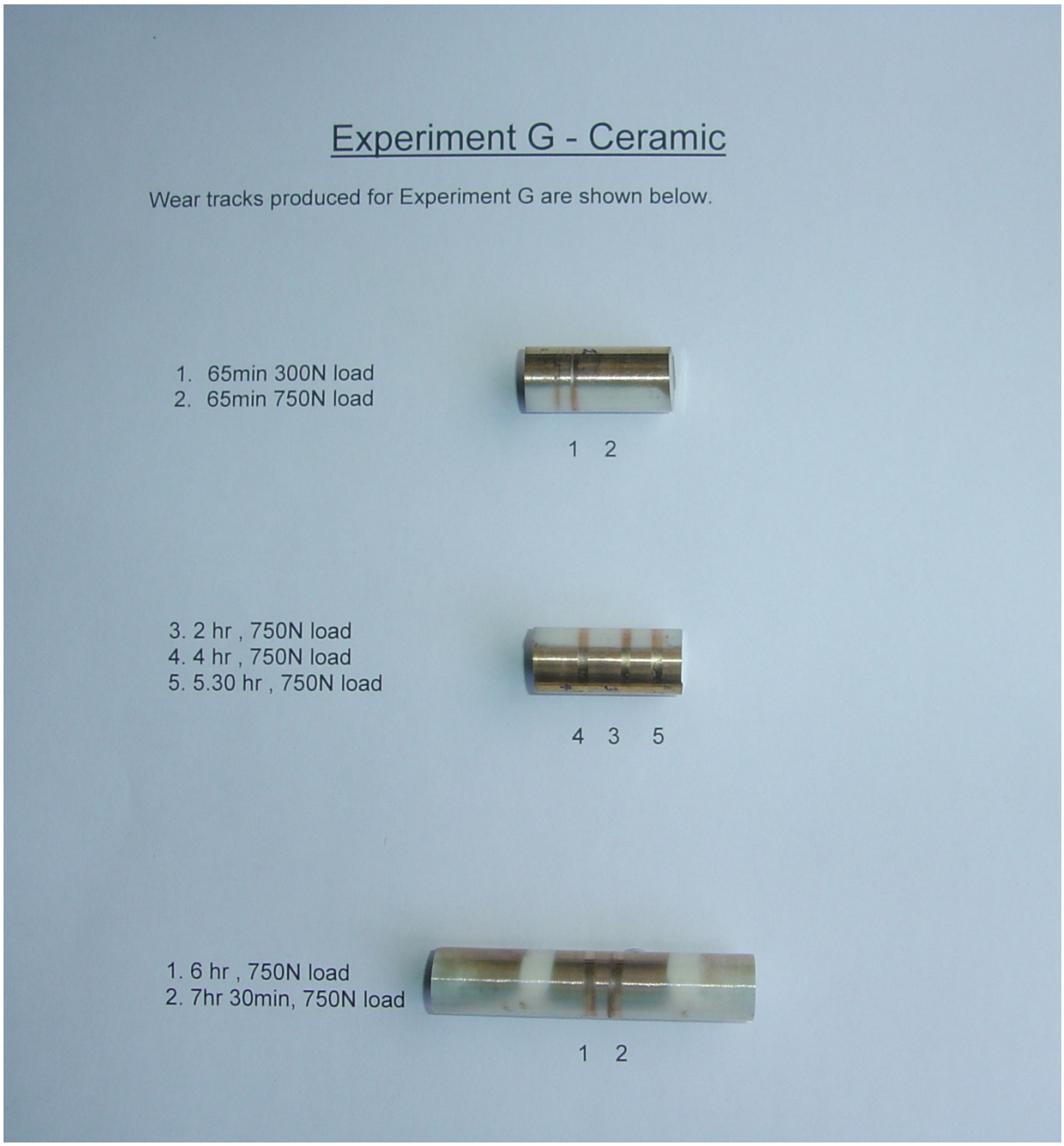


Figure 4.62 Wear Tracks on test samples for PSZ Ceramic - Experiment G.

### 4.5.1 Mass Loss – Experiment G

For each test the mass of the PSZ ceramic sample before and after the test was measured. The mass data for each test is recorded in Tables 4.24 and graphed in Graph 4.11. Graph 4.12 shows a comparison between mass loss data from previous steel tests and the ceramic results.

| | | | Mass of sample (grams) | | |
|---|---|---|---|---|---|
| Sample No | Load (N) | Duration (Minutes) | BEFORE (Mass grams) | AFTER (Mass grams) | Mass Loss (grams) |
| 1 | 300 | 65 | 42.4659 | 42.4657 | 0.0002 |
| 2 | 790 | 65 | 42.4657 | 42.4651 | 0.0006 |
| 3 | 790 | 120 | 42.0147 | 42.0132 | 0.0015 |
| 4 | 790 | 262 | 42.0132 | 42.01 | 0.0032 |
| 5 | 790 | 330 | 42.01 | 42.0072 | 0.0028 |

Table 4.24 - Mass Loss data for PSZ Ceramic at 300N and 790N Load

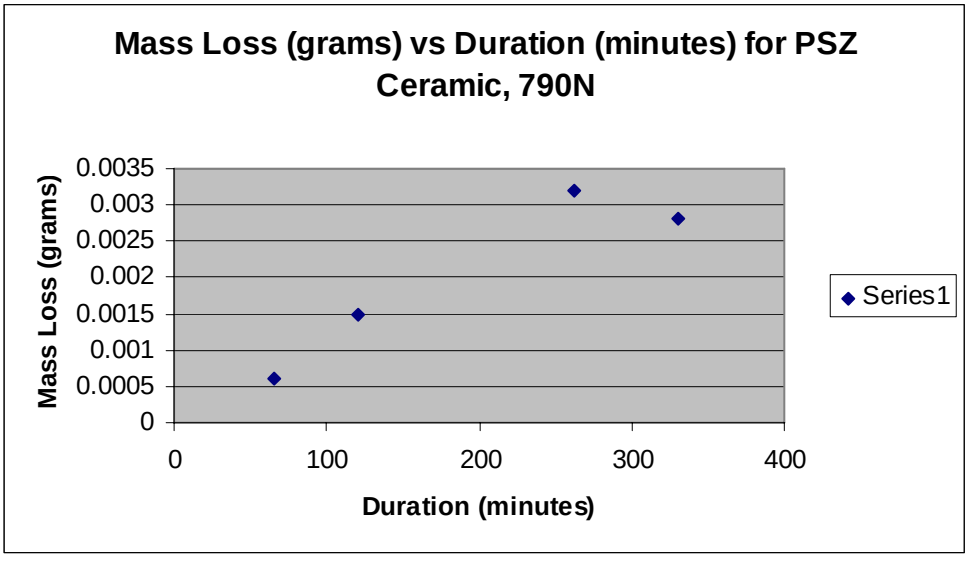


Graph 4.11 – Mass Loss (grams) vs. Duration (minutes) for PSZ Ceramic at 790N.

It is noted that the 330 minute duration sample has a lower value than the 262 minute sample. This does not correlate with wear depth data from the profilometer measurements in the next section which clearly show an increase in wear.

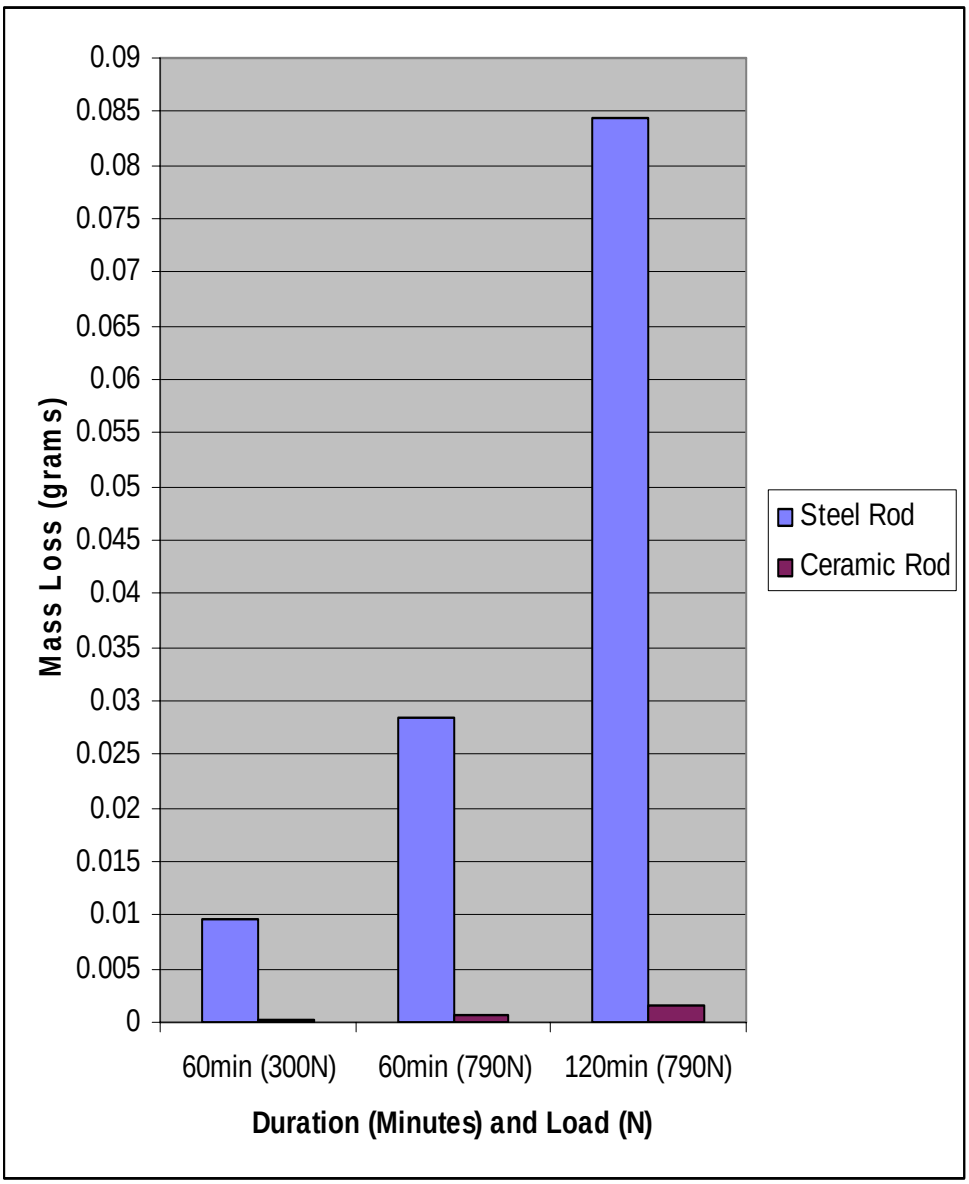


Graph 4.12 Comparison of mass loss for 52100 steel rods and PSZ ceramic rods in rolling contact at 300N and 790N loads. There is an order of magnitude difference in mass loss data with ceramic rods being the lower value.

### 4.5.2 Wear Depth – Experiment G

A profilometer was used to measure the wear depth for the wear tracks produced in Experiment G. The method used is detailed in Section 3. The profilometer traces are shown in Figures 4.63 – 4.65 for each of the tests conducted. Table 4.23 is a summary of the wear depth results. The data is plotted in Graph 4.13.

| Sample No | Load (N) | Duration (Minutes) | Wear Depth (um) |
|---|---|---|---|
| 2 | 790 | 65 | 3.8 |
| 3 | 790 | 120 | 6.6 |
| 4 | 790 | 262 | 8.3 |
| 5 | 790 | 330 | 10 |
| 1 (New rod) | 790 | 360 | 12.7 |
| 2 (New Rod) | 790 | 420 | 17.1 |

Table 4.23 - Wear Depth data for PSZ Ceramic, Experiment G, 790N

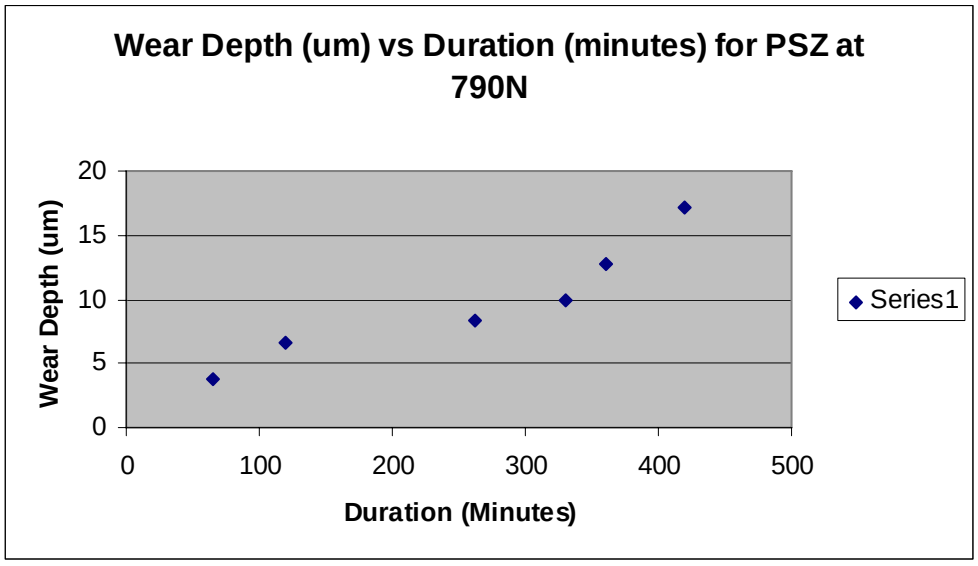


Graph 4.13 – Wear Depth (µm) vs. Duration for PSZ Ceramic, Experiment G, 790N

Graph 4.13 shows as duration / number of cycles increases the wear depth increases

**Experiment G – Profilometer Traces**

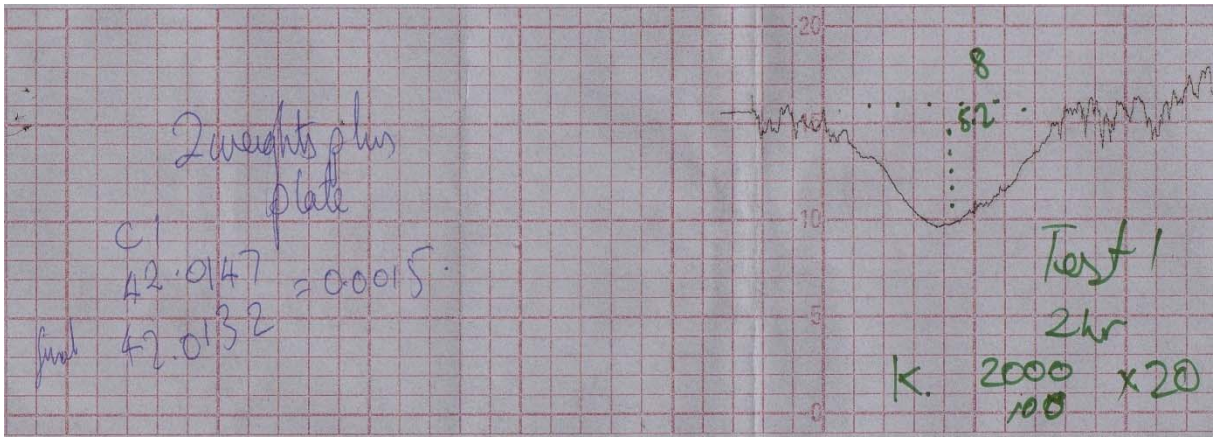


Figure 4.63 - Profilometer 120 minute Duration, 790N Load

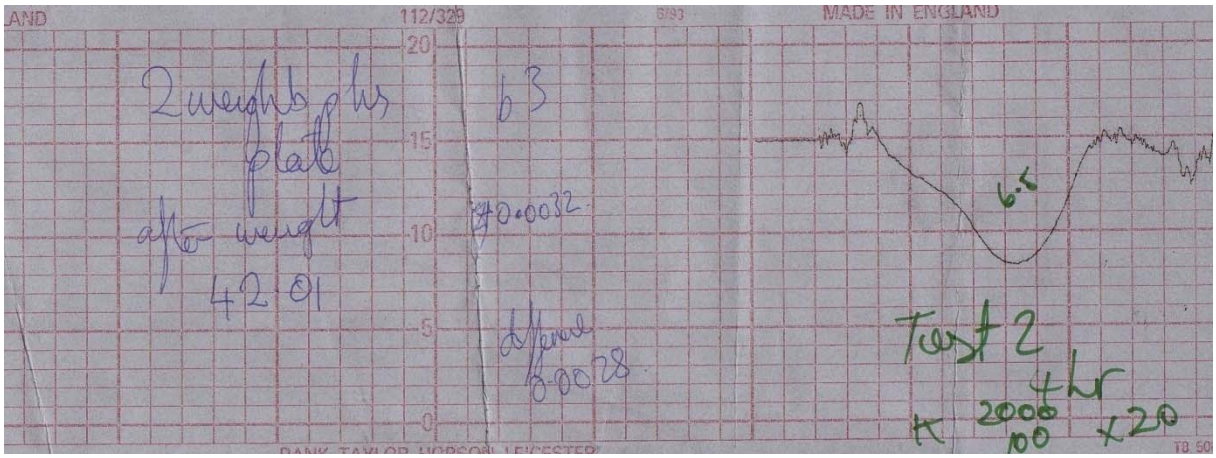


Figure 4.64 - Profilometer 262 minute Duration, 790N Load

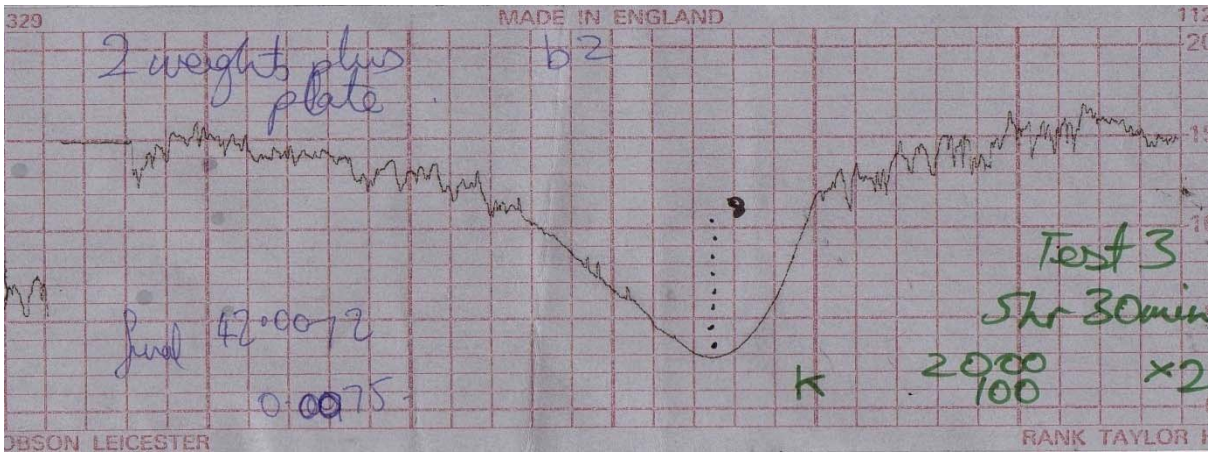


Figure 4.65 - Profilometer 330 minute Duration, 790N Load

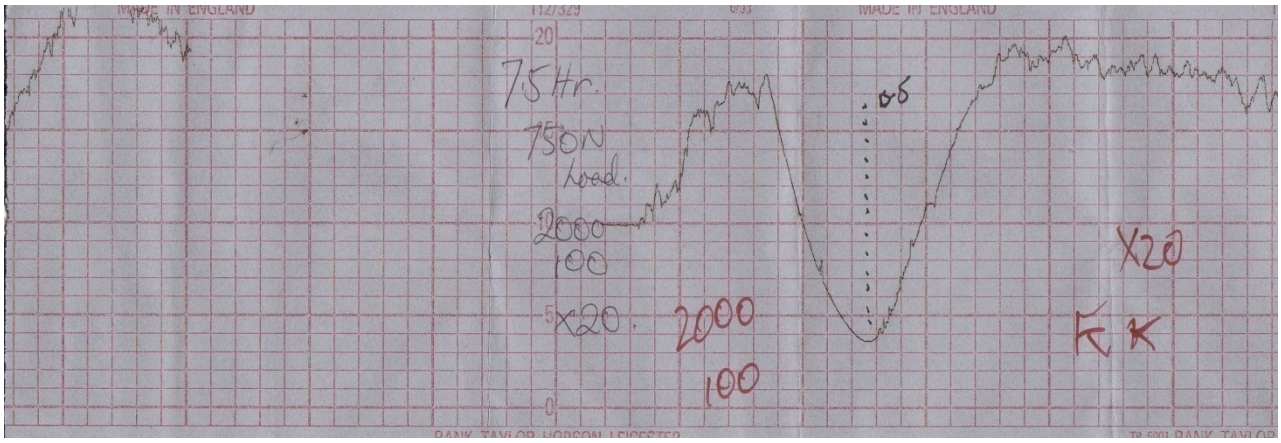


Figure 4.65 - Profilometer  420 minute Duration, 790N Load

Profilometer traces of the PSZ ceramic show a significantly smoother finish to the wear track compared to that of the steel samples of Experiments A, B, C.

### 4.5.3 Scanning Electron Microscope Observations for Experiment G, Mg-PSZ Ceramic on Steel at 790N load.

Observations – Wear Track Surface

Figures 4.66 to 4.71 show wear tracks of PSZ ceramic under rolling contact at 790N load. Figures 4.66 and 4.67 of 105 minute sample show original grinding marks of the surface have been removed and debris from the 52100 steel balls is present. There are long arc steaks that have yet to be identified. Figures 4.68 and 4.69 in the 120min sample show similar results. Figures 4.70 and 4.71 in the 330min sample show a highly polished surface with debris no longer present. The figures also show removal of material by a fatigue spallation.


Figure 4.66 - Sample 2, 105min, 790N Load, X50. Grinding marks removed, Debris from Steel Balls on surface.

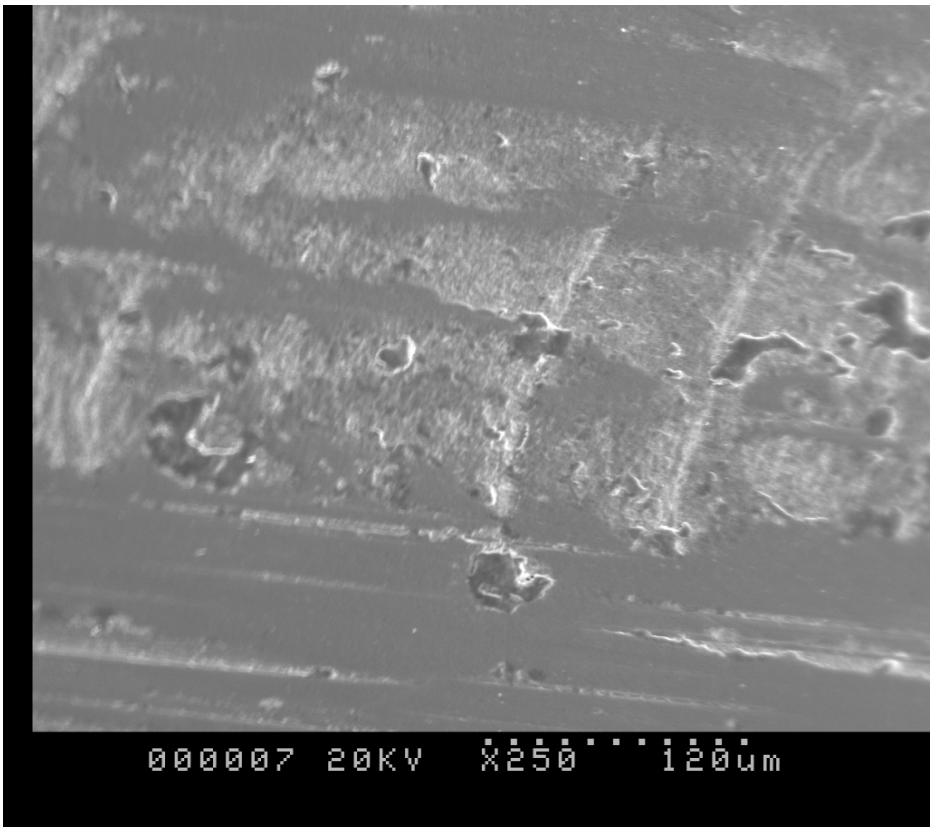


Figure 4.67 - Sample 2, 105min, 790N Load, X250


Figure 4.68 Sample 3, 120min, 790N Load, X50

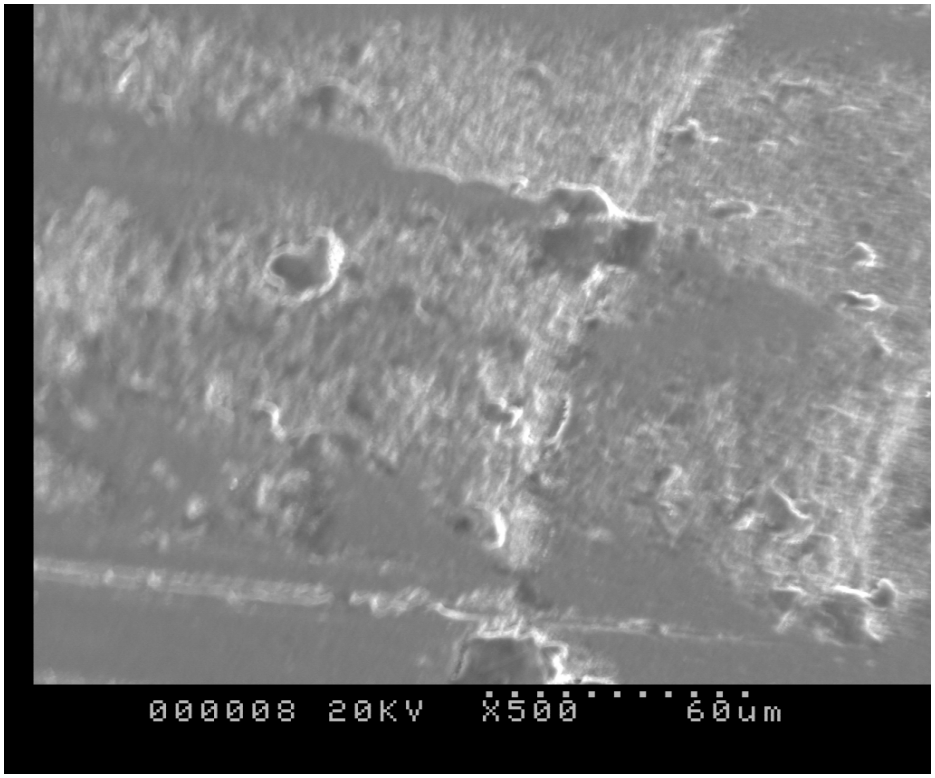


Figure 4.69 Sample 3, 120min, 790N Load, X500


Figure 4.70 Sample 1, 330 min, 790N load. Highly polished surface with Fatigue Spallation.

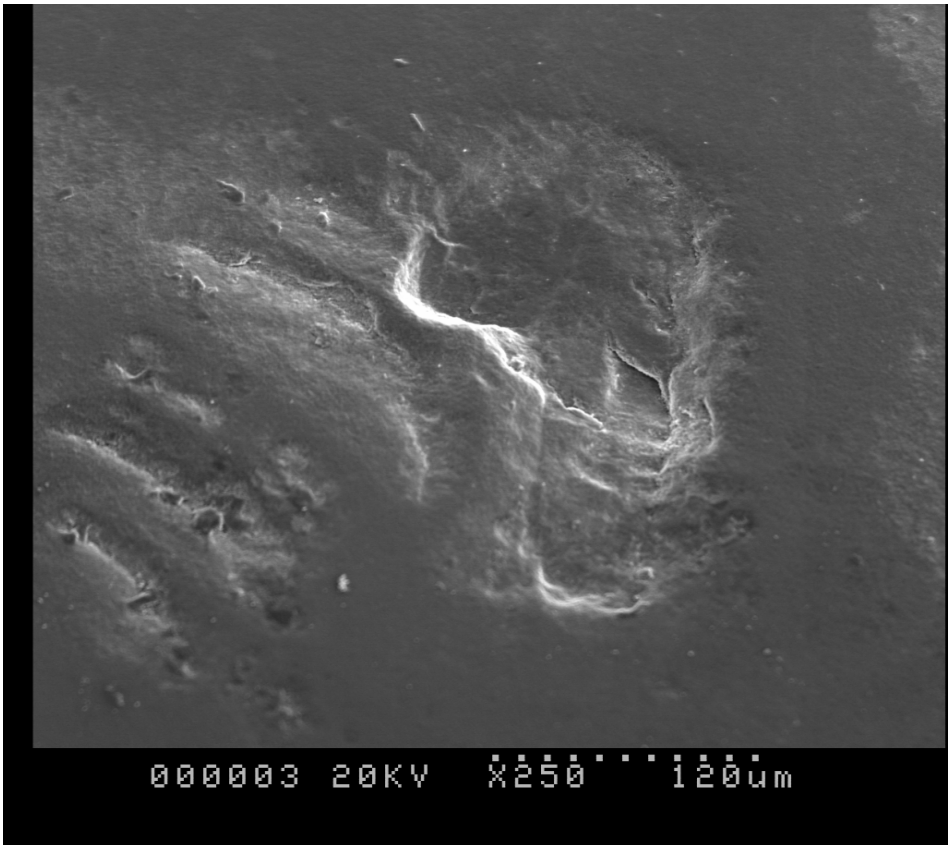


Figure 4.71 Sample 1, 330min 790N load, X250.

# Chapter 5
# Discussion

In this section the results of Section 4 are reviewed and discussed.

In this investigation the mass loss and wear depth at varied test loads and test durations were measured for 52100 bearing steel in rolling contact with 52100 bearing steel to simulate a standard steel ball bearing. To simulate a hybrid bearing the mass loss and wear depth were measured for 52100 bearing steel in rolling contact with OA-Mg-PSZ ceramic. In both cases the wear scar profile was also recorded using a talysurf profilometer. These results were presented in the previous Section 4.

These measurements and recordings allow wear to be quantified. In the discussion to follow mass loss (grams) is used to quantify the amount of wear. The wear scar profiles (wear volume ($mm^3$)) recorded by the talysurf profilometer could have also been used to quantify wear but for simplicity mass loss is used as they both show similar trends in behavior throughout Section 4.0. It should be noted that wear depth (mm) alone should not be used for comparison of wear behavior at varied loads. This is based on the results in Section 4.2.2 which showed that wear scar shape changes dramatically when load is increased due to change in width of wear groove rather than the wear depth. This indicates that wear volume would be fine to quantify wear and make comparisons at given loads as it takes into account wear depth as well as the width of the wear groove. Wear height alone is not sufficient to quantify wear.

## 5.1 Wear Behavior (Mass Loss) of 52100 Bearing Steel and OA-Mg-PSZ

Graph 4.4 in Section 4 showed the Mass Loss (grams) vs. Duration (minutes) at 300N, 450N and 790N for 52100 bearing steel. The graph shows that at any given load as the duration / no of cycles increases the mass loss increases. The gradient (rate of mass loss) increases as the load is increased.

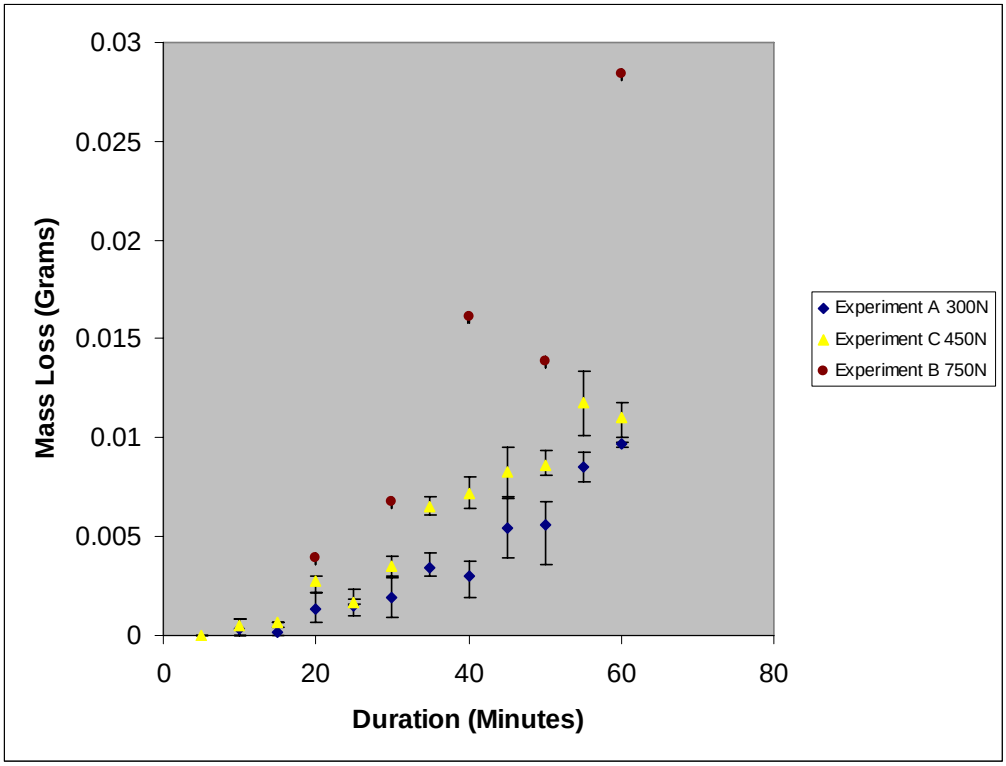


Graph 5.1 - Mass Loss (grams) vs. Duration (Minutes) at 300N, 450N & 790N. (Repeat of Graph 4.4 in Section 4.0)

Mass loss results for OA-Mg-PSZ ceramic at 300N and 790N loads were recorded in Table 4.24 and charted in Graph 4.11 of Section 4.0. The results also showed that at a given load the mass loss increases proportionally to test duration / no of cycles. A comparison of the mass loss of 52100 bearing steel vs. OA-Mg-PSZ ceramic at varied loads and test duration was shown in Graph 4.12 of Section 4.0. Graph 4.12 shows that the mass loss of OA-Mg-PSZ is at least one order of magnitude lower than that of the 52100 bearing steel.

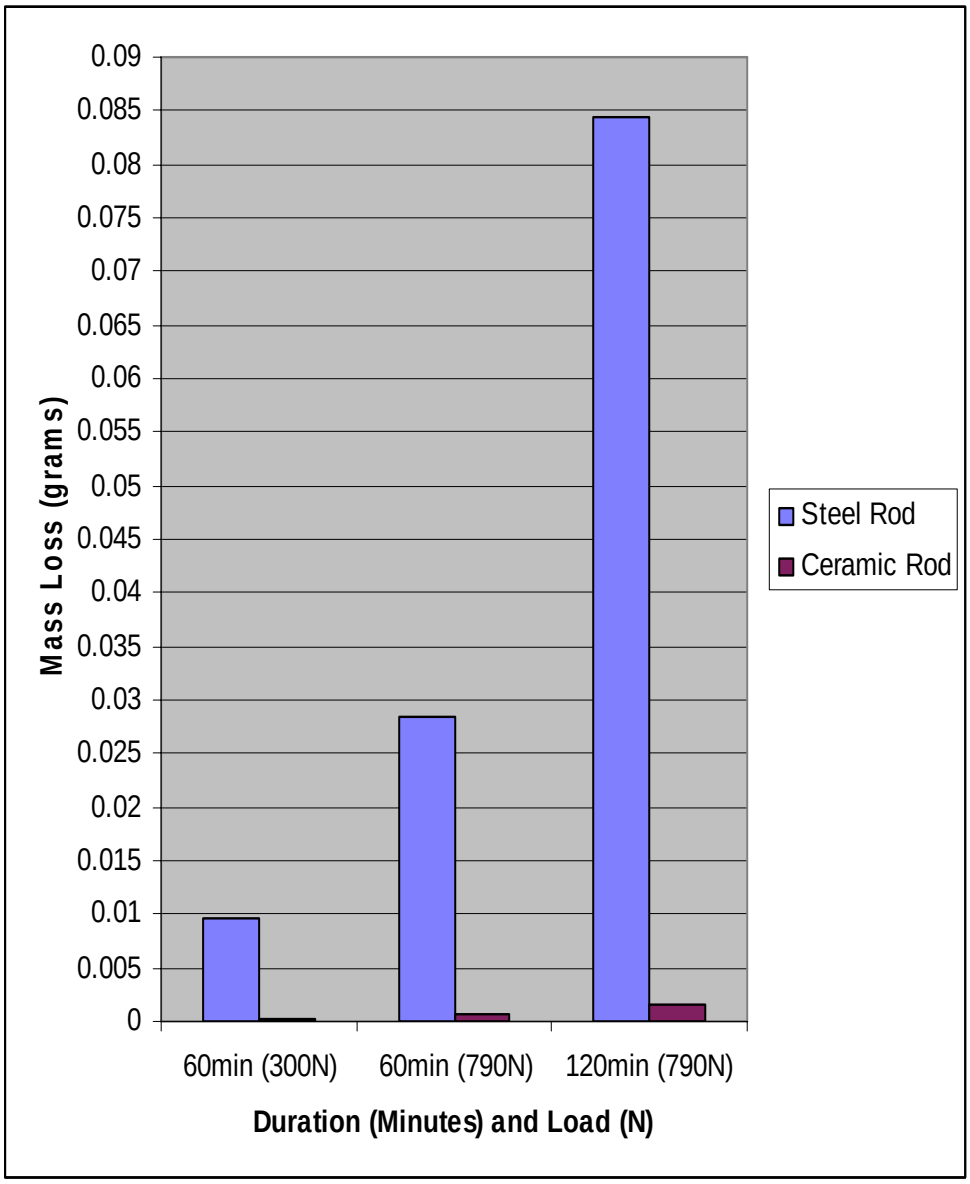


Graph 5.2 Comparison of Mass Loss for 52100 Steel Rods and OA-Mg-PSZ Ceramic Rods in Rolling Contact at 300N and 790N Loads. (Repeat of Graph 4.12 Section 4.0)

## 5.2 Wear Mechanism for Rolling Contact Wear of 52100 Bearing Steel in Contact with 52100 Bearing Steel, (Standard Steel Bearing)

SEM micrographs 4.28 - 4.47 showed the progressive change in surface features as wear progresses.

During the first 5 minutes of the tests, elastic plastic deformation on the scale of the surface asperities, results in change of surface quality. During these initial stages of wear, asperity polishing occurs by removal of initial grinding marks (Figure 4.30). This wear mechanism is either by adhesive and/or abrasive wear modes as discussed in Sections 2.3.1.1 and 2.3.1.2. After a short no. of cycles, typically 5 minute test duration as shown in Figure 4.33, the wear mode changes and surface cracking appears. Sub-surface examination of a sample at 450N was shown in Figure 4.57, revealed that the cracks originate at a distance below the surface. The distance was measured to be 10µm for a 55 minute test sample.

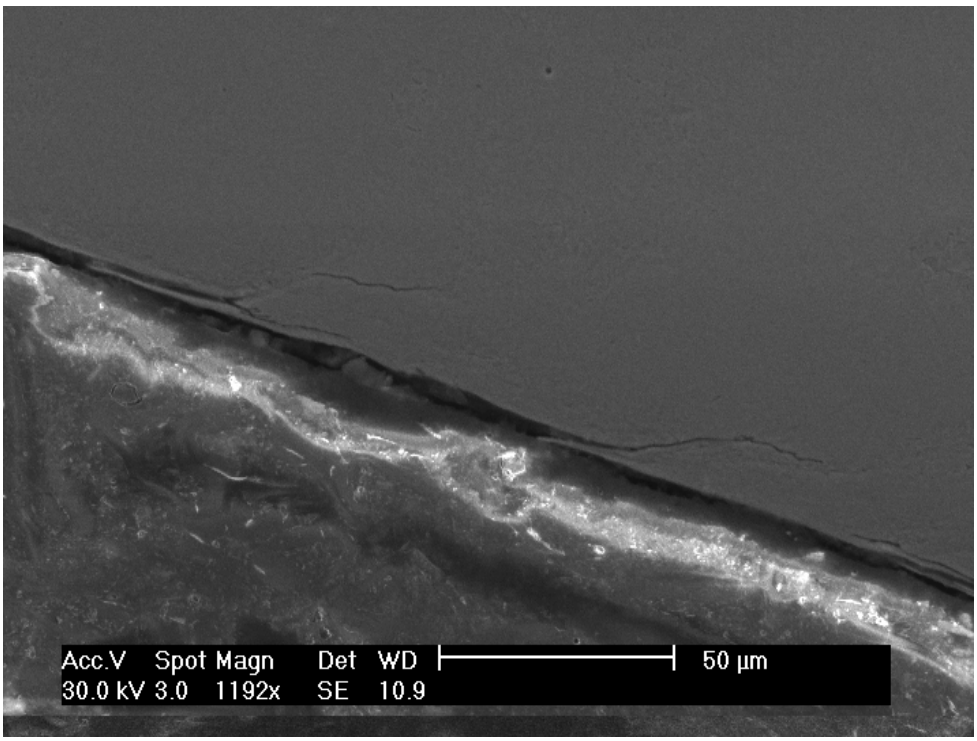


Figure 5.1 (Repeat of Figure 4.57 Section 4.0) – Sub-Surface examination of 450N sample at 55 minutes.

The location of crack initiation is possibly where the maximum shear stress is the greatest and will be calculated in the sections to follow. Cracks below the surface initially propagate parallel to the rolling direction then propagate at 45 degrees to the surface. If there are hard inclusions or defects (porosity) as was shown in Figure 4.60 and 4.61, at a distance below the surface near the potential maximum shear stress then they will be the preferred location for crack initiation.

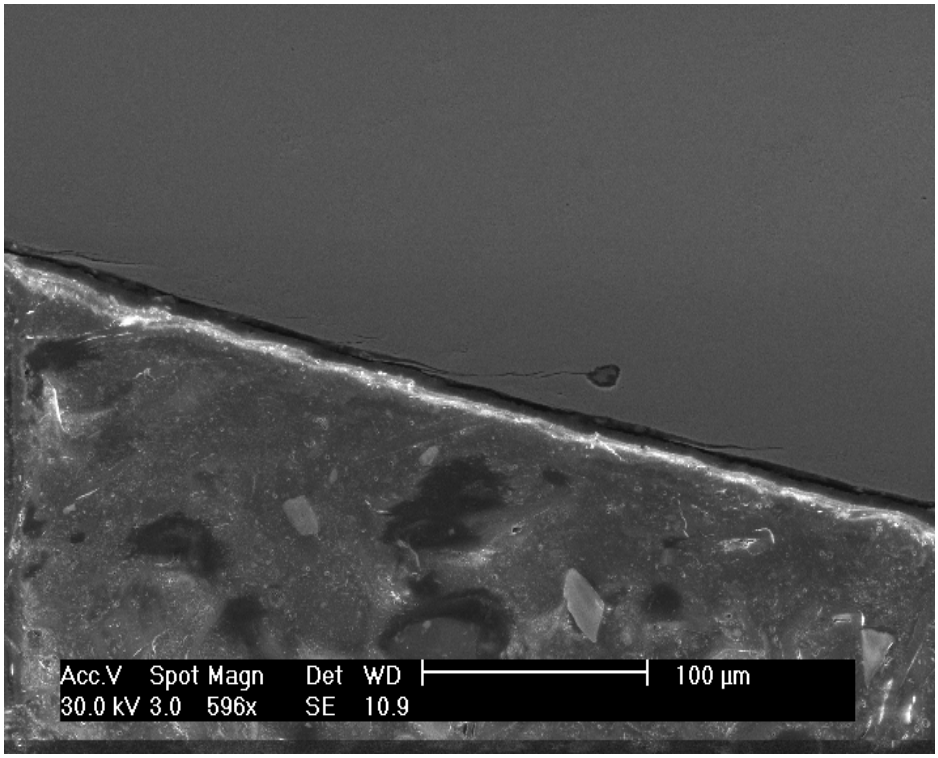


Figure 5.2 (Repeat of Figure 4.60 Section 4.0) Hard inclusion 10µm below the surface becomes the preferred site for Crack Initiation.

Plastic deformation and shearing occurs near and below the surface of rolling contact as was shown in Figure 4.59. Once cracks have extended to reach the surface, thin flat flake like sheets are produced as was shown in Figure 4.58. These flakes were clearly visible from the surface micrograph of Figure 4.54. The results described are in support of the Delamination Theory of Wear that was detailed in 2.3.1.3.

## 5.3 Wear Mechanism for Rolling Contact Wear of OA-Mg PSZ Ceramic.

Figures 4.66 to 4.71 showed the SEM micrographs of the wear tracks of PSZ ceramic under rolling contact at 790N load. Figures 4.66 and 4.67 of the 105 minute sample show original grinding marks of the surface have been removed and debris from the 52100 steel balls is present. As previously discussed with 52100 bearing steel, the initial

stages of wear of OA-Mg-PSZ are also asperity polishing occurring by removal of initial grinding marks by either adhesive and/or abrasive wear. This occurs for a significantly longer period (10 times longer in this investigation) than that of 52100 bearing steel at any given load. This accounts for the significantly lower mass loss of the ceramic material vs. bearing steel.

Following this period white lateral bands are then visible on the surface as was shown in Figure 4.67. These lateral bands have been observed by other authors [1,4,53,57] as typical lateral cracks seen in brittle failure of ceramics.

Near the site of these lateral cracks fatigue spallation occurs with increased test duration as shown in Figure 4.71. Spallation typifies material removal and volume loss.

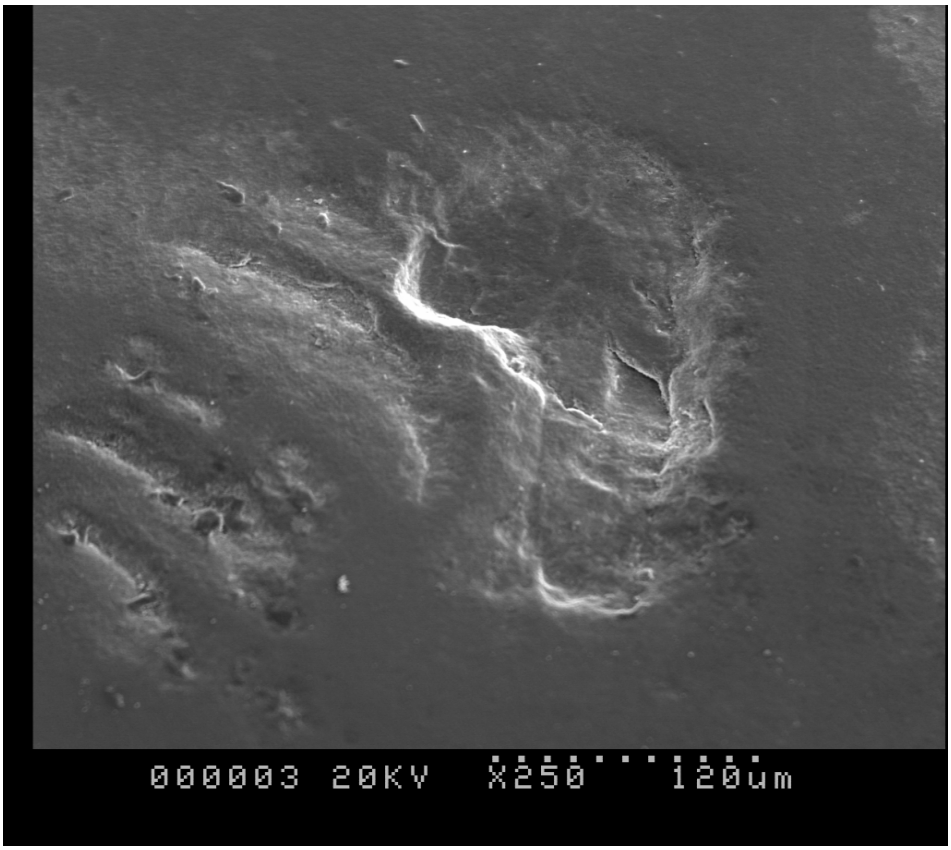


Figure 5.3 (Repeat of Figure 4.71 Section 4.0) Ceramic Sample 1, 330min 790N Load

## 5.4 Wear Equations for Rolling Contact Wear of 52100 Bearing Steel.

As mass loss and resulting wear volume was found to be proportional to load and test duration at a macroscopic level, equation of the form:

$$\text{Mass Loss (Wear Volume)} = K * \text{Load} * \text{Test Duration} \quad \ldots(13)$$

can be used to document mass loss and wear volume with K being the proportionality constant for the 52100 bearing steel used in this investigation. This equation is of the form described for adhesive and abrasive wear discussed in Section 2.3.1.1 and 2.3.1.2 with hardness being constant in this case.

At a microscopic level the amount of wear in the form of thin wear flakes removed will be proportional to the depth of the crack, the crack length, no of internal defects below the surface and time it takes for the crack to propagate to the surface (crack growth rate).

Mass Loss (Wear Volume) at given load =
Depth of crack * Crack Length * Crack propagation rate * No of internal Defects. …(14)

This equation is based on the results of this investigation and closely correlates with Equation (3) developed by Suh [20] for Delamination wear. All parameters in equation (14) can be measured by tests conducted using the new rolling contact test rig. The crack propagation rate can be calculated if the crack length at each of the time intervals (5 - 60 minute) samples is measured. The depth of crack will vary depending on the load as this will affect the maximum shear stress location.

Using Herztian equations the stress fields below the surface of contact can be calculated. The method is described by numerous authors [43,44,45,47] in the literature. Calculation of maximum normal stress, maximum shear stress and location of maximum shear stress was determined theoretically as well as modelled using finite

element analysis. The details of these calculations are described in a published paper by the current author in Appendix 1: Modelling the Contact Geometry of Ceramic Ball Bearings and Finite Element Method of Analysis.

The results of the theoretical calculations are shown in Table 5.1 for 52100 bearing steel on 52100 bearing steel.

Table 5.1 Theoretical calculation of maximum normal stress, maximum shear stress and location of maximum shear stress of 52100 bearing steel at 450N, 790N, 1500N load.

The depth below the surface where cracks were found to initiate in the 450N load sample was found to be 0.01mm (10μm). The calculated theoretical location of maximum shear stress was found to be 0.09mm. Based on this difference the location of crack initiation should be measured experimentally.

## 5.5 Wear Equations for Rolling Contact Wear of OA-Mg-PSZ Ceramic.

As mass loss and resulting wear volume for OA-Mg-PSZ was also found to be proportional to load and test duration at a macroscopic level, Equation (13)

$$\text{Mass Loss (Wear Volume)} = K * \text{Load} * \text{Test Duration} \quad \ldots(13)$$

can be used to document mass loss and wear volume with K being the proportionality constant for the OA-Mg-PSZ ceramic used in this investigation. This equation is of the form described for adhesive and abrasive wear discussed in section 2.3.1.1 and 2.3.1.2 with hardness being constant in this case.

At a microscopic level it is proposed that Equation (14) could also be used for OA-Mg-PSZ.

The key difference between 52100 bearing steel and OA-Mg-PSZ is the crack propagation rate. The crack propagation rate was found to be 10 times lower for OA-Mg-PSZ than that of 52100 bearing steel. All parameters can be found experimentally using the new rolling contact test rig and measured.

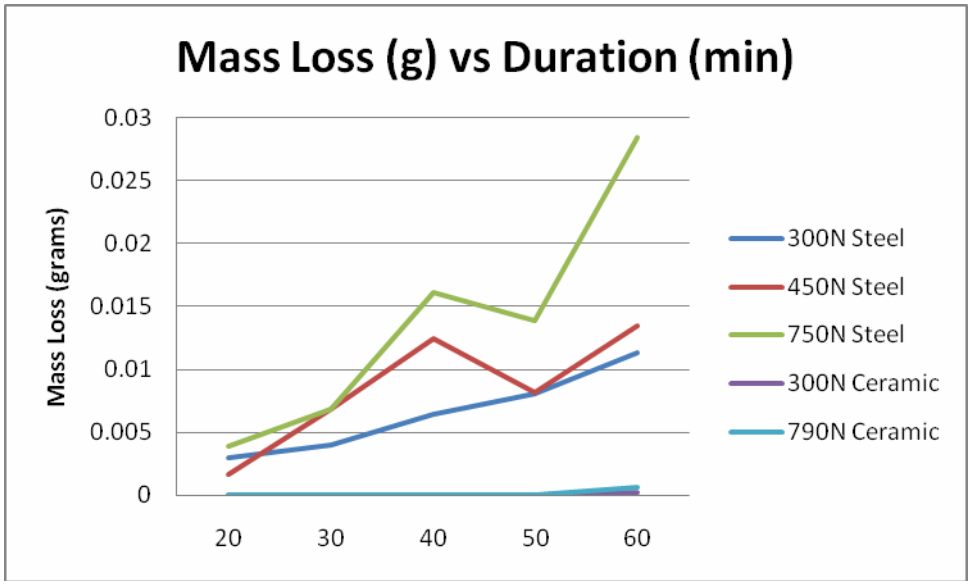


Graph 6.1 Mass loss vs Duration at various loads for 52100 Bearing Steel and OA-Mg-PSZ Ceramic. Graph is discussed in Chapter 6.

# Chapter 6
# Conclusion

The wear of a hybrid ceramic bearing system was investigated using a rolling contact wear test rig which included the operating variables and geometry seen in the full scale bearing. Wear test results were produced for varied loads and test duration variables for both 52100 bearing steel in contact with 52100 bearing steel as well as 52100 bearing steel in contact with OA-Mg-PSZ ceramic.

Based on the test results obtained by the new rolling contact wear test rig, the following conclusions are drawn.

## 6.1 Wear Behavior of 52100 Bearing Steel and OA-Mg-PSZ

### 6.1.1 Effect of Test Duration on Wear of 52100 Bearing Steel and OA-Mg-PSZ

At a fixed load, wear (mass loss and wear volume) increases proportionally to test duration (no of cycles). The wear rate of the 52100 bearing steel test specimens is an order of magnitude greater than that of the OA-Mg-PSZ ceramic test specimens.

### 6.1.2 Effect of Load on Wear of 52100 Bearing Steel and OA-Mg-PSZ

As the load increases the wear rate increases in both 52100 bearing steel and OA-Mg-PSZ. The wear rate at any given load is an order of magnitude greater in the 52100 bearing steel than the OA-Mg-PSZ ceramic test specimens. The mass loss vs duration for both 52100 bearing steel and OA-Mg-PSZ at various loads is shown in Graph 6.1 on the previous page.

## 6.2 Wear Mechanism and Wear Prediction Equations for 52100 Bearing Steel in Rolling Contact.

### 6.2.1 Wear Mechanism for 52100 Bearing Steel.

At initial stages of wear, asperity polishing occurs by removal of initial grinding marks by either adhesive and/or abrasive wear. After a short no of cycles for 5 minute test duration, the wear mode changes and surface cracking appears. Sub-surface examination revealed that the cracks originate at a distance below the surface. Cracks below the surface initially propagate parallel to the rolling direction then propagate at 45 degrees to the surface. If there are hard inclusions or defects (porosity) at a distance below then they will be the preferred location for crack initiation. Plastic deformation occurs near and below the surface of rolling contact. Once cracks have extended to reach the surface, thin flat flake like sheets are produced. The wear mechanism for rolling contact wear is in support of the Delamination Theory of Wear developed by Suh [20] for sliding wear.

### 6.2.2 Equations for Modeling Wear of 52100 Bearing Steel on Rolling Contact.

Mass loss and resulting wear volume was found to be proportional to load and test duration at a macroscopic level. Equation (13) was established to document mass loss and wear volume with K being the proportionality constant for the 52100 bearing steel used in this investigation.

At a microscopic level the amount of wear in the form of thin wear flakes removed is proportional to the depth of the crack, the crack length, no of internal defects below the surface and time it takes for the crack to propagate to the surface (crack growth rate) as described in equation (14). All parameters in equation (14) can be measured by tests conducted using the new rolling contact test rig.

## 6.3 Wear Mechanism and Wear Prediction Equations for OA-Mg-PSZ Ceramic

### 6.3.1 Wear Mechanism for OA-Mg-PSZ Ceramic.

At initial stages of wear, asperity polishing occurs by removal of initial grinding marks by either adhesive and/or abrasive wear. This occurs for a significantly longer period (10 times longer in this investigation) than that of 52100 bearing steel at any given load. Following this period white lateral bands are then visible on the surface. These lateral bands have been observed by other researchers as typical lateral cracks seen in brittle failure of ceramics. Furthermore, it was found near the site of these lateral cracks fatigue spallation occurs with increased test duration. Spallation typifies material removal and volume loss.

### 6.3.2 Equations for Modeling Wear of OA-Mg-PSZ in Rolling Contact.

Mass loss and resulting wear volume for OA-Mg-PSZ was also found to be proportional to load and test duration at a macroscopic level, Equation (13) can be used to document mass loss and wear volume with K being the proportionality constant for the OA-Mg-PSZ ceramic used in this investigation. As a result of this work, at a microscopic level Equation (14) can also be used for OA-Mg-PSZ.

The key difference between 52100 bearing steel and OA-Mg-PSZ was found to be the crack propagation rate. The crack propagation rate was found to be 10 times lower for OA-Mg-PSZ than that of 52100 bearing steel. All parameters can be found experimentally using the new rolling contact test rig and measured.

# Chapter 7
# Scope for Future Work

A significant amount of work has been completed in this investigation to understand the wear mechanisms in un-lubricated rolling contact of 52100 bearing steel and OA-Mg-PSZ ceramic. However further work needs to be done. This section details work that if time had permitted the author would have investigated

In order to quantify the wear volume of 52100 bearing steel and OA-Mg-PSZ shown in the Equation (14) below, the depth of crack, crack length, crack propagation rate and number of internal defects needs to be initially measured experimentally. Further measurements of experimental data collected from samples at 5 minute through to 60 minute is required. The subsurface crack length and depth below the surface of crack initiation for these samples needs to be measured.

Further work is suggested to improve the proposed wear Equation (14)

Mass Loss (Wear Volume) at given load =

Depth of crack * Crack Length * Crack propagation rate * No of internal Defects. …(14)

A detailed understanding of the mechanisms of crack propagation rate in OA-Mg-PSZ would assist greatly in wear modeling as it differs to that found in 52100 bearing steel. The stress induced transformation model equations could be utilized if the volume fraction and width of wake of transformation is measured.

If lubricant's are to be investigated in addition to dry contact as conducted in this investigation, then the test rig will need to be modified to collect and transfer lubricant to the area of contact. Test times will be significantly longer, hence loads would have to be revised to ensure enough samples can be tested to be statistically meaningful. Accurate measurement of coefficient of friction would be required to determine when the lubricant is no longer performing adequately and breaking down.

# References

[1] Zhen Chen, Jacques C.Cuneo, John, J. Mecholsky, Jr, Shoufeng Hu, Damage processes in $Si_3N_4$ bearing material under contact loading, Wear, 198, 197-207

[2] Luen-Yuan Chao and Dinesh K.Shetty, Development of Silicon Nitride for Rolling-Contact Bearing Applications: A review, J.Mater.Educ.,Vol 17, pp.245-303, 1995.

[3] D.Scott and J.Blackwell, Hot Pressed Silicon Nitride as a rolling bearing material – A preliminary assessment, Wear (1972), 61-67

[4] F.Guiu, M.J.Reece, D.A.J.Vaughan, Cyclic fatigue of ceramics, Journal of Materials Science 26 (1991) 3275-3286

[5] Yushu Wang, Stephen M.Hsu, The effects of operating parameters and environment on the wear and wear transition of alumina, Wear 195 (1996) 90-99

[6] G.B. Stachowiak, G.W. Stachowiak, Fretting wear and friction behaviour of engineering ceramics, Wear 190 (1995), 212-218

[7] N.Iyer and D.K. Shetty, Fatigue and Wear of M-50 Steel in Rolling Contact with Silicon Nitride Balls, Department of Materials Science and Engineering, University of Utah.

[8] R.Nathan Katz, Effects of Composition, Microstructure, and Processing on Ceramic Rolling Element Bearing Performance

[9] Crawford Meeks, Design and Life Prediction Issues for Ceramic Bearings

[10] R.Nathan Katz, Role of Composition, Microstructure and Processing on the Performance of Ceramic Rolling Element Bearings, NIST, 17April 1991

[11] R.Nathan Katz, Ceramic Materials for Rolling Element Bearing Applications

[12] M.B. Peterson and R.E. Lee, Jr, Sliding Characteristics of the Metal-Ceramic Couple, Wear, 7 (1962) 334-343

[13] S.S.Kim, K.Kato, K.Hokkirigawa, H.Abe, Wear Mechanism of Ceramic Materials in Dry Rolling Friction, Transactions of the ASME, Vol 108, October 1986, 522-526

[14] R.Lakshminarayanan, L-Y. Chao, N.Iyer and D.K.Shetty, Wear of steel in rolling contact with silicon nitride. University of Utah

[15] Yushu Wang and Stephen M.Hsu, Wear and Wear Transition modelling of ceramics, Wear 195 (1996), 25-46

[16] G.R. Bremble and B.G.Brothers, An Experimental Investigation into the friction and wea characteristics of unlubricated roller bearings, Wear, 17 (1971), 165-183

[17] A.Kasak and T.A. Neumeyer, Observations on Wear of High Hardness Steels, Wear, 14 (1969) 445-454

[18] W.D. Syniuta and C.J.Corrow, Scanning Electron Microscope Studies of Fracture Mechanisms of SAE 52100 Bearing Steel, Wear, 15 (1970), 171-186

[19] A.L. Zharin and G.P Shpenkov, Macroscopic Effects of Delamination Wear, Wear 56, (1979) 309-313

[20] Nam P.Suh, The Delamination Theory of Wear, Wear 25 (1973) 111-124

[21] S.Jahanmir, N.P.Suh and E.P. Abrahamson, Microscopic Observations of the wear sheet formation by delamination, Wear 28 (1974), 235-249

[22] Nam P.Suh, An overview of the delamination theory of wear, Wear 44 (1977), 1-16

[23] S.Jahanmir and N.P Suh, Mechanics of Subsurface Void Nucleation in Delamination Wear, Wear 44 (1977), 17-38

[24] J.R.Fleming and N.P Suh, Mechanics of Crack Propagation in Delamination Wear, Wear 44 (1977) 39-56

[25] J.R. Fleming and N.P Suh, The relationship between Crack Propagation Rates and Wear Rates, Wear 44 (1977) 57-64

[26] Gangopadhyay ET AL, Ceramic Cam Roller Followers

[27] Karl-Heinz Zum Gar, Microstructure and wear of Materials, 1987

[28] John B. Wachtman, Mechanical Properties of Ceramics

[29] J.F.Archard, Wear Theory and Mechanisms, Wear Control Handbook,

[30] M.B.Peterson, Design Considerations for Effective Wear Control, Wear Control Handbook, 1980

[31] Douglas Godfrey, Diagnosis of Wear Mechanisms, Wear Control Handbook

[32] Bayer, Mechanical Wear Prediction and Prevention, Wear Mechanisms, 1994

[33] Bayer, Mechanical Wear Prediction and Prevention, Wear Behavior and Phenomena, 1994

[34] Ernest Rabinowicz, Friction and Wear of Materials

[35] Sakar, Wear of Metals, 1976

[36] J.Halling, Introduction to Tribology, 1975

[37] ASM Papers, Fundamentals of Friction and Wear of Materials

[38] B. Pugh, Friction & Wear

[39] Kenneth C. Ludema, Friction, Wear, Lubrication, A textbook in Tribology

[40] Herzberg, R. Defromation and Fracture Mechanics of Engineering Materials, 1983

[41] Liebowitz, Fracture, 1971

[42] John Martin, Materials for Engineering, 1996

[43] Hamrock, Ball Bearing Lubrication, The Elastohydrodynamics of Elliptical Contacts

[44] Tedric A.Harris, Rolling Bearing Analysis, Second Edition, 1966

[45] K.L Johnson, Contact Mechanics

[46] J.Halling, Principals of Tribology, 1975

[47] P.S Houghton, Ball & Roller Bearings

[48] Luen-Yuan Chao, Dinesh K.Shetty, Development of Silicon Nitride for Rolling-Contact Bearing Applications, The Journal of Materials Education, Volume 17, Numbers 5&6

[49] Douglas Glover, A Ball – Rod Rolling Contact Fatigue Tester, ASTM STP 771, 1982, pp 107-124.

[50] H. Czichos, Systems Approach to the Analysis of Wear Problems, Conference on Lubrication Friction and Wear in Engineering, 1980, Melbourne, 1-5 December

[51] H.Muro, N.Tsushima, Microstructural, Microhardness and Residual Stress Changes due to Rolling Contact, Wear 15 (1970), 309-330

[52] Gustaf Lundberg & A.Palmgren, Dynamic Capacity of Rolling Bearings, Journal of Applied Mechanics, 1949, p165-173

[53] Evans, A.G. and Wilshaw, T.R., 1976, "Quasi-static solid particle damage in brittle solids I – Observations analysis and implications", Acta Metallurgica, Vol. 24, pp. 939-956.

[54] Evans, A.G. and D.B. Marshall, 1980, Wear Mechanisms in Ceramics, Fundamentals of Friction and Wear of Materials, Papers presented at the 1980 ASM Materials Science Seminar

**Thesis**

[55] Said, Jahamir, A fundamental Study on the Delamination Theory of Wear, Massachusetts Institute of Technology Jan 1977

[56] Peter John Mutton, The influence of Microstructure on the wear behaviour of rail and wheel materials, University of Melbourne, 1985

[57] Georgina L. Kelly, Rolling and Sliding Wear of Magnesia-Partially-Stabilised Zirconia, Monash University, Nov 1998

[58] Singhai Bian, Factors Affecting the Unlubricated Sliding Wear of Steel, University of Melbourne, Nov 1993

# APPENDIX 1: PUBLISHED PAPER – Modelling the Contact Geometry of Ceramic Ball Bearings and Finite Element Method of Simulation

## MODELLING THE CONTACT GEOMETRY OF CERAMIC BALL BEARINGS AND FINITE ELEMENT METHOD OF SIMULATION.

**Fazul M. HUQ, Michael PAPADOPOULOS and Varikan O. THOMAS**
Department of Mechanical Engineering
RMIT University, Melbourne, AUSTRALIA

ABSTRACT

In the present paper , the design of an accelerated rolling contact fatigue/wear (RCF) tester simulating the geometry and point contacts of a ceramic ball bearing is discussed. Details of a dynamic analysis for determining stress distributions associated with fatigue failure using finite element (FE) are presented. The FE simulation is based on the geometry of the RCF tester shown in Figure 1. The solution aspects presented are the stress distribution on the contacting area, the maximum shear stress and its location within the material. Correlation of the results produced using the FE method and by theoretical analysis are discussed.

Key words , Rolling Contact , Fatigue, Ceramic Bearing, Finite Element Simulation, Stress Distribution.

### 1. INTRODUCTION

The potential for significant performance increases, using candidate ceramic materials in rolling element bearings, has been the subject of research over the past two decades (Jahanmir 1991). Practical advantages over bearing steels have been reported (Parker 1975), with increased ability to withstand high loads, severe environments and high speeds. However, wide spread acceptance has been limited by the current inability to predict life for ceramic bearing applications (Jahanmir 1991).

Full scale bearing tests for investigating rolling contact fatigue and wear life of candidate ceramic materials are very expensive. This is due to high material costs, duration time of tests, and the large number of specimens that have to be tested as data must be treated statistically (Lundberg *et al.* 1949).

In order to study the fatigue/wear effects of ceramic materials in rolling contact and produce data within a reasonable time frame, an accelerated rolling contact fatigue/wear tester has been developed simulating the geometry and contacts experienced in ceramic ball bearings. The stress distributions produced by the RCF tester, are of particular interest in fatigue failure and have been modelled using an FE method of simulation. The results produced by the model are discussed in this paper.

### 2. THE ROLLING CONTACT FATIGUE/WEAR (RCF) TEST RIG.

The RCF tester simulates the geometry of a full scale ball bearing using two, 25.4mm AISI 52100 steel balls in point contact with a 14 mm diameter cylindrical ceramic specimen as shown in Figure 1. The two steel balls represent the inner and outer race of a bearing and simulate the surface interactions associated with the inner race and ball contacts, and outer race and ball contacts. The two steel balls and ceramic specimen are supported, and the geometry maintained, by three lower guide rollers and a drive roller as shown in Figure 2. The ceramic specimen is driven by the top roller and is edge loaded so as not to affect the contacts between the two steel balls and ceramic specimen which are of interest. Load is applied vertically with drive being produced by the top roller which in turn drives the ceramic specimen , rotating the two steel balls, and lower support rollers.

Figure 1 : Lower Section of the RCF Tester.

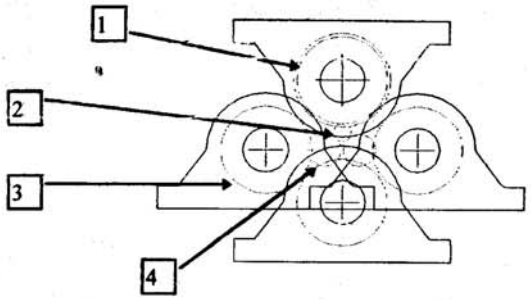


Figure 2 . Geometry and Components of the RCF tester.

(1) Top Drive roller (Load applied vertically), (2) Ceramic Specimen, (3) Guide Roller , (4) Steel Balls (Simulate Inner & Outer Race Contacts.

## 3.0 THEORETICAL MODEL ANALYSIS

The classical solution for the local stress and deformation of two elastic bodies apparently contacting at a single point was established by Hertz in 1881. Two bodies of revolution having different radii of curvature in a pair of principal planes passing through the contact between the bodies may contact each other at a single point under the condition of no applied load. Such a condition is called point contact. The contact area shape is a function of the curvature of the contacting bodies and Hertz assumption is that the shape of the deformed surface was that of an ellipsoid of revolution as shown in Figure 3a. Here, a and b are the semimajor and semiminor axes of the projected elliptical area of contact. For the condition of two rollers in contact, the stress distribution in the contact area degenerates to a semicylindrical form as shown in Figure 3b. We will be using this model as the FE simulation is 2- dimensional and models two cylinders of unit length in contact.

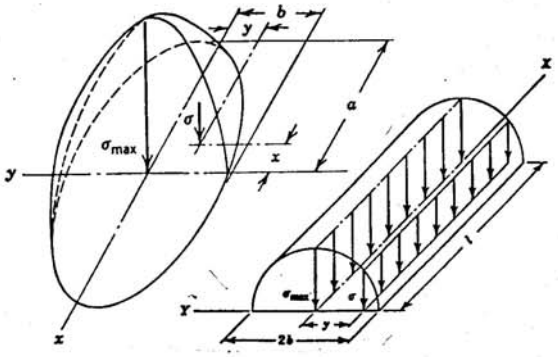


Figure 3a and 3b, Ellipsoidal (3a) and Semicylindrical (3b) surface compressive stress distribution of point and line contact.

For the condition of two rollers in contact it has been determined (Harris 1984), that the maximum normal stress is:

$$\sigma_{max} = \frac{2Q}{\pi l b},$$

$Q$ normal force between rolling element and raceway lb
$l$ roller effective length in.
$b$ semiminor axis of the projected contact ellipse in.

The normal stress at other points (y) within the contacting area is :

$$\sigma = \frac{2Q}{\pi l b}\left[1-\left(\frac{y}{b}\right)^2\right]^{\frac{1}{2}}$$

The semiminor axes of the projected line area of contact is :

$$b = \left\{\frac{4Q}{\pi l \Sigma\rho}\left[\frac{\left(1-\xi_I^{\,2}\right)}{E_I}+\frac{\left(1-\xi_{II}^{\,2}\right)}{E_{II}}\right]\right\}^{\frac{1}{2}}$$

$\xi$ Poisson's ratio, $\Sigma\rho$ curvature sum in.$^{-1}$
$E$ modulus of elasticity psi

For steel roller bearings the semwidth of the contact surface may be approximated by

$$b = 2.78\times10^{-4}\left(\frac{Q}{l\Sigma\rho}\right)^{\frac{1}{3}}$$

### 3.1 Maximum Shear Stress and its Location

Hertz analysis applies to surface stresses. Experiments conducted Lundberg and Palmgren (1949), indicate that failure of rolling bearings in fatigue emanates from points below the stressed surface. Therefore it is of interest to determine the magnitude and location of the subsurface stresses. Using value obtained for maximum normal stress and b (semiminor axis) , the maximum shear stress and its location below the surface can be determined using Figure 4 (Harris, 1984).

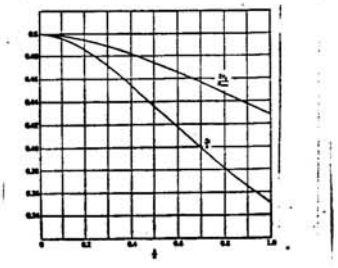

Figure 4 : $2\tau_o / \sigma_{max}$ and $z_o / b$ versus b/a

## 4. FE SIMULATION OF THE RCF TESTER

In order to determine the stress field associated with fatigue failure during the RCF tests a FE simulation of the two steel balls in contact with the ceramic specimen was performed. The finite element analysis (FEA) method can be used to obtain an approximate solution to the stress distribution in solids. The following commercial packages were used the construction of the finite element model and the processing of results.

Pre-processing: Patran v6.0
Processing: ABAQUS Explicit v5.6
Post-processing: ABAQUS Post v5.6

FEA software, ABAQUS was used to perform the finite element analysis and PATRAN pre-processor for setting up the finite element meshes. The static simulation is based on applying a displacement vertically to the top guide roller. The von Mises stress distributions beneath the contact positions are produced using Abaqus post (Post Processor).

The chief aims of the finite element simulation endeavour to:

- Corroborate analytical approaches to predicting contact stresses.
- To provide a quantitative description of the stress distributions for fatigue analysis of the specimens.

### 4.1 Modelling

Modelling of the physical system is pictured below in Figure 5. A cylindrical specimen lies on two steel spherical specimens and is loaded vertically. The spherical steel specimens are held respectively by guide rollers.

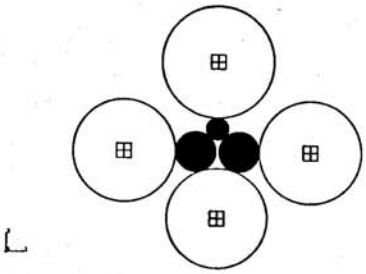

Figure 5 : Model of the RCF Tester

### 4.2 Simplifications.

#### 4.2.1 Dimensional problem.

First and foremost, the assumption was made that the problem can be simplified by adopting a two dimensional approach. This was supported by the geometric nature of the ceramic specimen and the fact that the ceramic stress distributions were of higher concern than any other member of the model. As such , 2 - dimensional plane linear elements were used to model all deformable specimens. Initially, the elements were constructed with very small dimensions, due to the nature of contact stresses.

#### 4.2.2 Deformable / non-deformable members

The rollers were modelled as rigid 2-dimensional circles, whereas the ceramic and steel specimens are fully deformable.

#### 4.2.3 Material model

Initially, the material model employed was a basic isotropic material, without plasticity or failure criteria.

#### 4.2.4 Geometry simplification.

Due to the symmetry of the problem only the left steel ball and half of the ceramic ball was needed to be modelled.

As a direct result of the above modelling simplifications, the modified finite element model is displayed in Figure 6. This shows the ceramic specimen in contact with the left steel ball in which the stress distribution is of interest.

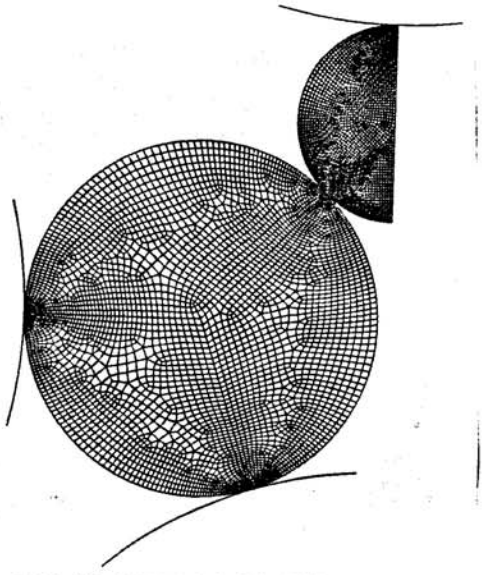

Figure 6: Modified FE Model of the RCF tester.

4.3 Loading

A linear analysis was sought for a pure static loading case. However, unforeseen numerical problems associated with the resolution of contact within an implicit procedure persuaded the use of a dynamic explicit analysis.

To ensure the dynamic effects were negligible in the analysis:

a) A long residence time was provided in the simulation (so that oscillations damp out).
b) The loading was applied gradually (sinusoidal).
c) A quasi-static check was made. The velocity, displacement time history of the top steel roller ensures that enough residence time has been used to damp out oscillations. The quasi-static check , which simply requires that the total kinetic energy of the deformable system be less than 5% of the internal energy of the deformable system at all times of the simulation, verified the simulation as being quasi-static.

A 250N , 750N and 1500N concentrated load case (acting vertically on the top roller) was used to evaluate stress distributions on the deformable specimens. Ideally, since this is a quasi-static linear model, the results of the latter load cases will be simple multiples of the first load case. The latter loads cases were still conducted as further verification to the use of a dynamic explicit analysis

For all the load cases employed, the displacement proved to be very small. The contact stresses spanned at the most two elements, which warrant further model modification.

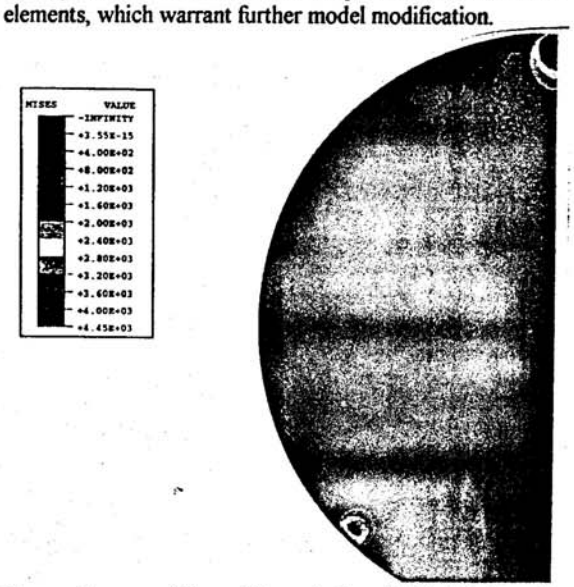


Figure 7 : von Mises (Normal Stress) Distribution for 1500N Loading.

5.0 FINITE ELEMENT AND THEORETICAL RESULTS

The von Mises stress distribution for the 2-dimensional model of the 1500N loading case is shown in Figure 7 . The shear stress distribution for the 1500N loading case is shown in Figure 8. The location of the maximum shear stress was calculated using the co-ordinates of the mesh nodes. The theoretical and FE results are summarised in Table 1. Values for b, the maximum normal stress , maximum shear stress and location were determined.

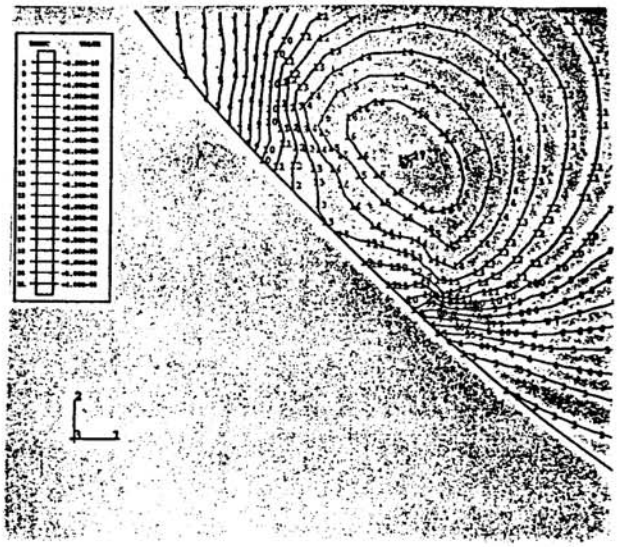

Figure 8 : Tresca (Shear Stress) Distribution for 1500N Loading.

| | | |
|---|---|---|
| Summary of Results for F.E and Theoretical Models | | |
| | | |
| For loading case 1500 N | Steel on Steel (Only) | |
| | FE Model | Theory |
| Maximum normal Stress (Mpa) | 3600 | 4300 |
| Maximum Shear Stress (Mpa) | 1600 | 1300 |
| Location of Maximum Shear Stress (mm) | 0.35 | 0.31 |
| b (Semiminor axis of contact mm) | 0.4688 | 0.2292 |

Table 1 : Summary of Results.

## 6.0 DISCUSSION/CONCLUSION

The refined model has captured the subsurface maximum stress concentrations (see von Mises and Tesca stress contours). This is largely due to a dramatic decrease in element size near the areas of contact. However a comparison of the theoretical and FE. results still illustrate a marked difference. The two models do not correlate to any acceptable degree. In light of this and the very high stress it is deemed reasonable to consider the theoretical results as more credible and further modification of the FE model is required.

The following factors have contributed to the lack of correlation between the models :

(1) The FE analysis was based on an explicit analysis for the first FE model, the dynamic effects were minimised by extending the residence time. For the refined model, the element size had been reduced dramatically, subsequently, the minimum time increment for stable solution progression in the explicit analysis reduced markedly. The overall time for a reasonable static solution was unacceptable (in the order of a week's computational time). To reduce the computational time, results were taken while the system was still vibrating.

(2) The material was isotropic and linear elastic. No plasticity was included in the FE model.

(3) The theoretical model was empirically modified/adjusted.

(4) The FE analysis was 2-dimensional and as such modelled as two unit rollers in contact whereas the real system has a ceramic roller and spherical balls.

### 6.1 Recommendations.

If an explicit analysis is conducted:

1) Review the contact algorithm used.

(2) Supply enough damping and total time to reduce dynamic effects.

(3) In addition, supply a realistic material model including plasticity effects.

(4) Model the system in 3 - dimensions.

## REFERENCES


Said Jahanmir, "Ceramic Bearing Technology" , Proceedings of the NIST/DARPA Workshop on Ceramic Bearing Technology, April 17-18 , 1991 Gaithersburg, Maryland.

R.J. Parker et al., " Fatigue Life of High- Speed Ball Bearings With Silicon Nitride Balls", Journal of Lubrication Technology, 1975, p 350-357

Gustaf Lundberg & A.Palmgren, "Dynamic Capacity of Rolling Bearings", Journal of Applied Mechanics, 1949, p165-173

Tedric R Harris, 1984. "Rolling Bearing Analysis", Second Edition, p434-480


## ABOUT THE AUTHORS


*Fazul M. Huq*, B.E (Mech), Grad IE Aust, is a postgraduate student in the Department of Mechanical Engineering at RMIT University, Melbourne Australia. He graduated as a mechanical engineer from Monash University , (Clayton Campus), Melbourne, Australia and is currently conducting research towards a PhD at RMIT University. His research interests include wear and fatigue modelling of rolling bearings using ceramic and steel materials.

*Michael Papadopoulos*, B.Eng (Aero), is a postgraduate student in the Department of Mechanical Engineering at RMIT University, Melbourne Australia. He is currently conducting research towards Masters of Engineering. His research interests include modelling of car body stamping processes using Finite Element Analysis.

*Varikan O. Thomas*, MEngSc, CPEng, is a Lecturer and co-ordinator of the Programs in the Department of Mechanical Engineering at RMIT University, Melbourne Australia. His research interests are in Robotics and the application of computer graphics to mechanical design enhancements. He can be reached by e-mail : rmevt@rmit.edu.au, by fax +613-9407-6003 or through postal address: Department of Mechanical Engineering, RMIT University, Bundoora East Campus, P.O. Box 71, Bundoora, Victoria, 3083, Australia.

# APPENDIX 2: METALLURGY OF THE CERAMIC AND STEEL MATERIALS BEING CONSIDERED.
# (Material directly taken from Zum-Gar [27])

## Classification of Materials

Materials can be divided into four main groups, namely metals, ceramics, plastics and composites. Metals differ from ceramics in the type of binding. Metallic binding is undirected, with valence electrons forming an electron cloud. Electrons can move freely between the atoms. Ceramics are inorganic materials with ionic and covalent atomic bindings, they embrace oxides, carbides, nitrides, graphites, cerments. The atomic bonds of ceramics are very stable and result in very high melting points and high chemical stability.

Depending on the surface structure the volume properties and surface properties can be substantially different. The volume mechanical properties and their dependence on microstructure will be discussed. The interaction between two contacting bodies may be elastic or plastic, depending among other things on the strength or hardness of the materials. Hence the strength and hardness of materials is very important for tribological processes. Strength can be defined as the resistance to plastic deformation and crack propagation. Plastic deformation occurs by slip, twinning, kinking or phase transformation in crystalline materials. Slip is the displacement of part of a crystal by a gliding motion of dislocations on a certain crystal plane, i.e. slip planes. Twinning is caused by the co-operative movement of atoms. The atoms move relative to each other by less than the atomic spacing in the lattice. Kinking is produced by a progressive rotation of the crystal lattice. Kink bands are separated from unkincked crystal walls of the edge dislocations.

## Hardening Mechanisms

Phase transformations are caused by a crystallographic transformation of crystal structure to another and may be connected with a volume change. Resistance to plastic deformation can be increased by impeding the movement of dislocations on slip planes.

For increasing the yield strength of a material, different obstacles can be thrown in the way of dislocations. The following hardening mechanisms based on microstructural elements are distinguished:

1. Solid solution hardening
2. Precipating hardening
3. dislocation hardening
4. grain boundary hardening
5. texture hardening
6. anisotropy hardening
7. transformation hardening

In considering wear, stronger emphasis is frequently put on improving the strength of metallic alloys than their ductility. However ductility can decrease dramatically with increasing strength or harness. Hence a compromise between high strength and sufficient ductility has often to be looked at in practice. Fracture toughness may be considered as a usual measure of sufficient “ductility in wear”. The critical stress intensity factor $K_{ic}$, also called the fracture toughness describes the resistance of a material against propagation of a crack. Increasing the yield stress results in decreasing fracture toughness. The concept of fracture toughness is founded on an existing crack in the material stressed. Another limiting condition in wear can be the formation of a crack. The formation of cracks is favored by:

- Inclusions or incoherent particles
- Embrittled grain, twin or phase boundaries
- Slip bands

Depending on the wearing system different mechanical properties, eg.: resistance against plastic deformation, crack formation or crack propagation have to be considered In the sequence from crack formation to crack propagation and finally fracture, crack propagation plays the determining part in most metallic alloys.

In contrast, crack formation seems to be the most important part in ceramics. Cracks can propagate relatively easily due to the substantially lower ductility of ceramic compared

with metals. In general the hardness and compression strength of ceramics decrease with increasing porosity and grain size. The fracture stress of hard ceramics is generally equal or lower than the yield stress. Thus ceramics fail brittleness before substantial yielding can occur. The energy of fracture and fracture toughness of ceramics are reduced by increasing porosity in the absence of microplasticity. Toughening of ceramics can be provided by microstructural elements which introduce more plasticity in the path of propagating cracks during loading.

**Zirconia Ceramics**

Zirconia ceramics are an important class of ceramic materials that are characterized by a high strength and toughness at room temperature. Zirconia, or zirconium oxide is a refractory oxide obtained from abundant zircon sand. Pure zirconia exists in three different crystal structures: monoclinic, tetragonal and cubic. The monoclinic phase is stable at room temperature and up to about 1170 deg C where it transforms to the tetragonal phase. The tetragonal phase is stable up to 2370 deg , it transforms to the cubic phase at this temperature.

An important characteristic of zirconia ceramics is that the microstructure of the material can be controlled by the addition of various cubic oxides such as MgO. The amount of the additive and the thermomechanical processing history can be chosen such that the tetragonal and cubic phases become stable at room temperature. Zirconia ceramics used in technical applications are classified into three types; cubic, partially stabilized and tetragonal zirconia. The cubic zirconia is obtained by fully stabilizing the high temperature cubic phase by addition of about 10% cubic oxides. Although cubic zirconia is used in certain applications, its relatively low fracture toughness and strength prevents its use in tribological applications.

**Partially stablised zirconia (PSZ)**

Partially stablised zirconia (PSZ) has a two phase structure, consisting of cubic grains with tetragonal and/or monoclinic precipitates, depending on the thermal history during processing. By careful process and microstructual control, PSZ can be made with a

larger fracture toughness and is therefore more important in structural applications. The metastable tetragonal precipitates undergo a stress induced phase transformation near an advancing crack tip. The compressive stress associated with the increase in volume in transformation of tetragonal to the monoclinic phase reduces the stress at the crack tip and results in high strength and toughness. It is also believed that the transformation absorbs energy which would otherwise be used for crack propagation. Thereby reducing the total energy available for advancing the crack and resulting in a toughening effect. Typical commercial PSZ materials contain about 8% MgO and have a composition of about 58% cubic, 37% tetragonal and 5% monoclinic.

**Tetragonal zirconia polycrystal (TZP)**

Tetragonal zirconia polycrystal (TZP) is made by addition of about 2-3% $Y_2O_3$ to stablise the tetragonal at room temperature and exhibits the highest toughness and strength among zirconia ceramics and other monolithic structural ceramic materials. The toughening mechanism in this material is similar to that of PSZ, that is tetragonal to monoclinic transformation. The TZP materials are not used as widely in tribological applications because of the severe degradation and degrease in strength at intermediate temperatures (200-400deg) in humid atmospheres.